Utilisation complémentaire des techniques de fractionnement flux-force asymétrique et en colonne tournante pour la caractérisation d'échantillons environnementaux de particules

Aleksandr Ivaneev

▶ **To cite this version:**

Aleksandr Ivaneev. Utilisation complémentaire des techniques de fractionnement flux-force asymétrique et en colonne tournante pour la caractérisation d'échantillons environnementaux de particules. Chimie analytique. Université de Pau et des Pays de l'Adour, 2020. Français. NNT : 2020PAUU3035 . tel-03209566

HAL Id: tel-03209566
https://theses.hal.science/tel-03209566

Submitted on 27 Apr 2021

HAL is a multi-disciplinary open access archive for the deposit and dissemination of scientific research documents, whether they are published or not. The documents may come from teaching and research institutions in France or abroad, or from public or private research centers.

L'archive ouverte pluridisciplinaire **HAL**, est destinée au dépôt et à la diffusion de documents scientifiques de niveau recherche, publiés ou non, émanant des établissements d'enseignement et de recherche français ou étrangers, des laboratoires publics ou privés.

№ |_|_|_|_|_|_|_|_|_|_|

UNIVERSITE DE PAU ET PAYS DE L'ADOUR
École doctorale des Sciences Exactes et de leur Applications (ED 211)
ET
UNIVERSITE NATIONALE DE SCIENCES ET TECHNOLOGIE "MISiS"
École doctorale

THESE

PRESENTEE PAR
Aleksandr IVANEEV

Pour obtenir le grade de docteur
de l'Université de Pau et des Pays de l'Adour
Spécialité: Chimie Analytique et Environnement

Utilisation complémentaire des techniques de fractionnement flux-force asymétrique et en colonne tournante pour la caractérisation d'échantillons environnementaux de particules

Soutenue le 17 décembre 2020

MEMBRES DU JURY

Directeurs de thèse

Petr FEDOTOV	Directeur de laboratoire, Université "MISiS"
Gaëtane LESPES	Professeur, Université de Pau

Rapporteurs

Serge BATTU	Professeur, Université de Limoges
Anna ZAVARZINA	Leading research scientist, Lomonosov Moscow State University

Examinateurs

Tatiana MARYATINA	Professeur, Vernadsky Institute of Geochemistry and Analytical Chemistry
Karen GAUDIN	Professeur, Université de Bordeaux
Stéphane FAUCHER	Docteur, Université de Pau

Acknowledgments

First, my sincere gratitude goes to my supervisors Petr Fedotov and Gaëtane Lespes for the obtained experience, consideration, encourage and support at all steps of the thesis work, discussion of results and planning of experiments.

I am grateful Mikhail Ermolin and Stéphane Faucher for their contribution and help in experimental work, valuable advices, discussion of results, and planning experiments.

I thank Vasily Karandashev and Natalia Fedyunina for their contribution in experimental work in part of digestion and analysis of samples under study, helpful suggestions and comments.

I express my acknowledgements to the Embassy of France in Moscow for Vernadsky PhD fellowship awarded for performing this doctoral thesis under co-supervision by Petr Fedotov and Gaëtane Lespes in University of Pau and University “MISiS”.

I would like to thank the Laboratory Of Separation and Pre-concentration in Chemical Diagnostic of Functional Materials and Environmental Objects (NUST “MISiS”) and Institut des Sciences Analytiques et de Physico-Chimie pour l’Environnement et les matériaux (UMR 5254 UPPA/CNRS, Pau) for the support and contribution towards this doctoral thesis.

Last, but not the least, I want to thank my colleagues and friends for continued support. I also express my sincere thank my wife Liubov for support and inspiration over the years.

TABLE OF CONTENTS

List of figures

List of tables

Glossary

NP – nanoparticle;

FFF – field-flow fractionation;

SPLITT – split flow thin cell fractionation;

FlFFF – flow field-flow fractionation;

SdFFF – sedimentation field-flow fractionation;

A4F – asymmetric flow field-flow fractionation;

RCC – rotating coiled column;

CTFFF – coiled tube field-flow fractionation;

CSF – conventional SPLITT fractionation;

FFDSF – full feed depletion SPLITT fractionation;

PSD – particle size distribution;

ICP-AES – inductively coupled plasma atomic emission spectrometry;

CV-ETAAS - cold vapour electrothermal atomic absorption spectroscopy;

ICP-MS – inductively couples plasma mass spectrometry;

sp-ICP-MS – ICP-MS in single particle mode;

SEM – scanning electron microscopy;

TEM – transmission electron microscopy;

EDS – energy dispersive X-ray spectroscopy;

LD – laser diffraction;

DLS – dynamic light scattering;

LDR – light intensity distribution reproduction;

SEI – second electron image;

MALS – multi angle light scattering;

UV – Ultraviolet detector;

SD – standard deviation;

RSD – relative standard deviation;

U – uncertainty;

B – relative accuracy bias;

LOD – limit of detection;

LOQ – limit of quantification;

MAD – maximum acceptable deviation;

REE – rare earth elements;

rG – gyration radii;

ar – aspect ratio.

General introduction

According to conventional definition, a nanoparticle is defined as a nano-object having its three external dimensions in the size range from about 1 to 100 nm [1]. However, from behavioural point of view, the sub-micrometric range (i.e. ≤ 1000 nm) has to be considered in order to account at once primary nanoparticles (NPs) and assemblies of nano-object [2]. Nanoparticles, which can have different origin (soil erosion, volcanic eruptions, dust storms, wildfires, etc.), are an intrinsic part of environmental compartments [2,3]. Environmental NPs have a potential risk for human health and ecosystems due to their ubiquity, specific characteristics and properties (extremely high mobility in the environment, abilities of accumulation of toxic elements and penetration in living organisms) and, hence, should be scrutinized.

The study of environmental NPs remains a challenge for analytical chemistry. In fact, NPs in a polydisperse environmental sample may represent only one thousandth or less of the bulk sample. Consequently, a considerable sample weight must be handled to separate amount of NP fraction sufficient for their dimensional and quantitative characterization. Moreover, there is the lack of unified analytical methodologies for recovering nanoparticulate fractions for their subsequent quantitative analysis [4,5]. Nowadays various techniques can be used for the separation of nanoparticles from environmental particulate samples. Environmental nanoparticles can be fractionated by membrane filtration, centrifugation, or field-flow fractionation (FFF) techniques. Due to their advantages (that will be discussed in detail in Chapter 1), the group of field-flow fractionation (FFF) techniques can serve as a basis for the development of unified methodology applicable to the study of environmental NPs.

This doctoral thesis focuses on the complementary use of asymmetrical flow and coiled tube field-flow fractionation techniques in the analysis of environmental particulate samples. Volcanic ashes from different regions of the world were taken as test samples. As compared, for example, to street dust, which has both anthropogenic and natural origin, volcanic ash is only from one source (volcanic eruption). The ash samples with particles size over a very wide range (from nanometre to millimetre) are characterized by an extremely low content of organic matter [6]. Therefore, volcanic ashes look to be appropriate “simple” samples for the comparative study of different separation methods and the development of a methodology for the recovery of nanoparticle fractions from polydisperse environmental solids. Furthermore, volcanic eruptions are one of the main sources of natural nanoparticles. During one eruption, more than 30 million tons of ash can be ejected to the height of tens of kilometers and reach the stratosphere, where volcanic ash

particles may spread worldwide and affect all areas of the Earth for years [7]. For example, it is known that airborne volcanic ash particles contribute to cooling of Earth surface due to ability of absorption and scatter solar radiation [8]. In addition, volcanic ash as a source of nutrient elements (e.g. iron and phosphorus) can increase bioproductivity of phytoplankton [9] and affect the global balance of CO_2 and hence climate change [10]. Along with nutrient elements, volcanic ash also contains toxic elements. Moreover, according to recent studies, particles of volcanic ash can accumulate toxic and potentially toxic elements; the concentration of these elements in NPs can be one or two order of magnitude higher than bulk ones [3,6].

The manuscript of doctoral thesis consists of three chapters. The first chapter is synthesis and assessment of bibliography concerning to the subject of the present study. It presents the examination of various approaches and techniques applied to the separation of environmental nanoparticles. Recent examples of studies on environmental nanoparticles of various origin for instance, dust, natural water colloids, and ashes, are also considered in this chapter.

The second chapter describes materials, reagents, techniques, and procedures which were used for the study of volcanic ash nanoparticles.

The third chapter considers results of the development of methodology based on the complementary use of asymmetrical flow and coiled tube field-flow fractionation techniques for the study of volcanic ash nanoparticles. Furthermore, the results related to the investigation of stability of environmental nanoparticles are also given. The new coiled tube field-flow fractionation procedure is proposed.

Finally, the general conclusion summarizes all the results obtained in the present study and describes possible perspectives.

The text of the present manuscript contains data of three articles published in international scientific journals and one submitted article. All the articles were prepared within the framework of this doctoral thesis. The list of articles is given in appendix.

Introduction générale

Selon la définition conventionnelle, une nanoparticule (NP) est un nano-objet ayant ses trois dimensions externes dans la plage de taille allant d'environ 1 à 100 nm [1]. Cependant, d'un point de vue comportemental, la gamme sub-micrométrique (c'est-à-dire inférieure ou égale à 1000 nm) doit être considérée pour tenir compte à la fois des nanoparticules primaires et des assemblages de nano-objets [2]. Les nanoparticules peuvent avoir différentes origines telles que l'érosion des sols, les éruptions volcaniques, les tempêtes de poussière, ou encore les feux de forêt. Elles font donc partie intégrante des compartiments environnementaux [2,3]. Les NP environnementales présentent un risque potentiel pour la santé humaine et les écosystèmes en raison de leur ubiquité, de leurs caractéristiques et de leurs propriétés spécifiques. Plus particulièrement les NP ont une mobilité extrêmement élevée dans l'environnement, une capacité à associer, voire à concentrer des éléments toxiques et à pénétrer dans les organismes vivants. Les nanoparticules doivent donc être considérées avec une attention particulière dans les études environnementales.

Néanmoins, l'étude des NP dans l'environnement demeure un défi pour la chimie analytique. En effet, les nanoparticules présentes dans un échantillon environnemental polydispersé peuvent représenter seulement un millième ou moins de la masse de l'échantillon global. Par conséquent, une masse d'échantillon considérable doit être manipulé pour séparer une quantité de nanoparticules suffisante pour leur caractérisation dimensionnelle et quantitative. De plus, il n'y a pas de méthodologie analytique unifiée pour récupérer différentes fractions nanoparticulaires en vue de leur analyse quantitative ultérieure [4,5]. De nos jours, diverses techniques peuvent être utilisées pour séparer les nanoparticules d'échantillons de particules environnementales. Les nanoparticules environnementales peuvent être fractionnées par des techniques de filtration sur membrane, de centrifugation ou de fractionnement flux−force (FFF). En raison de leurs avantages (qui seront examinés en détail au chapitre 1), l'ensemble des techniques de fractionnement par flux−force peut servir de base pour le développement d'une méthodologie unifiée applicable à l'étude des NP environnementales.

Cette thèse de doctorat porte sur l'utilisation complémentaire des techniques de fractionnement à flux asymétrique et à colonne tournante pour l'analyse d'échantillons de particules environnementales. Des cendres volcaniques de différentes régions du monde ont été prélevées afin de servir d'échantillons tests. Par rapport, par exemple, à la poussière de rue, qui a à la fois une origine anthropique et naturelle, les cendres volcaniques ne proviennent que d'une seule source (éruption volcanique). Les échantillons de cendres dont la taille des particules est très large (du nanomètre au millimètre) sont caractérisés par une teneur extrêmement faible en matière organique

[6]. Par conséquent, les cendres volcaniques peuvent être considérées des échantillons «simples» appropriés pour l'étude comparative des différentes méthodes de séparation et le développement d'une méthodologie pour la récupération de fractions de nanoparticules à partir de solides environnementaux polydispersés. De plus, les éruptions volcaniques sont l'une des principales sources de nanoparticules naturelles. Lors d'une éruption, plus de 30 millions de tonnes de cendres peuvent être éjectées à une hauteur de dizaines de kilomètres et atteindre la stratosphère, où les particules de cendres volcaniques peuvent se propager dans le monde entier et atteindre toutes les régions de la Terre pendant des années [7]. Par exemple, on sait que les particules de cendres volcaniques en suspension dans l'air contribuent au refroidissement de la surface de la Terre en raison de leur capacité d'absorption et de diffusion du rayonnement solaire [8]. De plus, les cendres volcaniques en tant que source d'éléments nutritifs (par exemple le fer et le phosphore) peuvent augmenter la bioproductivité du phytoplancton [9] et affecter l'équilibre global du CO_2 et donc le changement climatique [10]. Outre les éléments nutritifs, les cendres volcaniques contiennent également des éléments toxiques. Ainsi, selon des études récentes, les particules de cendre volcanique peuvent accumuler des éléments toxiques et potentiellement toxiques ; la concentration de ces éléments dans les nanoparticules peut alors être supérieure d'un ou deux ordres de grandeur à celle des éléments présents dans l'échantillon global [3,6].

Ce manuscrit de thèse de doctorat comprend trois chapitres. Le premier chapitre est une synthèse bibliographique concernant le sujet de la présente étude. Il examine les diverses approches et techniques appliquées à la séparation des nanoparticules environnementales. Des exemples récents d'études sont donnés concernant des nanoparticules de diverses origines, telles que des poussières, des colloïdes aquatiques naturels et des cendres.

Le deuxième chapitre décrit les matériaux, réactifs, techniques et procédures qui ont été utilisés pour l'étude des nanoparticules de cendres volcaniques.

Le troisième chapitre présente les résultats du développement méthodologique basée sur l'utilisation complémentaire des techniques de fractionnement à flux asymétrique et à colonne tournante pour l'étude des nanoparticules de cendres volcaniques. Complémentairement, la stabilité de ces nanoparticules y est abordée. Une nouvelle procédure de fractionnement en colonne tournante est également proposée.

Enfin, la conclusion générale reprend tous les principaux résultats obtenus et présente les perspectives possibles à cette étude.

Le texte du présent manuscrit contient les données de trois articles publiés dans des revues scientifiques internationales et d'un article soumis. Tous les articles ont été préparés dans le cadre de cette thèse de doctorat. La liste des articles est donnée en annexe.

Введение

Согласно общепринятому определению, наночастица – это объект, размер которого хотя бы в одном из измерении составляет от 1 до 100 нм [1]. Следует отметить, что частицы окружающей среды в нанометровом диапазоне обладают различной морфологией (наностержни, наносферы, нанопластины, нановолкна и др.) и могут образовывать скопления (агломераты), свойства и характеристики которых отличны от свойств и характеристик образующих их частиц [2]. В связи с вышеизложенным частицы и их скопления в субмикронном диапазоне размеров (≤ 1000 нм) тоже следует рассматривать с точки зрения изучения окружающей среды, чтобы при исследовании сложных полидисперсных образцов (например, пыль и пепел) были учтены их разнообразные составляющие и свойства, в том числе наночастицы и их скопления, параметры и свойства данных наночастиц и скоплений [2]. Наночастицы, которые имеют различные источники происхождения (эрозия почв, вулканические извержения, пылевые бури, лесные пожары и др.), являются неотъемлемой частью окружающей среды [2,3]. Наночастицы окружающей среды могут быть потенциально опасны для здоровья людей и состояния экосистем из-за своих характеристик и свойств (повышенная подвижность в окружающей среде, возможность аккумулировать токсичные элементы и проникать в живые организмы) и, следовательно, требуют тщательного изучения.

Исследование наночастиц осложнено их незначительным количеством в исходных полидисперсных образцах окружающей среды, которое обычно составляет сотые и в редких случаях десятые доли процентов. Кроме того, наночастицы должны быть выделены из исходных образцов в необходимом для их последующего изучения и анализа количестве. Кроме этого, в настоящее время отсутствует единый подход в выделению фракций наночастиц для их последующего количественного анализа [4,5]. Различные методы можно использовать для выделения наночастиц из полидисперсных образцов окружающей среды. Наночастиц окружающей среды могут быть выделены методами мембранной фильтрации, седиментации и проточного фракционирования в поперечном силовом поле (ПФП). Благодаря своим преимуществам, которые будут подробно описаны в первой главе, группа методов ПФП может послужить основой для создание единого подхода, применяемого к изучению наночастиц окружающей среды.

Настоящая докторская работа направлена на развитие подхода, основанного на взаимодополняющем применение методов асимметричного проточного фракционирования

с поперечным потоком и фракционирования частиц во вращающейся спиральной колонке при исследовании полидисперсных образцов окружающей среды. Вулканический пепел, отобранный в разных региона мира, изучали в настоящей работе. вулканический пепел может быть «удобным» образцом для разработки методологии исследования наночастиц окружающей среды из-за его относительно однородной минеральной структуры. По сравнению с частицами городской пыли, которые имеют как естественные, так и антропогенные источники происхождения, частицы пепла образуются только в результате вулканической активности. Образцы вулканического пепла содержат частицы с широким диапазоном размеров от нанометра до миллиметра и характеризуются низким содержанием органического вещества [6]. В дополнение к изложенному следует отметить, что извержения вулканов являются одним из основных источников образования природных наночастиц. Во время одного извержения более 30 миллионов тонн пепла могут выбрасываться на высоту десятков километров и достигать стратосферы. Частицы вулканического пепла в нанометровом диапазоне размеров могут распространятся по всему миру и являться причиной негативного воздействия на многие регионы Земли в течение многих лет [7]. Наночастицы вулканического пепла, находящиеся в атмосфере, изменяют температурный режим планеты, рассеивая и поглощая длинные и короткие волны солнечной радиации [8]. Питательные элементы (железо и фосфор), содержащиеся в наночастицах вулканического пепла, увеличивают биопродуктивность фитопланктона, что приводит к изменениям в биогеохимических процессах в мировом океане [9] и оказывает влияние на мировой баланс CO_2 и, следовательно, изменяет климат [10]. Наночастицы вулканического пепла могут концентрировать на своей поверхности токсичные элементы и вещества [14,15,91]. Следует отметить, что содержание токсичных элементов в данных наночастицах может быть на порядок и более выше, чем в микрочастицах пепла [14,15]. Таким образом, наночастицы вулканического пепла могут быть потенциально опасны для экосистем и здоровья людей в локальном и мировом масштабах. Вместе с питательными веществами, наночастицы также могут содержать токсичные элементы; содержание токсичных элементов в данных наночастицах может быть на порядок и более выше, чем в микрочастицах пепла [3,6].

Текст докторской диссертации состоит из трёх глав. В первой главе проведён обзор литературы, соответствующей предмету настоящего исследования. В данной главе представлены различные подходы и методы, применяемые для разделения полидисперсных образцов окружающей среды. Кроме этого, в данной главе также приведены примеры

современных исследований наночастиц окружающей среды, имеющих различные источники образования, например, пыль, естественные водные коллоиды и пепел.

Вторая глава описывает материалы, реактивы, методы и методики, используемые в настоящем исследовании наночастиц вулканического пепла.

Третья глава содержит результаты развития методологии, основанной на взаимодополняющем применении метода ассиметричного проточного фракционирования с поперечным потоком и фракционирование частиц во вращающейся спиральной колонке. Кроме этого, в третьей главе приведены результаты исследования стабильности суспензий наночастиц окружающей среды. Новая методика фракционирования частиц во вращающейся спиральной колонке была также предложена в настоящей главе.

Заключение содержит описание всех полученный результатов в настоящей работе и возможные перспективы развития настоящего исследования.

Текст диссертационной работы содержит информацию, изложенную в трёх опубликованных в международных научных журнал статьях и в одной статье, которая была направлена в редакцию. Все перечисленные статьи сделаны в рамках настоящей докторской работы. Список статей приведён в приложение.

Chapter 1 State of the art

1.1 Introduction

The characterization of particles over a size range of less than 100 μm remains a challenge in field of environmental studies [3,11–17]. Such characterization is all the more important since most physical and chemical properties of these objects are linked to their size [3,11]. Therefore, determining the characteristics of polydisperse sample as a function of size and obtaining the associated size distributions are needed for a comprehensive investigation. Among the different analytical strategies for obtaining this information, the size fractionation of the sample under study is an attractive way of investigation.

Nowadays various techniques can used for the fractionation of (sub) micron-sized objects. Analytes with size 1-100 μm can be fractionated by membrane filtration, field-flow fractionation (FFF), split flow thin cell fractionation (SPLITT), sedimentation, or centrifugation. Analytes with size less than 1 μm can be fractionated by capillary electrophoresis, gel chromatography, membrane filtration, centrifugation, or FFF [18–21]. Among this set of techniques, on line separation is the most efficient; and among on line separation techniques, only FFF enables analytes to be fractionated over the nano- and micrometric size ranges.

FFF is a rapidly elaborating family of techniques, with increased selectivity, sensitivity, resolution and wide applications. The concept of FFF was proposed by J.C. Giddings in 1960s [22]. Analytes of very varied nature such as biological cells, particles, and/or macromolecules can be fractionated on the basis of their physical and/or chemical characteristics in a carrier liquid which can also be of varied nature, typically aqueous or organic. Unlike chromatography FFF does not require a stationary phase, which minimizes sample breakthrough effects or the analytes or their interactions with the stationary phase. The separation is performed in a thin (0.05-0.5 mm) ribbon-like channel under the action of a physical force applied at a right angle to the channel and owing the non-uniform flow velocity profile of a carrier liquid. FFF enables analytes from 1 nm to 100 μm to be fractionated with a higher resolution than offline techniques and most online techniques [18,23,24]. The group of FFF techniques can be divided into sub-techniques according to the nature of the applied force field, which can be hydrodynamic, gravitational, thermal, magnetic, acoustic, electrical, etc. Flow FFF (FlFFF) can be considered as the most versatile FFF subtechnique; it employs a nonspecific hydrodynamic force across the channel [18,23]. In turn, sedimentation FFF (SdFFF) employs a centrifugal force field to fractionate analytes in a wide size

range, from approximately some tens nanometers up to some hundreds micrometers [12,24–26]. Moreover, as compared to other FFF subtechniques including asymmetrical flow FFF (A4F), the advantage of SdFFF is absence of membrane, which is an integral part of A4F technique; there are no interactions between membrane material and particles to be separated in SdFFF.

Nevertheless, it should be noted that FFF has an important limitation, namely, the mass of injected sample, which should not exceed 1 mg to avoid overloading the system. Therefore, FFF is mainly used in analytical couplings with sufficiently sensitive detectors and not as a preparative tool. In addition, since the separation performance is strongly related to the quantity injected, the sample preparation and in particular homogenization prior separation is essential in order to provide representative results [4,18].

The fractionation in a rotating coiled column (RCC) can also be attributed to FFF family, and also using a centrifugal force field. This non-conventional SdFFF technique is called coiled tube FFF (CTFFF).[27] One of its interests is that the mass of the loaded sample introduced in a long column can be increased up to at least 1 g (see details in the next part). The method was applied to samples of soil, street dust and volcanic ash, for which the particles were sorted into different size fractions [6,28–30].

Split flow thin cell fractionation technique should be also mentioned since it is similar to FFF[18,31] and can also employ gravitational or centrifugal force field [32–35]. In addition to the gravitational and centrifugal fields, magnetic [36] and electric [37] force fields may be used for SPLITT fractionation. Like in CTFFF, large amounts of sample (up to gram level) can be fractionated using SPLITT technique. However, during one experimental run SPLITT technique is capable to recover only two fractions (e.g. particles with size <10 and >10 μm). Therefore, for the separation of more than two fractions, the use of multi-stage procedures is required [18,31].

The present chapter mainly focuses on the recent advances in theory and applications of A4F, sedimentation FFF in thin channels and rotating coiled columns. SPLITT technique is also considered. The four types of methods are compared and critically evaluated. The promising directions for the further development of the methods are also discussed.

1.2 Theoretical background and instrumentation

1.2.1 Sedimentation field-flow fractionation

In the SdFFF, the fractionation is performed in a circular flat channel inserted inside a centrifugal basket (Fig. 1). For this method, which employs flat channels with volumes of about a few millilitres and laminar flows, the theory is relatively well developed.[23,38] Firstly, the behaviour of analytes can be explained in a simple and general way, without taking into account the type of force applied, and in the case of hard spherical particles. In normal mode, the force induced by the field applied perpendicularly to the flow initially leads to the accumulation of particle on the channel wall (named accumulation wall). This generates an opposing diffusive force, which gives the particle its position at a certain height above the wall. Since the flow has parabolic velocity profile, this position leads the particle to acquire a specific longitudinal velocity. Therefore, a retention time that can be expressed by:

$$t_R = \frac{<v>t_0}{<U_z>}, \quad (1)$$

where $< v >$ is the average velocity of the mobile phase in the section of the channel, t_0 is the void time and $< U_z >$is the average longitudinal velocity of the particles injected.

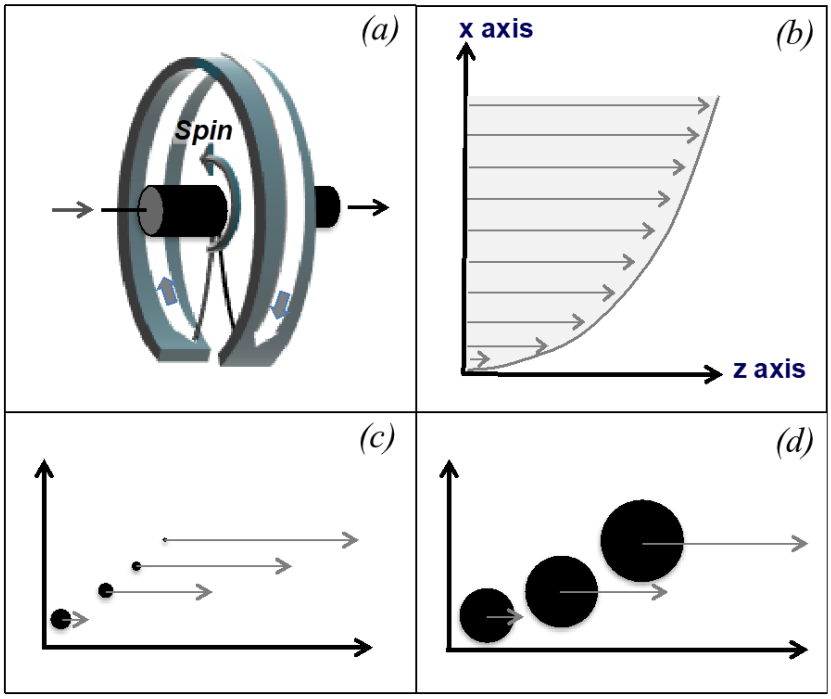

Figure 1. Schematic formalization of (a) SdFFF instrumentation, (b) parabolic flow of the mobile phase in the channel, and (c) normal and (d) steric modes of elution in FFF; x: transverse axis; z: longitudinal axis

The average longitudinal velocity depends on the longitudinal velocity in each point x of the channel height (due to the laminar flow), the particle concentration at the point x (described on the basis of Fick's second law and Maxwell-Boltzmann distribution), and the particle distribution in the channel height, which lead to:

$$< U_z >= -6 < v > \frac{D}{WU_x}\left[\frac{e^{\frac{-wU_x}{D}}+1}{e^{\frac{-wU_x}{D}}-1}+\frac{2D}{wU_x}\right], \quad (2)$$

where D is the diffusion coefficient, w is the channel height, U_x is the particle transverse velocity (in the channel height). By replacing (2) in (1), the retention time in normal mode can be generally expressed as:

$$t_R = \frac{t_0}{6\frac{D}{WU_x}\left[\frac{1+e^{\frac{wU_x}{D}}}{1-e^{\frac{wU_x}{D}}}-\frac{2D}{wU_x}\right]} \quad (3)$$

The transverse velocity can be expressed specifically according to the nature of the force applied. Thus, in SdFFF,

$$< U_x >= \frac{VD}{kT}(\rho' - \rho)g, \quad (4)$$

where ρ' is the particle density, ρ is the mobile phase density, V is the particle volume, g is the centrifugal acceleration, k is the Boltzmann' constant and T is the temperature. The retention time in normal mode can be then specifically expressed as:

$$t_R = \frac{t_0}{6\frac{kT}{wV(\rho'-\rho)g}\left\{coth\left[\frac{wV(\rho'-\rho)g}{2kT}\right] - \frac{2kT}{wV(\rho'-\rho)g}\right\}} \quad (5)$$

When there is a significant retention of the particles, the terms in parenthesis in the equations (3) and (5) tends to 1. In addition, the amount $V(\rho' - \rho)g$ is defined as the effective mass, noted m_e (the second part of this expression, $V\rho g$, corresponding to the buoyant mass). Then, equation (5) can be simplified, and re-written as follows:

$$m_e = \frac{6kT}{t_0 wg} t_R \quad (6)$$

This expression is more useful in analytical sciences since the effective mass can be deduced from the measurement of the retention time. Taking into account the analyte as a population of hard spherical particles, V can be expressed according to the particle radius (r_p); with the same simplification and rewriting concerning equation (5), one can obtained:

$$t_R = \frac{2\pi w(\rho'-\rho)gt_0}{9kT} r_p^3 \quad (7)$$

This equation illustrates the strong dependence of retention time on size (as a cubic function of the radius), and also on density of the analyte.

In steric mode, the diffusive force opposing the force induced by the applied field is relatively weak as compared to the repulsive and/or lift forces. Therefore, the position of the particle in the height of the channel, i.e. its distance from the accumulation wall, depends mainly on the size of the particle (or its radius in the case of a sphere). The expression of the retention time can be obtained from equation (3) according to:

$$t_R = \frac{t_0}{6(a-a^2)+6\frac{D}{wU_x}(1-2a)\left[\frac{1+e^{\frac{-wU_x}{D}(1-2a)}}{1-e^{\frac{-wU_x}{D}(1-2a)}}-\frac{2D}{(1-2a)wU_x}\right]} \quad (8)$$

where a is the ratio between the particle radius and the channel height (r_p/w).

Specifically to SdFFF, and also expressing the volume V according to the radius of a spherical particle, equation (8) can be rewritten as:

$$t_R = \frac{t_0}{6(a-a^2)+9\frac{kT}{2w\pi r_p^3(\rho'-\rho)g}(1-2a)\left\{coth\left[\frac{2w\pi r_p^3(\rho'-\rho)g}{3\mathrm{kT}}(1-2a)\right]-\frac{3kT}{2(1-2a)w\pi r_p^3(\rho'-\rho)g}\right\}} \quad (9)$$

This expression also shows that in steric mode, as in normal mode, the retention time strongly depends on the size of the analyte, and also on its density.

1.2.2 Flow field-flow fractionation

It has been already mentioned that flow field flow fractionation is the most versatile subtechnique employing the cross-flow as the external force field. This technique provides a nonspecific hydrodynamic force field along the channel formed by a secondary mobile phase, namely, cross-flow. The particles under separation are migrated by the cross-flow toward the surface of accumulation channel (permeable membrane). The separation is based on the difference in diffusion coefficients which are corresponded to the positions of individual species in the laminar carrier fluid profile. The type of utilization membrane depends on the properties of particles to be separated. The application of flat and smooth membranes is required because any membrane flaws would have impact on separation process. Regenerated cellulose is widely used material for FlFFF membranes. Separation by FlFFF is on the basis of the of the particles effective size, and separation is independent of density. In case of SdFFF, the separation is provided depended on size and density [18,23,39]. Two different types of FlFFF can be highlighted: asymmetric and symmetric flow FFF (Fig. 2).

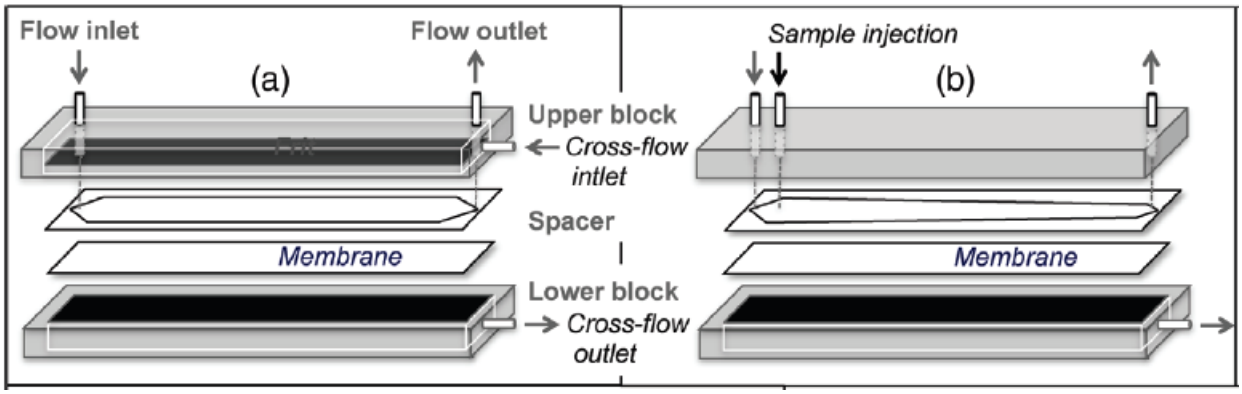

Figure 2. Schematic view of symmetric (a) and asymmetric (b) flow field-flow fractionation.

In the case of symmetrical FlFFF, the carrier fluid is pumped directly across the channel thought porous frits and formed the cross-flow. Both walls of the channel are permeable, but ultrafiltration membrane impermeable to the analytes covers the accumulation wall [40]. Symmetrical FFF can be applied to separation of samples with various nature such as viruses, dissolved organic matter, colloids, manufactured nanoparticles etc. [18,23,41–43].

In asymmetric FlFFF (also called A4F), the most commonly used FlFFF type, only one channel wall (accumulation wall) is permeable for carrier-fluid, which passing through it formed cross-flow. The channel in A4F technique has a trapezoid shape to avoid losses of axial flow of carrier fluid across the channel [44]. Separation efficiency in A4F significantly depends on the channel geometry [18,23,45]. This technique has widely field of application in characterization of environmental as well as biological and technological samples. It also can be used for the characterization of PSD of PM under study [46–54].

The theory of FlFFF technique has been described in detail in various papers [23,45,55,56]. Therefore, in the present work it is given briefly. The transverse velocity can be expressed in FlFFF can be express as follows[23]:

$$< U_x >= \frac{Q_c}{V_0} w, \tag{10}$$

where Q_c is the cross-flow rate, V_0 is the void volume.

The retention time in normal mode is given as follows [23]:

$$t_R = \frac{t_0}{6\frac{DV_0}{w^2Q_c}\left\{coth\left[\frac{w^2Q_c}{2DV_0}\right]-\frac{2DV_0}{w^2Q_c}\right\}} \quad (11)$$

Retention time in steric mode is expressed as follows [23]:

$$t_R = \frac{t_0}{6(a-a^2)+6\frac{DV_0}{w^2Q_c}(1-2a)\left\{coth\left[\frac{w^2Q_c}{2DV_0}(1-2a)\right]-\frac{2DV_0}{(1-2a)w^2Q_c}\right\}} \quad (12)$$

A4F technique has become highly demanded compared to symmetric flow FFF in environmental studies which are discussed below.

1.2.3 Coiled tube field-flow fractionation

CTFFF can be attributed to the family of FFF techniques as a variation of conventional SdFFF (the latter simply being called SdFFF, thus differentiating from the CTFFF below). Unlike SdFFF, the separation channel in CTFFF is coiled onto the drum of a planetary centrifuge. The coiled column (bobbin) rotates around its axis and at the same time revolves around the central axis of the centrifuge with the aid of a planetary gear. The axes of rotation and revolution are parallel (Fig. 3). It should be noted that planetary centrifuges have been widely applied to countercurrent chromatography[57] As compared to SdFFF, the separation process in CTFFF has two significant differences. Firstly, the sample to be fractionated is not injected into a thin channel but is pumped with the carrier flow through a long rotating coiled tube (inner capacity of common analytical column is about 20-25 mL). Secondly, the separation in CTFFF occurs under the action of the complex asymmetrical force field generated by the planetary centrifugal motion [18,58]. Hence, the behaviour of particles is much more complicated than in the channel for conventional SdFFF.

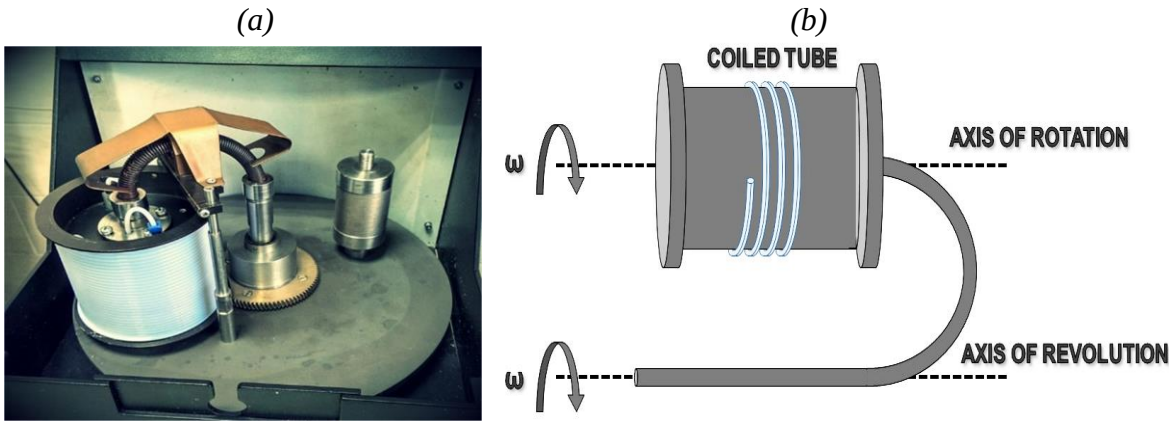

Figure 3. The planetary centrifugal motion for CTFFF. Photo of the instrument *(a)* and principal scheme *(b)*.

For the first time the uneven distribution of polymer particles of different sizes in rotating coiled columns was observed by Y. Ito in 1960s.[59] However, the studies on particle separation by CTFFF were continued only in early 2000s by P. Fedotov.[60] The behaviour of particles of different nature and size in CTFFF under controlled operating conditions was systematically studied.[58,61] The particles were fractionated at a constant rotation speed of the column and stepwise increasing of the flow rate of the carrier liquid. As a theoretical background, two hypothetical modes of the motion of particles in rotating coiled columns were suggested: migration of the particles in the mobile phase (carrier liquid) flow and migration of particles along the column walls.[58,61] After the suspended particles are injected into the column, they began to migrate in the carrier liquid flow and the distance covered by a particle before the sedimentation of the column wall can be expressed as follows [61]:

$$L_s = U_w t_s \approx \left[v - K_v \frac{R^2 \omega^2 r_p^4 \Delta\rho^2}{2\pi r \eta^2}\right] \frac{d\eta}{r\omega^2 r_p^2 \Delta\rho}, \qquad (13)$$

where U_w is the speed of a particle relative to the tube walls, v is the linear velocity of the carrier liquid, t_s is the time needed for the sedimentation of a particle, K_v is the shape-dependent coefficient, R is the revolution radius, r is the column rotation radius, ω is the column rotational speed, $\Delta\rho$ is the difference in density between particles and mobile phase ($\rho' - \rho$), η is the dynamic viscosity of the mobile phase; d is the inner diameter of the tube.

If the distance covered by a particle before the sedimentation of the column wall is greater than the length of the column, this particle is not retained. The retained particles are distributed along the column wall depending on their radii and other parameters given in Eq. 10. These particles can further migrate along the column walls if the sum of Archimedean (buoyancy, F_A) and hydrodynamic (F_{hyd}) forces is greater than the force of mechanical interaction of particles (F_{mech}) with column material (the force "retaining" particles on the walls) [61]:

$$F_a + F_{hyd} > F_{mech} \quad (14)$$

This expression can be transformed[61]:

$$v\eta > Kr\omega^2 \Delta\rho r_p^n \quad (15)$$

where K is a constant, $n = {}^1/_2 \div 1$ (depending of the shape of particles and/or the smoothness of the column walls).

Theoretical and experimental dependencies of the critical linear velocity of the carrier liquid flow, which is needed for the migration of particles along the column walls, on the particle radius are in agreement [58,61]. This has been demonstrated for the fractionation of reference sample of quartz sand BCR-70 and mixture of silica samples Silasorb-300 and Silasorb-600 at stepwise increasing of the flow rate of the carrier liquid.[58]

On the basis of theoretical modeling it was suggested that modification of geometry of column drum could enable submicron and nanoparticles to be fractionated without a significant increase in the column rotation speed. A conical column and a cylindrical column with two symmetrical protrusions were designed, fabricated, and tested using a series of synthetic and natural samples.[58] However, significant retention of submicron particles was not observed, while the increase in resolution was demonstrated. Taking as example the fractionation of silica standards (150, 390, and 900 nm), it has been shown that the purity of three fractions separated in the cylindrical column with two symmetrical protrusions is 87–98% whereas the fractions separated in the conventional cylindrical column contain only 70–84% of the target particles.[58] In general, despite the insufficiently developed theory, CTFFF has given rise to a series of interesting and promising applications.

1.2.4 Split flow thin cell fractionation

The idea of particle fractionation across in a SPLITT channel came from J. Giddings [31]. Ordinary SPLITT channel is equipped by stream splitters. Thus, the SPLITT system has two inlets at one side of the channel and two outlets at the other side. The fractionation is performed under the combined action of a gravitational force field and flow rates. The sample to be separated is usually introduced into the upper inlet as continuous flow. The injected sample forms a thin layer along the upper wall of the channel; the thickness of this layer is equal to the distance between the upper channel wall and inlet splitting plane. Close to outlets of channel is the outlet plane; its position depends on the ratio of the upper and lower flow rates [18].

The schematic illustration of SPLITT technique is shown in Fig. 4. The theory of SPLITT technique has been described in details in various papers [32,62–64]. In general, the separation of particles in SPLITT system is governed by Stokes' law. The retention time that correspond to the time required for particles migrating to traverse the transport region of thickness can be expressed as follows:

$$t_R = \frac{18w\eta}{\Delta\rho g d_p^2}, \tag{16}$$

where w is the thickness of SPLITT cell, η is the viscosity of the mobile phase, $\Delta\rho$ is the difference in density between particles and mobile phase, g is the centrifugal acceleration, and d_p is the diameter of particle.

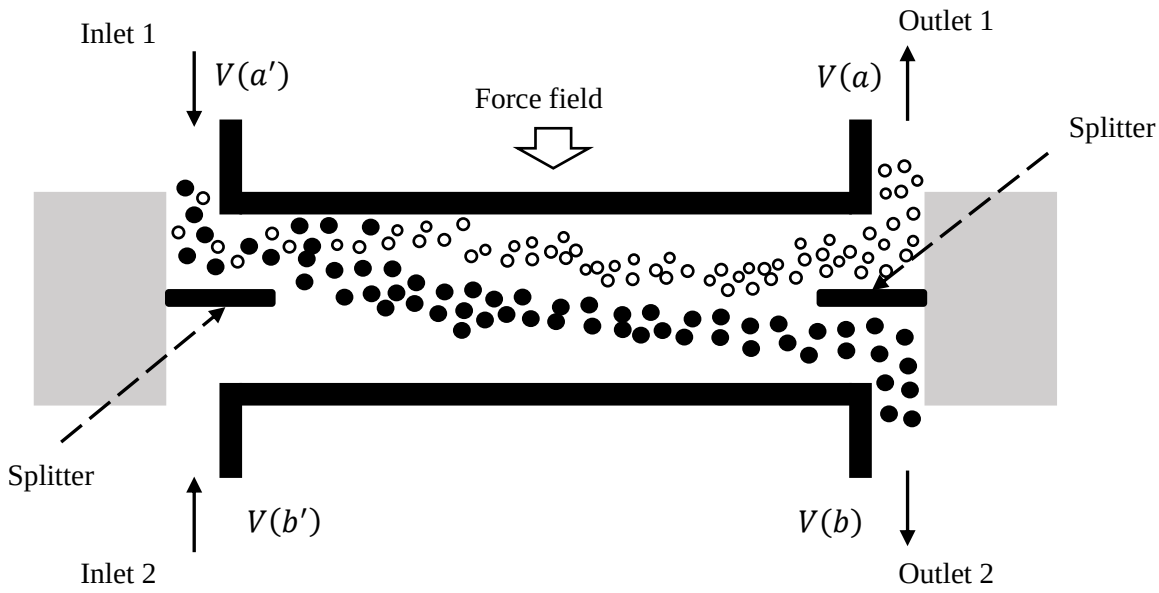

Figure 4. Schematic view of SPLITT channel

In turn, in the case of conventional SPLITT fractionation (CSF) mode, when two inlets (inlets 1 and 2) are used, the volumetric flow rate $V(t)$ coursing through the transport region between the two splitting planes can be expressed in either of two forms.

$$V(t) = V(a) - V(a') = V(b') - V(b), \tag{17}$$

where $V(a')$ and $V(b')$ are volumetric flow rates entering inlets 1 and 2, respectively, while $V(a)$ and $V(b)$ are volumetric flow rates exiting outlets 1 and 2.

In the case of using only inlet 1 (full feed depletion SPLITT fractionation (FFDSF) mode), it becomes [65–67]:

$$V(t) = V(a') - V(b) \tag{18}$$

Generally, the expression of the volumetric flow rate ΔV can be given as follows:

$$\Delta V = \frac{bLg\Delta\rho d_p^2}{18\eta}, \tag{19}$$

where b and L are the breadth and length of the SPLITT cell, respectively (and, therefore, bL is the working area of the cell in the plane perpendicular to the field). All particles will exit from the outlet 2 when:

$$\Delta V > V(t) \tag{20}$$

The fractionation retrieval parameter F_2, which corresponds to the separation efficiency at outlet 2 (fig. 4) for CSF mode, can be given as follows[64]:

$$F_2 = \frac{\Delta V - V(t)}{V(a')} \tag{21}$$

In FFDSF mode it will be

$$F_2 = \frac{\Delta V - V(t)}{V(b)} \tag{22}$$

Depending on study [32,37,64,68–72] the cut-off diameter (d_c) can be considered as the diameter at which 50% or 100% of the particles of a mixture to be separated exit outlet 2 (fig. 4) and, thus, F_2 equals 0.5 or 1, respectively. Therefore, for CSF, the cut-off diameter can be calculated by substituted $F_2 = 0.5$, eq. 14, and 16 in eq. 18 and expressed as follows:

$$d_c = \sqrt{\frac{18\eta[V(a) - 0.5\,V(a')]}{bLg\Delta\rho}} \tag{23}$$

In the case of using $F_2 = 1$, the eq. 20 is modified into

$$d_c = \sqrt{\frac{18\eta[V(a) - V(a')]}{bLg\Delta\rho}} \tag{24}$$

In turn, for FFDSF mode, the cut-off diameter can be expressed depending on the values of F_2 (0.5 or 1) as follows:

$$d_c = \sqrt{\frac{18\eta[V(a') - 0.5\,V(b)]}{bLg\Delta\rho}} \tag{25}$$

or

$$d_c = \sqrt{\frac{18\eta[V(a') - V(b)]}{bLg\Delta\rho}} \tag{26}$$

The SPLITT technique has a niche application in environmental studies.

1.3 Applications to environmental studies

SdFFF, A4F, CTFFF, and SPLITT techniques have been used for fractionation and characterization of complex polydisperse environmental. The main information relative to the applications of SdFFF, A4F, CTFFF, and SPLITT is summarized in Tables 1, 2, 3, and 4, respectively

The fate in the environment, and health effects of nano- and microparticles strongly depend on their size and chemical composition [2,3]. The investigation of nano- and microparticles depending on their size is directly related to their separation from polydisperse environmental samples. In this sense, separation techniques play a crucial role in the study of size-dependent properties of particles in the environment.

Particle size distribution (PSD) is an important characteristic of environmental particulate matter. SdFFF, due to advanced theoretical background, can be used as a tool not only for fractionation of particles, but also for the determination of PSD of environmental samples. For example, SdFFF enabled PSD of fly ash particles (<44 μm) emitted from coal thermo-electric power stations[26] as well as dust particles (10-50 μm) [73] to be characterized. In addition, the size distribution of various elements can be determined by offline or online associating SdFFF with an elemental analysis technique. Offline association involved inductively coupled plasma-atomic emission spectrometry (ICP-AES) for the determination of various elements such as Cu, Zn, Fe, Mn, or, more specifically, cold vapour electrothermal atomic absorption spectroscopy (CV-ETAAS) for the study of mercury. The use of SdFFF associated offline with ICP-AES or CV-ETAAS enabled element size distribution in size fractions less than 2 μm including several submicron fractions to be established.[26,73–75] In clay materials, different fractions starting from 60 nm were investigated; such an approach led to better understanding clay properties such as charge, swelling, delamination, and chemical composition depending on size [75]. Online association of SdFFF with elemental analysis technique was also reported. In environmental studies, such coupling preferentially involved inductively coupled plasma-mass spectrometry (ICP-MS) due to its higher sensitivity. As a typical example, engineered TiO_2 nanoparticles were determined in both sea and lake waters [76]. Such study demonstrates that SdFFF-ICP-MS can be considered as a relevant tool for the monitoring of engineered NPs in natural waters, which is challenging due to very low

analyte concentrations in matrices containing many various dissolved and colloidal species possibly in high concentrations.

The A4F as the most popular type of flow field-flow fractionation techniques has wide field of application in characterization of environmental samples. The transport of arsenic [77,78], uranium [79], and phosphorus [80] by soil colloids as well as transport of phosphorus by river colloids [81] have been investigated using offline and online coupling of A4F and ICP-MS techniques. The online coupling of A4F with ICP-MS can be served as reliable tool for the characterization of environmental colloids in natural [81–85] and drinking [86] water. In addition, this approach was successfully used in the study of polymer-coated quantum dots (CdSe/ZnS and Ag_2S) in environmental media such as soils and natural waters for understanding their behaviour and prediction of their fate in the environment [51,87,88]. Moreover, in recent studies [89–98] it has been demonstrated the efficiency of relatively new approach based on coupling of A4F and ICP-MS in single particle mode (sp-ICP-MS) applied to the study of engineered and natural nanoparticles. For instance, the Ag [89–93], modified Ag [94,95], Au [96,97] and natural [98] NPs were detected and characterized by the both online and offline coupling of A4F and sp-ICP-MS.

Despite the advantages of SdFFF and A4F, especially in terms of selectivity and fractionation power, there is a limitation, which is related to the weight of handling sample to be separated. Indeed, to avoid overloading of the system, usually mass of the particulate matter does not exceed 10-20 μg, while volume of suspension is less than 100 μL [26,73–76]. This limitation impedes the quantitative or exhaustive offline analysis of separated fractions, especially the determination of trace elements. Moreover, the number of elements determined online can be limited due to the significant dilution induced by the SdFFF as well as the elution process and therefore the continuous introduction of the fractionated particles into the ICP-MS detector. Besides, taking into account the negligible relative content of NPs (about 0.1% or less) and the high polydispersity of the bulk sample, NP detection and characterization can be impossible without a preparation step. Typically this step aims to selectively recover the particles of interest and hence concentrate these particles and narrow down the initial particle size distribution of the bulk sample.

Table 1. Selected applications of "conventional" sedimentation field-flow fractionation in a thin channel

Sample Type	Sample description	Main objectives	Parameters of injection of the sample	Size	Methods of characterization and analysis of separated fractions	Reference
Environmental particulate matter	Clay	Determination of swelling and delamination properties of clay particles of different size	Volume: 100 µL	Two fractions with mean particle size 60 and 250 nm	ICP-AES (offline)	[75]
	Fly ash (<44 µm)	Characterization of particle size distribution	Volume: 20-100 µL	<10.3 and 10.3-44 µm	ICP-AES (offline)	[26]
	Soil (<2 µm)	Characterization of the colloidal Hg-bearing fractions	Weight of particles: 10 µg; Sample volume: 10 µL	Five fractions in the range <2 µm	CV-ETAAS (offline)	[74]
	Dust (<53 µm)	Characterization of particles size distribution	Volume: 20-40 µL	10-50 µm	UV (online)	[73]
Engineered nanoparticles	TiO_2 nanoparticles	Separation and detection of TiO_2 NPs in natural waters	-	Aggregated/agglomerated fractions with size 250 and 150 nm	MALS-ICP-MS (online)	[76]

Table 2 Selected applications of asymmetric field-flow fractionation in a thin channel

Sample type	Sample description	Main objectives	Parameters of injection of the sample	Size, nm	Methods of characterization and analysis of separated fractions	References
Soil	Soil colloids (< 0.45 μm)	Study of aggregate formation of soil colloids	Volume: 100 μL	< 450	UV, ICP-MS, organic carbon detector (online), LD (offline)	[99]
		Study of uranium transport by soil colloids	Volume: 100 μL	< 450	UV, MALS, ICP-MS (online)	[79]
		Study of phosphorus transport by soil colloids	Volume: 100 μL	< 450	UV, organic carbon detector, ICP-MS (online)	[80]
	Soil colloids (< 0.2 and < 1 μm)	Study of arsenic transport by soil colloids	Volume: 100 μL	< 1000	UV, ICP-MS (online), X-ray absorption spectroscopy (offline)	[77,78]
Colloids	Colloids in river water (< 0.45 μm)	Characterization of colloids	Volume: 500 μL	< 450	UV (online), ICP-MS (offline)	[82]
	Colloids in river water (< 1.2 μm)	The study of phosphorous transport by natural colloids	Volume: 100 μL	< 450	UV, ICP-MS (online)	[81]
	Colloids in river water (< 5 μm)	Characterization of colloids	Not indicated	< 200, 200-5000	UV, organic carbon detector, ICP-MS (online)	[83,84]
	Colloids in groundwater (< 0.45 μm)	Characterization of colloids	Not indicated	< 450	UV, ICP-MS (online)	[85]
	Colloids in drinking water	Characterization of colloids	Volume: 1 mL (with pre-concentration in FFF channel)	< 450	UV, ICP-MS (online), SEM, DLS (offline)	[86]

Gas condensates	Natural nanoparticles from gas condensates	Characterization of natural NPs	Volume: 50 µL	< 1000	UV, MALS, ICP-MS (online), TEM-EDS, sp-ICP-MS (offline)	[98]
Engineered nanoparticels	Ag NPs (mean size 20, 30, 40, 50, 60, 70, 80, 100, and 200 nm) in aquatic suspensions	Detection, quantification, and characterization of Ag NPs	Volume: 20 and 50 µL	< 200	UV, MALS, ICP-MS (online), sp-ICP-MS, ICP-MS, TEM-EDS, DLS, (offline)	[89–92]
	Ag NPs (40, 60, 80, and 100 nm) in aquatic suspensions	Characterization of Ag NPs	Volume: 20 µL	< 120	UV, ICP-MS, sp-ICP-MS (online), TEM (offline)	[93]
	Modified Ag nanoparticles (20, 50, and 75 nm)	Characterization of Ag NPs	Volume: 20 µL	< 140	UV, MALS, ICP-MS (online), sp-ICP-MS (offline)	[94,95]
	Au NPs (10, 30, and 60 nm) in soil and sediment extract matrices	Characterization of Au NPs	Volume: 100 µL	< 1000	UV, MALS (online), DLS, ICP-MS, sp-ICP-MS (offline)	[96,97]
	Quantum dots CdSe/ZnS (< 10 nm) in soils	Study behaviour of CdSe/ZnS in soils	Volume: 50 µL	< 100	UV, MALS, ICP-MS (online), TEM-EDS (offline)	[51]
	Quantum dots Ag_2S and CdSe/ZnS in aqua solutions	Characterization of QDs	Volume: 20 µL	< 220	UV, MALS, ICP-MS (online), X-Ray diffrection, TEM-EDS (offline)	[87,88]

CTFFF due to the high capacity of the rotating column enables the mass of handling sample to be increased up to at least 1 g. This enables additional pre-separation steps to be avoided, because samples with wide particle size distribution can be directly injected into the rotating column. This opens possibilities for the separation of bulk sample followed by isolation of weight amounts of nano-, submicro-, and microparticle fractions for further characterization and quantitative analysis. Thus, CTFFF was applied to the fractionation and analysis of a series of particulate samples of natural origin and/or environmental interest including soil, volcanic ash and urban dust.[6,28–30,100–104] Size fractions ranging from less than 0.2 μm up to 100 μm were separated from bulk samples. Then, these fractions could be either digested for exhaustive elemental determination by ICP-AES and/or ICP-MS, or characterized in size, shape and elemental composition using scanning electron microscopy (SEM) with energy dispersive X-ray spectroscopy (EDS), laser diffraction (LD) or dynamic light scattering (DLS). In addition, speciation analysis could be also performed in the size fractions by sequential chemical extraction of elements.[104] Such a CTFFF-based approach enabled uneven distribution of toxic elements between size fractions to be obtained. This investigation strategy also highlighted that the concentration of toxic elements increased with decreasing particle size, the accumulation of elements being related to their sorption onto particle surface. For example, the concentrations of some toxic metals and metalloids (As, Se, Te, Hg, Tl, Bi) in volcanic ash nanoparticles were hundred fold higher than in bulk samples. Since nanoparticles of volcanic ash can serve as a carrier for the toxic elements on the global scale, these results is of particular importance.[6,102,103]

Despite the abovementioned advantages, the CTFFF separation efficiency remains lower than that of SdFFF and A4F. In addition, coupling CTFFF with different detectors (such as multi-angle light scattering (MALS), ICP-MS) has not been yet reported. It should be noted that in the case of environmental studies, the flow rates applied in CTFFF technique for recovery of nanoparticles usually vary from 0.2 to 0.4 mL/min depending on samples under study. Due to optimal flow rate in MALS, which typically equals up to 1 mL/min, the coupling of CTFFF and MALS is complicated. However, CTFFF, SdFFF, and A4F separation techniques are intrinsically complementary. This means the injection of a large quantity of sample and separation over a wide size range by CTFFF, then the analysis of each fraction that can include physico-chemical characterization of the nanoparticulate fraction in the size continuum by SdFFF or A4F multidetection. Therefore, approach based on the combined use of CTFFF and SdFFF or A4F techniques seems to be promising for the fractionation and characterization of polydisperse environmental samples.

Table 3. Applications of "non-conventional" sedimentation field-flow fractionation in a rotating coiled column

Type of sample	Sample description	Main objectives	Parameters of injection of the samples	Size	Methods of characterization and analysis of fractionation sample	Reference
Environmental particulate matter	Contaminated soil (<250 μm)	Study on the distribution of heavy-metal species in silty, dusty, and sandy fractions	Weight: 0.5 mg; Volume: 5 mL	Silty 0.1-0.2 μm; dusty 2 – 50 μm; sandy >50 μm	SEM, ICP-MS, ICP-AES (offline)	[104]
	Road dust (<100 and <250 μm)	The study of heavy metal association with nanoparticles	Weight: 1 g; Volume: 10 mL	<200 and <300 nm	LD, SEM-EDS, ICP-AES, ICP-MS (offline)	[29,105]
	Street dust (<100 μm)	Studies on the association of elements of natural and anthropogenic origin with nano-, submicro-, and microparticle fractions of dust	Weight: 100 mg; Volume: 2 and 5 mL	<0.2; 0.2-2; >2 μm; <0.3; 0.3-1; 1-10; 10-100 μm	LD, SEM-EDS, ICP-AES, ICP-MS (offline)	[28,30]
	Volcanic ash	Separation, characterization, and quantitative elemental analysis of volcanic ash nanoparticles	Weight: 1g; Volume: 5 and 10 mL	<100 and <200 nm	LD, SEM, ICP-AES, ICP-MS (offline)	[6,102,103]
	Quartz sand (< 20 μm)	Fractionation of natural microparticles of irregular shape	Weight: 10-20 μg; Volume: 0.5-5 mL	<1, 1-2, 2-3, 3-4, 5-7, 7-8, 10 and 10-20 μm	SEM	[100]

SPLITT technique, like CTFFF, enables large amount of environmental particulate samples (up to several grams) to be separated.[26,66,106–108] For example, two size fractions were separated from marine sediment (<1 and 1-38 μm),[108] fly ash (<10.3 and 10.3-44 μm),[26] and natural water colloid (<1 and >1 μm).[66] SPLITT, like SdFFF and CTFFF, can be also combined with various characterization techniques. It should be noted that the study of fly ash particles was performed by the combined use of SPLITT and SdFFF techniques. SPLITT fractionation can serve as a useful tool for pre-separation of complex environmental samples such as the fly ash before characterization by SdFFF or other methods of characterization and/or analysis.[26] SPLITT separation of marine sediments demonstrated that the enriched preservation of soil-derived carbon was a common phenomenon across the finest particle fraction.[108] The behaviour of colloids in lake water was also investigated using SPLITT.[66]

The multi-stage application of SPLITT enables more than two size fractions to be recovered; for example, two and three experimental run yielded separation of the lake and sea sediments into three (<5, 5-10, 10-30 μm) [106] and four[107] (<2, 2-5, 5-10, and >10 μm) particle fractions, respectively. The results obtained have shown that phosphorus is mainly accumulated in the <5 μm size fraction of lake sediment.[106]

Despite the benefits of SPLITT, the cross-contamination of recovering fractions is a common phenomenon.[66,107] The recovery for the micrometer size fractions is usually about 80 %.[66,107] It has been shown that recovery is decreased with decreasing in size (<1 μm) of separated fractions.[66,108] Therefore, for trace elements speciation, questions are raised related to the suitability of SPLITT technique application.

Table 4. Applications of split flow thin cell fractionation in a centrifugal force field

Type of sample	Sample description	Main objectives	Parameters of injection of the samples	Size	Methods of characterization and analysis of fractionation sample	Reference
Environmental particulate matter	Lake sediments (<30 μm)	Study of phosphorus accumulation in different size sediment particles	Continuous flow of particle suspension (after wet sieving)	<5, 5-10, 10-30 μm	LD (offline) Spectrometric (offline)	[106]
	Sea sediments (<44 μm)	Increasing of SPLITT channel for separation of large amount of sediments	Continuous flow of particle suspension (0.5 % w/v)	< 2, 2-5, 5-10, > 10 μm	OM (offline)	[107]
	Marine Sediments (<38 μm)	Preservation of soil-derived carbon across different size sediment particles	Continuous flow of particle suspension (after wet sieving)	<1, 1-38 μm	C,N,S analyzer coupled online to isotope mass spectrometer and liquid chromatography–mass spectrometer (offline)	[108]
	Fly ash (<44 μm)	Separation, characterization, and analysis of fly ash particles	Continuous flow of particle suspension (total mass 3 g)	<10.3 and 10.3-44 μm	SdFFF, ICP-AES (offline)	[26]
	Aquatic colloids	Study of behavior of environmental colloids	Continuous flow of initial water samples	<1 and >1 μm	spectrophotometer (online), atomic force microscopy (offline)	[66]

1.4 Conclusion

SdFFF and A4F are versatile techniques for the fractionation and characterization of complex environmental particulate matter. Owing to the well-developed theory, both SdFFF and A4F techniques can be used not only for the separation but as well as for the sizing of investigated samples. Nevertheless, SdFFF A4F have an important limitation, namely, the mass of analytes in the injected sample does not usually exceed 10-20 μg to avoid overloading the system. Therefore, SdFFF and A4F are mainly used in analytical couplings with sufficiently sensitive detectors and not as a preparative tool. In addition, since the separation performance is strongly related to the quantity injected, the sample preparation and in particular homogenization prior to the separation is essential in order to provide representative results.

The non-conventional SdFFF technique, coiled tube-based FFF, enables the mass of the particulate sample introduced in a long column to be increased up to at least 1 g. Despite its relatively low resolution as compared to conventional field-flow fractionation, CTFFF has a series of important niche applications. It opens a new door into the isolation of nano- and submicron particles from bulk samples of different origin and nature. Its interest has been demonstrated in environmental studies.

SPLITT technique can also be used for the separation of particulate samples at gram levels due to injection of sample to be separated in continuous flow. However, only two fractions can be recovered during one experimental run at SPLITT fractionation. The separation of three and more fractions can be performed by the use of multi-stage procedures. SPLITT fractionation has some other limitations. SPLITT cannot be used for the fractionation and investigation of particles with a size less than 1 μm. Cross-contamination of separated fractions is often observed, and is increased with decreasing in size of particles to be separated.

It can be concluded that CTFFF, SdFFF, and A4F separation techniques can be regarded as complementary ones. The fractions of particles characterized by a relatively wide size range (typically on several hundred nanometers, even tens of micrometers) can be recovered from the bulk sample by CTFFF, then the analysis of each fraction can be performed by SdFFF or A4F with multidetection. Therefore, an approach based on the combined use of CTFFF and SdFFF or A4F techniques seems to be promising for the fractionation and characterization of polydisperse environmental samples.

Chapter 2 Materials and methods

The present chapter contains the information related to the volcanic ash bulk samples, materials and instrumentation used in the study, methodology of NPs separation from polydisperse samples by filtration, sedimentation, and CTFFF techniques, trapping the NPs on membrane filters, descriptions of digestion procedures as well as methodologies applied to the characterization and quantitative analysis of recovered NPs. The approaches used for the calculation of NPs weights and comparison of the results of the ICP-MS analysis of NPs suspensions after their digestion and acidification are also described.

2.1 Volcanic ash samples

The present study was carried out using ash samples of volcanoes Tolbachik, Klyuchevskoy (Kamchatka, Russia, eruptions of 2012 and 2015, correspondingly), and Puyehue (Puyehue-Cordón Caulle volcanic complex, Andes, Chile, eruption of 2011). Klyuchevskoy and Puyehue are stratovolcanoes, therefore, content of ash may attain one third of the total ejected mass. It should be noted that Klyuchevskoy is among the most productive arc volcanoes on Earth [44,109]. Tolbachik is a predominantly basaltic volcanic complex in the Central Kamchatka depression and belongs to the Klyuchevskoy volcanic group. However, Tolbachik is a volcano formed by lava flows (so called Hawaiian type) and content of its ash is less than 1 % of the total mass ejected during the eruption. Puyehue ash sample (about 2 kg) was collected in June 2011 immediately after eruption of volcano and put into a polyethylene bag. Ash-containing snow samples (about 2 kg) of Tolbachik and Klyuchevskoy volcanoes were collected in 2012 and 2015 respectively, during winter season after eruptions from the snow surface and put into polyethylene bags. After melting the ash-snow mixture, the ashes were dried at 25 °C in a well-ventilated room. The weight of each ash sample was not less than 1 kg. The weight of each ash sample was not less than 1 kg. Some properties of volcanic ash samples are presented in table 5.

Table 5. Properties of volcanic ash samples under study

Sample	Density, mg cm $^{-3}$	pH
Puyehue	2.9 ± 0.7	6.65 ± 0.12
Tolbachik	3.2 ± 0.7	6.67 ± 0.15
Klyuchevskoy	3.1 ± 0.3	6.91 ± 0.09

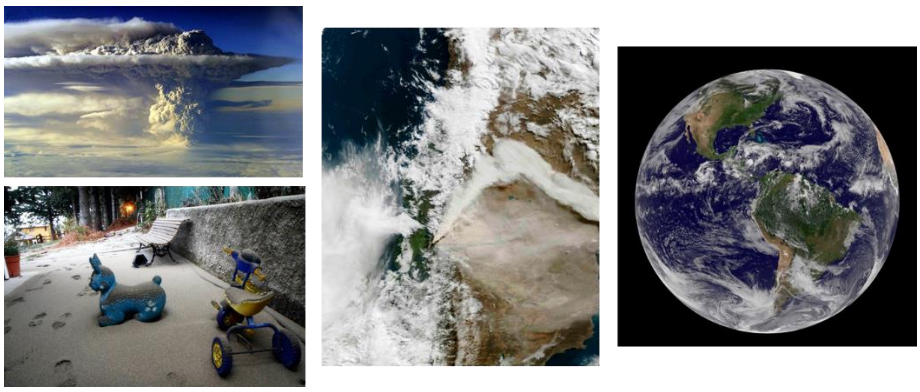

Figure 5. Photos of Puyehue (Chile) eruption of 2011. Sources: Reuters and NASA

2.2 Reagents

Different acids were used: HNO3 (Nitric acid 65%; GR, ISO), HF (Hydrofluoric acid 40%; GR, ISO, Merck); HCl (Hydrochloric acid 37 %; PA-ACS-ISO; Panreac), and HClO4 (Perchloric acid 70%; PA-ACS-ISO; Panreac). The solutions of multielement (ICP-MS-68A-A: Al, As, Ba, Be, Bi, B, Ca, Cd, Ce, Co, Cr, Cs, Cu, Dy, Er, Eu, Fe, Ga, Gd, Ho, In, K, La, Li, Lu, Mg, Mn, Na, Nd, Ni, P, Pb, Pr, Re, Rb, Sc, Se, Sm, Sr, Tb, Th, Tl, Tm, U, V, Y, Tb, Zn) and single-element standards (Na, Al, Si, K, Ca, Fe, Ni, Cu, As, Se, Ag, Cd, Sn, Te, Hg, Tl, Pb, Bi, La, Ce, Pr, Nd, Y, Gd, Dy, Ho, Th, and U) from the High-Purity Standards (USA) were used for calibration in ICP-AES and ICP-MS analyses. Standard sample 'Trace Metals in Drinking water' (High-Purity Standards, USA) was used as reference sample. Ultrapure deionized water with resistivity of 18.2 MΩ cm (Millipore Simplicity, Water Purification System) was used at all steps of the research.

Standard geological samples (*Gabbro GSO 521-84P* (Russian Standard Sample), *Andesite, AGV-2* (United States Geological Survey) and *Granodiorite, Silver Plume, Colorado, GSP-2* (United States Geological Survey)) were used for controlling of digestion procedure applied for bulk samples of volcanic ash.

For dimensional analysis by A4F, ammonium nitrate (99.999%, from Sigma-Aldrich, Steinheim, Germany) and ultra-pure milli-Q water (Millipore system, Bedford, MA, USA) were used. An aqueous solution was prepared such that ammonium nitrate concentration was 10^{-5} mol L^{-1}, with pH at 7.05 ± 0.01. This solution was filtered at 100 nm to obtain the mobile phase of the separation system. Standard samples of monodispersed polystyrene nanospheres (PS from 20 to 200 nm of geometric radii, NIST traceable standards, Gaithersburg, MD) were used to verify fractionation, to ensure the accuracy of the dimensional analysis, and to determine the shape of peaks of fractionated monodisperse populations.

For the elemental calibration of ICP-MS detector in A4F-MALS-ICP-MS hyphenated system and further analysis, standard solutions containing aluminium, iron, copper and lanthanum (at (999 ± 3), (998 ± 4), and (1000 ± 3) mg L^{-1} respectively, SCP Science, France) were used. Additionally, a solution of indium (at (1000 ± 4) mg L^{-1}, SCP Science, France) was used as internal standard solution. Nitric acid (HNO_3, 70% from Atlantic laboratory, Bruges, Belgium) was used for sample acidification.

2.3 Separation of nanoparticles from volcanic ash samples

The filtration, sedimentation and CTFFF methods were applied to separate NP fractions from the three volcanic ashes studied. Each method being based on different principles, separation operational parameters were preliminary optimized for each method independently. This explains why some parameters were not necessarily the same from one method to another.

2.3.1 Filtration

Prior to the NP fraction separation by membrane filtration and sedimentation methods, a mixing procedure was carried out on the basis of Standard NF ISO 18772 [110]. For that, 1 g of ash sample and 20 mL of deionized water were placed in a 50 mL polypropylene tube. Then, the tubes were fixed on the rotary agitator (Intelli-Mixer RM-1, Latvia) and shaken for 24 h with a speed of 20 rpm at room temperature (25 °C). Ultrapure deionized water with the resistivity 18.2 MΩ cm (Millipore Simplicity, Water Purification System, USA) was used at all steps of the study. Once the mixing procedure was finished, the tubes were left for 2 h to settling of coarse particles (> 2 μm).

For the separation of NPs by membrane filtration, preliminary tests were performed in order to select the best membrane materials. For that, cellulose acetate (CA, Vladipor, Russia), polyethersulfone (PES, Millipore, USA), and polytetrafluoroethylene (PTFE, Millipore, USA) membranes with 0.45 μm pore size were used. As a result, results obtained by dynamic light scattering (DLS) analysis (DynaPro NanoStar, Wyatt Technology, Germany) showed that separation of nanoparticles by filtration using CA membrane led to the best recovery. This was expected due to its high surface electric charge density and high hydrophilicity enabling interactions of particles with membrane to be minimized [111]. So CA membrane was used in this study. Then, the separation was performed as follows: the whole volume of suspension was passed

through filter at a constant flow rate of 1 mL/min (peristaltic pump 120 U/DV, Watson-Marlow, UK) according to recommendations for separation of environmental samples [111]. Then, filtered suspensions were transferred into a polypropylene tube.

2.3.2 Sedimentation

The sedimentation method is based on the Stokes' law. In a first step, the sedimentation time was selected by repeated measurements of a size distribution of the volcanic ash particles in the suspension for all three samples. For that, afterward the mixing, the tubes with suspension were left for sedimentation process at ambient temperature (25 °C) and successive aliquots of suspension (≈1 mL) were regularly taken and characterised for particles size distribution by DLS analysis. Thus, the sedimentation time enabling recovering of NP fractions with size less than 400 nm was determined to be 48h. In a second step, the mixing procedure and the sedimentation method were redone and when the sedimentation was finished (48 h), the suspension of NP fraction was carefully taken with a pipette and transferred into a polypropylene tube.

2.3.3 Coiled tube-field flow fractionation

The separation of NP fractions by CTFFF method from volcanic ash samples was performed on a planetary centrifuge with a vertical single-layer coiled column (fig. 3) according to previously developed methodology [6]. The planetary centrifuge was fabricated in the Institute of Analytical Instrumentation, St. Petersburg, Russia. The planetary centrifuge has a revolution radius R = 90 mm and a rotation radius r = 50 mm. The β value (β = r/R) is 0.55. The separation column is made of a PTFE tube with an inner diameter of 1.6 mm. The solid sample (1 g) was introduced into the column (filled with deionized water) as an initial suspension in 10 mL of water. Then, the column was rotated at 800 rpm and water was continuously fed into the column. The inner capacity of the column is 20 mL and particulate matter has even distribution along the column. Therefore, the sample introduced in the column is equivalent to a suspension composed of 1g of ashes in 20 mL water as in sedimentation and filtration methods. The separation of nanoparticles was achieved at a flow rate of 0.3 mL min^{-1}. The rotation speed and flow rate parameters were chosen in order to enable the fractionation of NPs with size less than 400 nm from the bulk sample. The particulate matter in the column effluent was monitored using a flow spectrophotometer. The separated fractions of NPs were collected into a polypropylene tube. All separation methods were performed in three replicates (i.e. n=3).

2.4 Size characterization of recovered fractions and initial samples

Once the separation by membrane filtration, sedimentation and CTFFF was finished, each fraction of NPs was immediately characterized by laser diffraction method (Shimadzu SALD-7500nano, Japan) and, in parallel, several drops of NP fractions from all the samples were taken for study by scanning electron microscopy (Tescan MiraLMU, Czech Republic).

For laser diffraction characterization of separated fractions, 5 mL of each fraction were added to the batch cell of the device. Semiconductor laser (wavelength 405 nm) and batch cell (SALT-BC75) are used in the technique. Size distribution was studied within the range of particle refractive indices from (1.00 - 0.00i) to (2.00 - 1.00i). The appropriate refractive index and corresponding PSD was evaluated using LDR (Light Intensity Distribution Reproduction) method [112], integrated in the device software. The measurement of each aliquot was done in three replicates.

Characterization by scanning electron microscopy was carried out after drying of a droplet of each fraction on the silicon wafer without conductive coating; secondary electron image (SEI) mode and accelerating voltage 5 kV were used.

2.5 Trapping of recovered nanoparticles on filters

The separated NPs fractions were trapped on the membrane filters (20 kDa, Vladipor, Russia) using a filtration cell. The volume of filtration cell is 10 mL. The cell is equipped with magnetic stirrer to prevent clogging of membrane pores. The principle scheme of the filtration cell is illustrated in figure 6. The filtration is performed under the pressure of 2 bar.

Initially, the membrane was fixed in the filtration cell. Then, 2 mL of deionized water were added to the filtration cell for wetting the membrane. After 20 min of membrane wetting, the filtration of samples was performed. Since the volume of filtration cell was 2 fold greater than the volume of recovered suspensions, the filtration process was done in 2 steps; the suspension was divided into two portions of volume 10 mL. The blank samples were also passed through membranes. Afterwards, the filters were dried in a desiccator (for 3 days) digested, and analysed by ICP-AES and ICP-MS techniques.

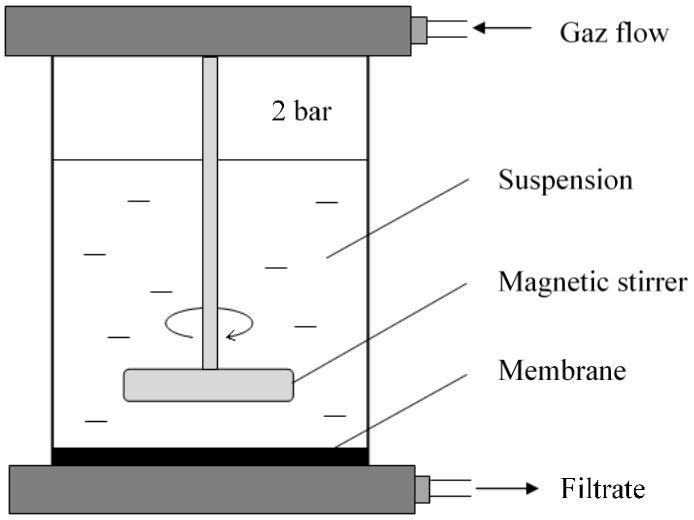

Figure 6. Principle scheme of filtration cell for trapping of recovered nanoparticle on filters

2.6 Elemental analysis of initial samples and recovered nanoparticles

2.6.1 Pre-treatment procedures

2.6.1.1 Digestion of initial samples

Samples of the volcanic ash as well as standard geological samples Gabbro GSO 521-84P, Andesite, AGV-2 and Granodiorite, Silver Plume, Colorado, GSP-2 were digested in autoclave system using a combination of acids. The autoclave system was ANKON-AT-2, Russia [113,114].

The digestion procedure was described in detail and validated for geological samples by Karandashev et al. [115]. The particulate samples of weight 50 mg were put into Teflon beakers together with 2mL HF, 0.5 mL HNO_3, and 0.05 mL of solution containing 8mg L^{-1} ^{146}Nd, 5 mg L^{-1} ^{161}Dy, and 3 mg L^{-1} ^{174}Yb, which were necessary to control completeness of digestion, covered with caps and stored for 6-8 h at room temperature. Then, the beakers were opened and boiled down at 170-180 °C. After cooling, 2 mL HF, 0.5 mL $HClO_4$, and 0.2 mL HNO_3 were added to each sample, the beakers were closed and placed in the autoclave titanium housings. The autoclaves were put in an electric furnace and held at 160 °C (1 h), 180 °C (1 h), 200 °C (1 h) and 220 °C (0.5 h). After cooling, the samples were boiled down at 170-180 °C. Then, 1 mL HCl and 1 mL HNO_3 were added to each of the sample, the beakers were closed and held for 1 h at 160 °C. After the autoclaves were cooled down, they were opened, and the solution was evaporated to dryness. Then, 1 mL HCl and 1 mL HNO_3 were again added to the beakers and the steps of heating

at 160 °C and evaporation to dryness were repeated. The dry residue was dissolved in 0.8 mL HCl and 0.8 mL HNO_3 at 80-100 °C heating and transferred to polyethylene test tubes, the solution volume was brought up to 10 mL with deionized water. The solutions from the beakers without analysed sample were used as control ones. Before measurements all the solutions were diluted by 5 times and an internal standard of 10 mg L^{-1} In was added.

This digestion procedure leads to the losses of Si (as volatile SiF_4) as well as Hg and As. Therefore, another 50 mg of bulk ash were taken for the extraction of Hg and As with boiling aqua regia. The extraction procedure was described in detail and validated for soil, ground, and bottom sediments by Karandashev et al. [116]. Briefly, it is employed the shaking and heating of the mixture of sample and aqua regia for the extraction, followed by filtration of the extract through ashless paper filters and dilution with deionized water.

2.6.1.2 Digestion of filters with trapped nanoparticles

The digestion of filter with NPs as well as blank filters was also performed using an autoclave system. The digestion procedure was also already described in detail and validated by Fedotov et al. [30]. The filter sample was transported in Teflon beakers. The 0.5 mL of HNO_3 and 1 mL of HCl were added into the beakers with filter. Then, the beakers were closed and placed in the autoclave titanium housings. The autoclaves were put in an electric furnace and held during 1 h at 160 °C, 2 h at 180 °C, and 1 h at 200 °C. After cooling of autoclave, they were opened, obtained solutions were transferred to polyethylene test tubes and their volume was brought up to 10 mL with deionized water. Before measurements, an internal standard of 10 mg L^{-1} In was added to all the solutions. For the control samples, above-described procedure was done in Teflon beakers without analysed sample.

2.6.1.3 Digestion of nanoparticle suspension

To confirm the reliability of the direct analysis of NP suspensions by ICP-MS, conventionally acid digestion followed by ICP-MS analysis is used. It should be noted that NP suspensions were recovered from volcanic ash sample by sedimentation process described in *2.3*. For each ash, suspensions were prepared three times, and then pooled to obtain a single composite suspension in order to overcome the heterogeneity of volcanic ash. From this suspension, for each sample preparation procedure tested (digestion and acidification), three aliquots were taken. For analytical control, blanks containing deionized water instead of NP suspensions were prepared in three

replicates as described below for procedures of digestion and acidification of NP suspensions.

This procedure is similar to the autoclave digestion of the bulk samples described in *2.6.1.1.* Three aliquots consisting in 6 mL of suspension were transferred into Teflon reaction vessels; 0.05 mL of the solution of isotope tracers (8 mg L^{-1} ^{146}Nd, 5 mg L^{-1} ^{161}Dy, and 3 mg L^{-1} ^{174}Yb) was also added to the vessels for controlling of digestion completeness. The obtained solution was evaporated. The mixture of concentrated acids (1 mL HF, 0.3 mL $HClO_4$, and 0.3 mL HNO_3) was added to the dry residue. Then, vessels were closed with caps, placed in the autoclave, and heated in an electric furnace at 160 °C (1 h), 180 °C (1 h), 200 °C (1 h) and 220 °C (0.5 h). After cooling, the reaction vessels were opened and placed on the heating plate and the solution was evaporated to dryness at 170-180°C. For the digestion of insoluble fluorides, the residue was twice treated with the mixture of concentrated 1 mL HCl and 0.5 mL HNO3 in autoclave at 160 °C (1 h) with the subsequent evaporation to dry salts. After the dry residue was dissolved in the mixture of 0.2 mL HCl and 0.2 mL HNO3 at 80-100 °C and transferred to polyethylene test tubes. Before measurement, the solution volume was brought up to 6 mL with deionized water, in order to obtain a final matrix of 2 % HNO3 and 1 % HCl. Then the internal standard of 10 μg L^{-1} Rh was added to each aliquot for the indirect analysis by ICP-MS.

2.6.1.4 Acidification of nanoparticle suspension

Prior to the direct analysis of NP suspensions by ICP-MS, they were acidified to 4 % HNO_3. The internal standard of 10 μg L^{-1} Rh was added to 6 mL of each aliquot of the acidified solution. It should be noted that NP suspensions as well as standard solutions for calibration were prepared for each final preparation matrix in order to overcome acid effect and avoid memory effect.

2.6.2 Elemental analysis

2.6.2.1 Inductively coupled plasma atomic emission spectrometry analysis

The contents of Na, Mg, Al, Si, P, K, Ca, Ti, Mn, Fe, and Cu in bulk samples and in NPs trapped on filter were determined by ICP-AES (iCAP-6500 Duo, Thermo Scientific, USA). The measurements were made using the following parameters [115]:

- a RF generator power of 1200W;
- a VeeSpray nebulizer;
- a plasma-forming Ar flow rate of 12 L min^{-1};

- an auxiliary Ar flow rate of 0.5 L min^{-1};
- an Ar flow rate into the nebulizer of 0.6 L min^{-1};
- an analysed sample flow rate of 1.8 mL min^{-1}.

The concentration of element in samples under analysis was calculated by software of ICP-AES technique (ThermoSPEC, version 4.1). The limit of detection (LOD) was calculated according to Eurachem/CITAC guide [117] as:

$$LOD = C_i + 3\sigma, \quad (27)$$

where C_i is the mean concentration of i element obtained from measurement of blank samples; σ is standard deviation of i element concentration obtained from measurements of blank samples.

2.6.2.2 Inductively coupled plasma mass spectrometry analysis

In case of the analysis of filter with NPs as well as bulk samples, the contents of Na, Al, Ti, Mn, Fe, Ni, Cu, As, Se, Y, Ag, Cd, Sn, Te, La, Ce, Pr, Nd, Gd, Dy, Ho, Hg, Tl, Pb, Bi, Th, and U in the samples were determined using an ICP-MS (X-7, Thermo Scientific, USA). The measurements were made using the following parameters:

- a RF generator power of 1250W;
- HF resistant polyimide a PolyCon nebulizer;
- Quartz torch with 1.5 mm injector for X Series;
- a plasma-forming Ar flow rate of 13 L min^{-1};
- an auxiliary Ar flow rate of 0.9 L min^{-1};
- an Ar flow rate into the nebulizer of 0.9 L min^{-1};
- an analysed sample flow rate of 0.8 mL min^{-1}.

In case of the analysis of digested and acidified nanoparticle suspension, the content of Al, Fe, Y, La, Ce, Pr, Gd, Ho, Ni, Cu, Se, Sn, Te, Tl, Pb, Bi, and Th in the solutions was determined by ICP-MS (Agilent 7900, USA). The measurements were made using the following parameters:

- a RF generator power of 1550 W;
- set of standard nickel cones;
- a MicroMist nebulizer;
- quartz Scott-style spray chamber;
- a plasma-forming Ar flow rate of 15 L min-1;
- an Ar flow rate into the nebulizer of 1.05 L min-1;

- an analysed sample flow rate of 1.0 mL min-1.

All these elements were selected because they enable a complete elemental characterization of bulk and NP fraction of volcanic ashes to be achieved. For all the analyses, the internal standard (In and Rh) was used for accurate correction of non-spectral interferences. The absence of these elements in samples was preliminary verified. The treatment of the results of the analysis was provided by ICP-MS techniques software. The limit of detection (LOD) was calculated according to equation 27.

2.7 Calculation of weight of separated nanoparticles

The quantitative determination of the NP weight in suspension is generally difficult to achieve precisely after separation. To overcome this difficulty, another approach was used from the calculation of element concentrations in volcanic ash nanoparticles. The mineral particles of volcanic ash primarily consist of aluminosilicate and their chemical composition can be represented as a sum of the oxides of major elements. For instance, basalt can be considered as 45–55 % SiO_2, 14 % or more Al_2O_3, 5–14 % FeO, MgO in the range from 5 to 12 %, about 10% CaO, 2–6 % total alkalis, and 0.5–2.0 % TiO_2 [118]. The determined absolute amounts of major elements (Si, Na, Mg, Al, P, K, Ca, Ti, Mn and Fe) were recalculated to their oxides (SiO_2, Na_2O, MgO, Al_2O_3, P_2O_5, K_2O, CaO, TiO_2, MnO_2, Fe_2O_3) and the total amount of oxides was considered as representative of the weight of the NP fraction. The approach was described and validated earlier by Ermolin et al. [6].

2.8 Comparison of the results of direct and indirect elemental analysis

The concentrations of elements in NPs measured by direct ICP-MS analysis and after acid digestion of the suspensions (simply named “indirect analysis” hereinafter) were compared. Due to the lack of certified reference material and so to certified concentration value, the comparison was performed taking into account the uncertainties associated with the two mean concentration values ($mean \pm U$, with $U = 2 \times Standard\ Deviation\ (SD)$) obtained after direct and indirect analysis, by calculating the relative accuracy bias according to:

$$B = \frac{[\max(C_{direct}; C_{indirect}) - U_1] - [\min(C_{direct}; C_{indirect}) + U_2]}{C_{indirect}} \times 100 \quad (28)$$

with C_{direct} and $C_{indirect}$ the concentrations obtained by direct and indirect analysis; U_1 and U_2 the uncertainties associated with the concentrations selected by the tests max and min respectively. $B \leq 0$ means there is no significant difference between the concentrations i.e. there is no bias, while $B > 0$ is the direct evaluation of the relative accuracy bias.

2.9 Study of volcanic ash nanoparticles by hyphenated system (Asymmetric flow field-flow fractionation-UV detector-multi-angle light scattering-inductively coupled plasma mass spectrometry)

The nanoparticle fraction was recovered by sedimentation as was described in the section *2.3.2*. Two aqueous solutions were considered to preliminary evaluate the settling process: a synthetic river water (prepared according to work [119] and deionized water (from 18 MΩ milliQ system).

2.9.1 Dimensional analysis

Dimensional characterisation and monitoring were performed using Asymmetric Flow Field-Flow Fractionation (A4F, Eclipse 3, Wyatt Technology, Dernbach, Germany) coupled to UltraViolet-Visible Diode Array Detector (UV-Vis DAD 1260 Infinity, Agilent Technology, Tokyo, Japan) and Multi-Angle Light Scattering detector (MALS, DAWN HELEOS, Wyatt Technology, Santa Barbara, USA).

A4F operating conditions were the following: injector and focus flows were 0.2 and 2.5 mL min^{-1} respectively; the cross-flow programming, optimized for fractionating particles up to 200 nm geometric radius, was from 2.5 (for 1 min) to 0.5 mL min^{-1} in 5 min, left at 0.5 mL min^{-1} for 30 min, then adjusted and kept at 0 mL min^{-1} for 11 min; detector flow was 1 mL min^{-1}. All the flows were controlled by a HPLC pump (Agilent Technologies 1100 series, Waldbronn, Germany). The channel was 26.5 cm in length, with a trapezoidal cross-section from 2.1 (in) to 0.6 cm (out). It was used with a cellulose-regenerated membrane with a 10 kDa cut-off. The injected volume was 100 µL. The A4F mobile phase (see 2.1) was chosen in order to avoid any agglomeration/aggregation (salt nature and concentration), and also in agreement with detector requirement (no surfactant for MALS and low salt concentration for ICP-MS) [23]. MALS information was collected at 15 angles between 29.6 and 157.7°. It was processed with Astra software (Wyatt technology) using the sphere formalism for standard nanospheres and Berry's first-order formalism for all particle types. Then, the shape index, defined as the ratio between the gyration radii of the nanoparticles of volcanic ash and the standard nanospheres, was deduced [79].

The shape index enables the gap with the "sphericity" of fractionated nanoparticles with respect to standard nanospheres to be evaluated, and thus shape information to be obtained.

2.9.2 Elemental analysis

The elemental analysis was performed with ICP-MS (Agilent 7900) instrument equipped with a cooled Scott-type spray chamber, a concentric nebulizer (Meinhard) and an octopole Collision/Reaction Cell (CRC). The CRC with helium 4.3 mL min^{-1} was used to eliminate polyatomic interferences. For A4F-ICP-MS analysis, the operating conditions were chosen in order to simultaneously monitor Al, Fe, Cu and La taken as major and trace elements of complementary interest to the ash nanoparticle fraction considered. Indeed, the question of concentrations was important for obtaining reliable results due to the large dilution induced by A4F. The monitored isotopes were ^{27}Al, ^{56}Fe, ^{63}Cu, ^{139}La, and ^{115}In. A coupling module comprising a T-connector and a second HPLC pump was used to connect the A4F system and the ICP-MS detector. It enabled the element standards (including the internal standard) to be introduced, and the mobile phase to be acidified for the ICP-MS quantitative analysis.

The total concentration of nanoparticles in suspension was also determined using the UV-Vis signals. Indeed, the maximum intensity of a UV–Vis absorption spectrum is a function of the concentration of NPs in suspension. It can therefore be used to determine the concentration [120,121]. In addition, such an approach was used to determine the total NP concentration using A4F coupling, which is easier and faster than offline procedures [122]. Consequently, the signals recorded at 300 nm (which was the most absorbing wavelength for this sample; see below in the result and discussion part) were used to determine the total concentration of nanoparticles. The calibration of the UV-Vis detector was carried out using the mass of nanoparticles determined in the initial suspension by the exhaustive elemental analysis of the suspension was also used. The total concentrations of nanoparticles and the corresponding UV-Vis signal areas were obtained in the initial unfractionated (total samples) and fractionated suspension.

The accuracy (exactness and precision) of the offline and online elemental analyses was verified in two ways: (i) by injecting a certified reference water (CRM TMDA64-3, river water) via the coupling module and comparing the determined element values with those of the certificate, and (ii) by injecting the sample directly into the ICP-MS and then introducing it via the A4F system without any fractionation, and comparing the element values obtained. For the CRM TMDA64-3 (not certified for La), the concentrations found were: (269.2 ± 1.3), (302.1 ± 4.2) and (247.7 ± 5.9)

µg L^{-1} for Al, Fe and Cu respectively (certified values: (290 ± 23), (298 ± 21) and (260 ± 18) µg L^{-1} for Al, Fe and Cu). The values found are therefore in accordance with the reference values, with recoveries equal to (93 ± 7), (101 ± 5) and (95 ± 5) % respectively. For the sample of volcanic ash nanoparticles, the offline/online concentrations (reported in Table 9) were also in agreement, and their associated standard deviation of the same order of magnitude. In addition, the detection limits (LOD), calculated from the signal height, were 0.5, 3, 0.09 and 0.005 µg L^{-1} for Al, Fe, Cu and La respectively, and the Relative Standard Deviation (RSD) evaluating the quantification precision was about 7% for all monitored isotopes. The elemental approach enabled the accuracy of the UV-Vis analysis to be verified, with recovery (considering the elemental approach as the reference since it was previously validated) of (95 ± 3) %. In addition, the limits of detection, calculated from the signal height, was 500 µg L^{-1}, and the Relative Standard Deviation evaluating the quantification precision was about 6%.

2.9.3 Signal processing from fractograms

For each analytical sequence, blank and standard solutions were analyzed. Then, the UV-Vis and ICP-MS temporal signals (from the fractograms) were filtered using a low-pass digital filter. Standard monodispersed samples fractionated by A4F showed Gaussian peaks. The deconvolution process was therefore carried out on the basis of Gaussian peaks, simultaneously considering the signals of all the detectors. The adjustment of the analytical expression (sum of the Gaussian peaks) to the experimental fractogram enabled the deconvolution solution to be optimized. The accuracy of the process was estimated by the coefficient of determination R^2. Deconvolution was considered optimal when R^2 was equal to or greater than 0.99.

Chapter 3 Analytical study of the nanoparticle fraction of volcanic ash

3.1 Separation of nanoparticles from volcanic ash samples: comparative study of filtration, sedimentation, and coiled tube field-flow fractionation

The common approaches applied to the separation of nanoparticle fractions include filtration and sedimentation methods [4]. As was mentioned coiled tube field-flow fractionation can be also used for the separation of NPs from environmental samples.

In the present part of work, filtration, sedimentation and CTFFF were applied to the separation of NPs from volcanic ash samples for subsequent dimensional and quantitative characterization. The size populations obtained by these methods were characterized in order to establish their similarities and differences in terms of size, size distribution, concentrations and composition. The aim was to perform a comparative description, given that each method used has its own optimal operating conditions [6,28,129,29,30,123–128].

3.1.1 Dimensional characterization of nanoparticle fractions

The NP fractions of volcanic ash recovered by filtration, sedimentation, and CTFFF were characterized by laser diffraction and SEM. The measured size distributions of particles in all separated NP fractions are presented in figure 7. Additionally, the micrographs of the corresponding NP fractions are shown in figure 8. As is seen in figure 7, for all samples, the filtration and CTFFF methods enabled particles less than 400 nm to be separated. For filtration, the position of peak maximum was always in a narrow range of 30-40 nm, the distribution ranging from several nanometres up to 150, 250 and 400 nm depending on the sample. For CTFFF, both the peak maximum (from 30 to 140 nm, respectively) and the distribution width (about 10-60, 50-350 and 20-350 nm respectively) depended on the sample. The sedimentation mainly provided particles less than 400 nm (≥ 95%). Both the peak maximum (about 90, 110 and 100 nm, for Puyehue, Tolbachik, and Klyuchevskoy ash samples, respectively) and the distribution width (about 10-350, 40-350 and 20-350 nm for Puyehue, Tolbachik, and Klyuchevskoy ash samples, respectively) depended on the samples, as for CTFFF. However, unlike the other two methods, sedimentation provided a second population of submicron particles in the range of 400-900 nm. The maximum of the respective peak corresponded to a size of about 600 nm for all the samples. It should be noted that this second population represented less than 5 % of the whole particle fraction separated.

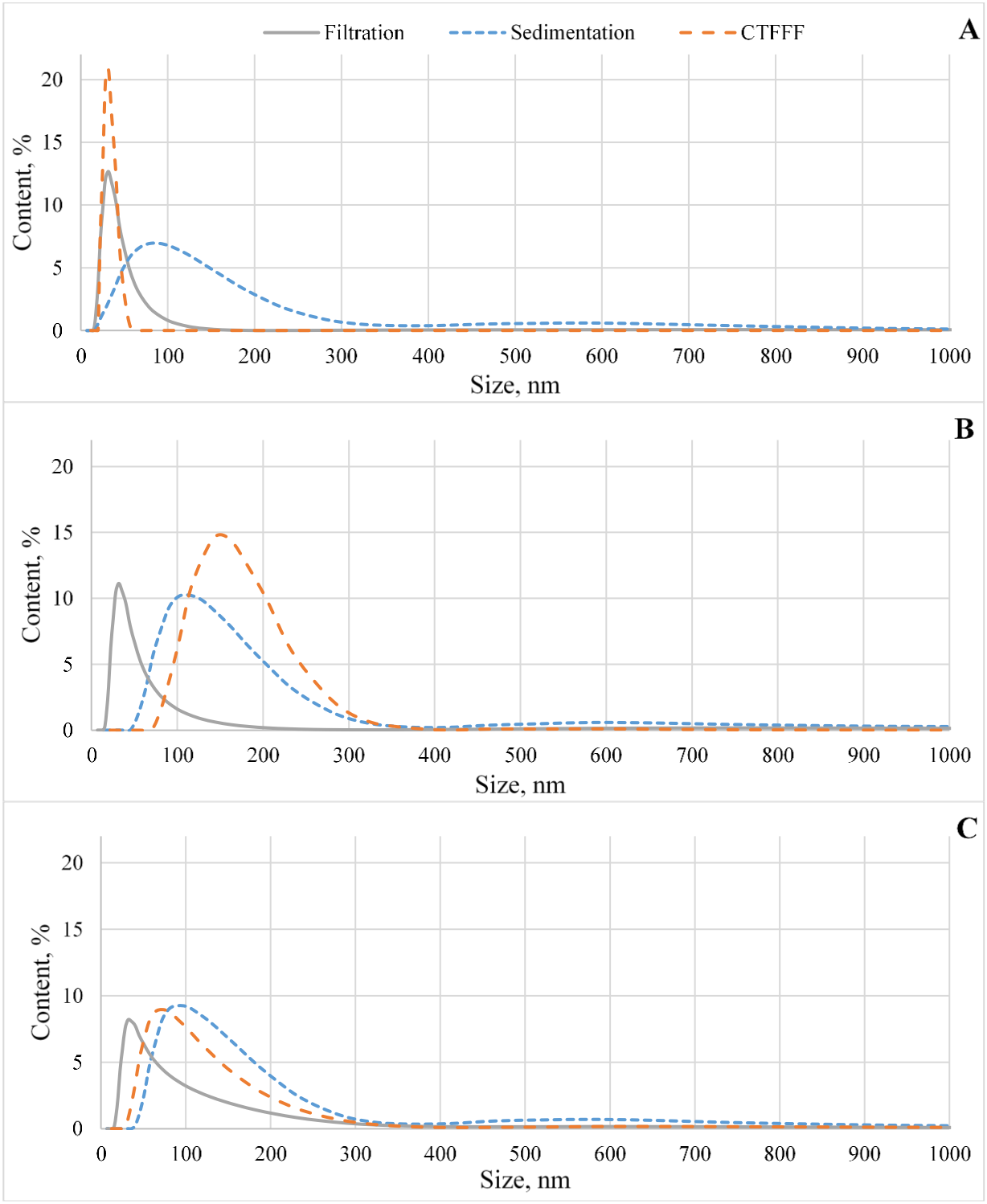

Figure 7. The size distribution of NP fractions of Puyehue (**A**), Tolbachik (**B**), and Klyuchevskoy (**C**) volcanic ash samples as measured by laser diffraction.

Thus, dimensional results show that filtration enabled smaller NPs to be selectively separated. This indicates that larger NPs were mostly retained on the filter although their size was smaller than the filter cut-off. This observation is in agreement with literature [129].

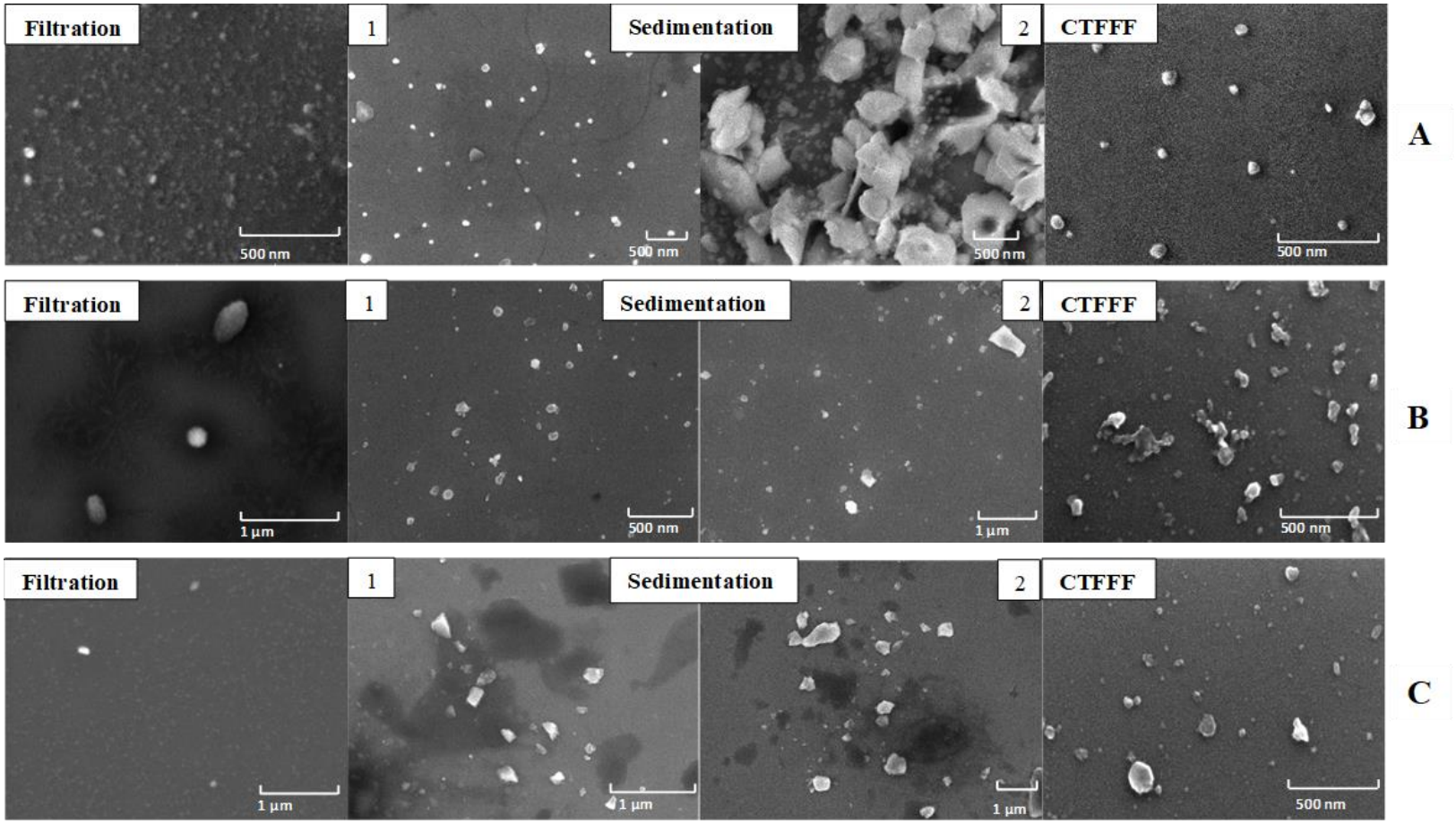

Figure 8. Micrographs of NP fractions of Puyehue (A), Tolbachik (B), and Klyuchevskoy (C) volcanic ashes separated by filtration, sedimentation, and CTFFF, techniques. For NP fraction separated by sedimentation, a population of particles with size < 400 nm and submicron population are illustrated in micrographs 1 and 2, respectively

CTFFF provided the separation of NPs with same PSD as sedimentation for Tolbachik and Klyuchevskoy volcanic ash in contrast to Puyehue sample, which had PSD similar to the fraction separated by filtration method. In particular, for Puyehue volcanic ash, a high adhesion of NPs to the tube wall of the rotating coiled column was observed, which decreased the recovery of NPs. This phenomenon was systematically observed for all the replicates of NPs separation from Puyehue by CTFFF. The adhesion of particles in column is strongly dependent on mineral composition of volcanic ash particles, their surface properties, and properties of liquid media, first of all, the ionic strength [130]. Indeed in the present study, Tolbachik and Klyuchevskoy ashes are basaltic ones [35], while Puyehue ash is andesitic one [36]. The adhesion was also enhanced by the action of centrifugal forces generated in CTFFF during the separation process.

Figure 8 enables nanoparticles with a spherical or ellipsoidal shape and a smooth surface to be visualized in all samples and whatever the separation method used. This is evidently the result of high-temperature processes of particle formation occurred during eruption [131,132]. The submicron particles found in the fractions separated by sedimentation were of irregular shape, which could be attributed to the fragmentation of larger particles during the eruption [131,132].

3.1.2 Elemental characterization of bulks and nanoparticle fractions

The determined concentrations of major and trace elements in bulks and corresponding NP fractions of volcanic ash samples are given in table 6.

In NP fractions separated by filtration, most of trace elements were under the limit of detection (except Cd, Tl, Pb and La in Puyehue sample, Ni, Cu, Tl, Pb and La in Tolbachik sample, and Tl and La in Klyuchevskoy sample). In addition, concentrations were systematically inferior to the ones determined after separation by sedimentation and CTFFF. This tendency is in accordance with dimensional information get in 3.1. Indeed, for all samples, using filtration method, larger NPs were retained on the filter although their sizes were smaller than the pores size of the filter cut-off. Therefore, the determination of major and trace element concentrations was complicated due to the low amount of recovered NP fractions using filtration method. The repeatability, expressed by the relative standard deviation (RSD) associated to the concentration values, were also calculated. RSD ranged from 11% to 52% for Puyehue and Tolbachik samples, and from 4% to 29% for Klyuchevskoy sample.

Table 6. Concentration of major and trace elements in bulk samples (relative to measured bulk ash weight) and NP fractions (relative to measured NP fraction suspension volume) of volcanic ash separated by filtration, sedimentation, and CTFFF techniques (*mean ± Standard Deviation (SD) (n=3) and Relative Standard Deviation (RSD) into brackets*)

Element	Puyehue				Tolbachik				Klyuchevskoy			
	Bulk [6]	Filtration	Sedimentation	CTFFF [6]	Bulk [6]	Filtration	Sedimentation	CTFFF [6]	Bulk [6]	Filtration	Sedimentation	CTFFF [6]
	mg/g	ng/mL	ng/mL	ng/mL	mg/g	ng/mL	ng/mL	ng/mL	mg/g	ng/mL	ng/mL	ng/mL
1	**2**	**3**	**4**	**5**	**6**	**7**	**8**	**9**	**10**	**11**	**12**	**13**
Na	36 ± 4 (11 %)	46 ± 13 (28 %)	846 ± 385 (46 %)	56 ± 24 (43 %)	28 ± 3 (11 %)	39 ± 6 (15 %)	419 ± 78 (19 %)	167 ± 47 (28 %)	24 ± 2 (8 %)	27 ± 8 (29 %)	421 ± 35 (8 %)	545 ± 47 (9 %)
Mg	< 0.03	15 ± 3 (20 %)	37 ± 14 (38 %)	12 ± 2 (17 %)	20 ± 2 (10 %)	45 ± 16 (36 %)	422 ± 68 (16 %)	459 ± 86 (19 %)	28 ± 3 (11 %)	30 ± 2 (7 %)	520 ± 82 (16 %)	554 ± 48 (9 %)
Al	74 ± 7 (9 %)	45 ± 6 (13 %)	1041 ± 526 (51 %)	261 ± 80 (31 %)	84 ± 8 (10 %)	42 ± 22 (52 %)	1679 ± 301 (18 %)	1133 ± 312 (28 %)	86 ± 9 (10 %)	27 ± 1 (4 %)	1791 ± 88 (5 %)	2744 ± 153 (6 %)
Si	n.d.*	251 ± 92 (37 %)	2315 ± 355 (15 %)	968 ± 329 (34 %)	n.d.*	239 ± 126 (53 %)	2902 ± 414 (14 %)	3588 ± 738 (21 %)	n.d.*	< 197	2284 ± 163 (7 %)	4321 ± 926 (21 %)
P	0.57 ± 0.05 (9 %)	3.6 ± 0.7 (19 %)	35 ± 12 (34 %)	10 ± 2 (20 %)	3.0 ± 0.2 (7 %)	6 ± 3 (50 %)	188 ± 16 (9 %)	354 ± 24 (7 %)	0.8 ± 0.1 (13 %)	5.1 ± 0.6 (12 %)	43 ± 4 (9 %)	40 ± 3 (8 %)
K	8 ± 1 (13 %)	< 12	259 ± 123 (47 %)	< 12	20 ± 2 (10 %)	< 12	258 ± 57 (22 %)	97 ± 35 (36 %)	8 ± 0.8 (10 %)	< 12	28.4 ± 0.8 (3 %)	124 ± 19 (15 %)
Ca	57 ± 6 (11 %)	151 ± 37 (25 %)	414 ± 129 (31 %)	< 32	51 ± 5 (10 %)	110 ± 31 (28 %)	858 ± 111 (13 %)	498 ± 134 (27 %)	57 ± 6 (11 %)	146 ± 14 (10 %)	1680 ± 59 (4 %)	1459 ± 130 (9 %)
Ti	3.6 ± 0.4 (11 %)	36 ± 19 (53 %)	94 ± 42 (45 %)	13 ± 4 (31 %)	11 ± 1 (9 %)	128 ± 33 (26 %)	168 ± 10 (6 %)	266 ± 93 (35 %)	6.4 ± 0.6 (9 %)	< 4	84 ± 14 (17 %)	465 ± 41 (9 %)
Mn	0.67 ± 0.05 (7 %)	4.0 ± 0.4 (10 %)	30 ± 4 (13 %)	2.5 ± 0.6 (24 %)	1.0 ± 0.1 (10 %)	3.2 ± 0.7 (22 %)	30 ± 9 (30 %)	46 ± 5 (11 %)	1.1 ± 0.1 (9 %)	5.5 ± 0.3 (5 %)	29 ± 4 (14 %)	46 ± 3 (7 %)
Fe	62 ± 6 (10 %)	27 ± 9 (33 %)	569 ± 144 (25 %)	74 ± 35 (47 %)	69 ± 7 (10 %)	122 ± 40 (33 %)	2133 ± 368 (17 %)	3432 ± 192 (6 %)	62 ± 6 (10 %)	23 ± 4 (17 %)	1199 ± 99 (8 %)	2346 ± 130 (6 %)
	µg/g	pg/mL	pg/mL	pg/mL	µg/g	pg/mL	pg/mL	pg/mL	µg/g	pg/mL	pg/mL	pg/mL
Ni	0.7 ± 0.1 (14 %)	< 410	< 410	732 ± 41 (6 %)	9 ± 1 (11 %)	1495 ± 212 (14 %)	2425 ± 82 (3 %)	8437 ± 2558 (30 %)	22 ± 2 (9 %)	< 410	1042 ± 184 (18 %)	1173 ± 100 (9 %)
Cu	16 ± 2 (13 %)	< 474	< 474	1694 ± 130 (8 %)	240 ± 25 (10 %)	1122 ± 429 (38 %)	16023 ± 3365 (21 %)	40491 ± 3830 (9 %)	68 ± 7 (10 %)	< 474	5246 ± 87 (2 %)	21418 ± 1600 (7 %)
As	4.0 ± 0.4 (10 %)	< 95	< 95	< 95	3.4 ± 0.3 (9 %)	< 95	4104 ± 227 (6 %)	12464 ± 1024 (8 %)	0.60 ± 0.06 (10 %)	< 95	< 95	1084 ± 125 (12 %)
Se	1.6 ± 0.2 (13 %)	< 501	< 501	< 501	< 2.5	< 500	1921 ± 326 (17 %)	5240 ± 511 (10 %)	< 0.7	< 500	< 500	1100 ± 127 (12 %)
Ag	0.10 ± 0.01 (10 %)	< 4	10.9 ± 0.6 (6 %)	12 ± 3 (25 %)	0.10 ± 0.01 (10 %)	< 4	59 ± 8 (14 %)	111 ± 21 (19 %)	0.10 ± 0.01 (10 %)	< 4	33 ± 6 (18 %)	71 ± 6 (8 %)

Table 6 (continued)

1	2	3	4	5	6	7	8	9	10	11	12	13
Cd	0.10 ± 0.01 (10 %)	12 ± 5 (42 %)	27 ± 12 (44 %)	< 2	< 0.03	< 2	< 2	31 ± 8 (26 %)	0.10 ± 0.01 (10 %)	< 2	26.1 ± 0.9 (3 %)	77 ± 11 (14 %)
Sn	2.6 ± 0.3 (12 %)	< 532	< 532	< 532	1.6 ± 0.2 (13 %)	< 532	< 532	1111 ± 107 (10 %)	0.9 ± 0.1 (11 %)	< 532	< 532	884 ± 38 (4 %)
Te	<0.07	< 18	< 18	< 18	< 0.05	< 18	109 ± 19 (17 %)	457 ± 12 (3 %)	< 0.05	< 18	35.9 ± 0.8 (2 %)	218 ± 44 (20 %)
Hg	<0.08	< 15	< 15	19 ± 8 (42 %)	0.10 ± 0.01 (10 %)	< 15	210 ± 51 (24 %)	418 ± 31 (7 %)	0.10 ± 0.01 (10 %)	< 15	122.0 ± 0.8 (1 %)	843 ± 63 (7 %)
Tl	0.50 ± 0.05 (10 %)	19 ± 2 (11 %)	101 ± 52 (51 %)	30 ± 6 (20 %)	0.20 ± 0.02 (10 %)	35 ± 10 (29 %)	157 ± 22 (14 %)	333 ± 33 (10 %)	0.10 ± 0.01 (10 %)	20 ± 4 (20 %)	51 ± 1 (2 %)	151 ± 15 (10 %)
Pb	23 ± 2 (9 %)	203 ± 106 (52 %)	1946 ± 724 (37 %)	472 ± 128 (27 %)	7.0 ± 0.7 (10 %)	252 ± 80 (32 %)	1051 ± 241 (23 %)	4096 ± 409 (10 %)	3.0 ± 0.3 (10 %)	< 54	145 ± 15 (10 %)	1441 ± 80 (6 %)
Bi	0.20 ± 0.02 (10 %)	< 7	126 ± 62 (49 %)	96 ± 23 (24 %)	0.10 ± 0.01 (10 %)	< 7	140 ± 27 (19 %)	603 ± 26 (4 %)	0.10 ± 0.01 (10 %)	< 7	< 7	140 ± 5 (4 %)
La	29 ± 3 (10 %)	19 ± 9 (47 %)	400 ± 201 (50 %)	115 ± 44 (38 %)	21 ± 2 (10 %)	12 ± 4 (33 %)	320 ± 49 (15 %)	659 ± 155 (24 %)	7 ± 1 (14 %)	3 ± 1 (33 %)	100 ± 3 (3 %)	295 ± 10 (3 %)
Ce	66 ± 7 (11 %)	< 956	906 ± 440 (49 %)	279 ± 96 (34 %)	51 ± 5 (10 %)	< 956	779 ± 146 (19 %)	1669 ± 383 (23 %)	18 ± 2 (11 %)	< 956	238 ± 4 (2 %)	712 ± 48 (7 %)
Pr	8.6 ± 0.9 (10 %)	5 ± 2 (40 %)	125 ± 64 (51 %)	35 ± 11 (31 %)	7.5 ± 0.8 (11 %)	5 ± 1 (20 %)	115 ± 20 (17 %)	240 ± 54 (23 %)	2.8 ± 0.3 (11 %)	< 1	39 ± 2 (5 %)	105 ± 6 (6 %)
Nd	37 ± 4 (11 %)	23 ± 5 (22 %)	554 ± 251 (45 %)	152 ± 51 (34 %)	33 ± 3 (9 %)	23 ± 9 (39 %)	529 ± 117 (22 %)	1094 ± 236 (22 %)	13 ± 1 (8 %)	6.6 ± 0.6 (9 %)	189 ± 3 (2 %)	510 ± 6 (1 %)
Y	53 ± 5 (9 %)	< 22	635 ± 326 (51 %)	129 ± 60 (47 %)	40 ± 4 (10 %)	< 22	545 ± 113 (21 %)	881 ± 189 (21 %)	22 ± 2 (9 %)	< 22	313 ± 13 (4 %)	625 ± 10 (2 %)
Gd	8.6 ± 0.9 (10 %)	5 ± 1 (20 %)	132 ± 69 (52 %)	27 ± 12 (44 %)	7.7 ± 0.8 (10 %)	< 1	120 ± 29 (24 %)	214 ± 45 (21 %)	3.9 ± 0.4 (10 %)	< 1	60 ± 1 (2 %)	130 ± 2 (2 %)
Dy	8.8 ± 0.9 (10 %)	5 ± 2 (40 %)	126 ± 66 (52 %)	28 ± 10 (36 %)	7.2 ± 0.7 (10 %)	< 2	108 ± 24 (22 %)	171 ± 36 (21 %)	4.0 ± 0.4 (10 %)	< 2	62 ± 4 (6 %)	124 ± 3 (2 %)
Ho	1.8 ± 0.2 (11 %)	< 2	27 ± 14 (52 %)	6 ± 2 (33 %)	1.5 ± 0.2 (13 %)	< 2	22 ± 3 (14 %)	35 ± 7 (20 %)	0.9 ± 0.1 (11 %)	< 2	13.4 ± 0.6 (4 %)	25.6 ± 0.9 (4 %)
Th	8.6 ± 0.9 (10 %)	< 7	97 ± 41 (42 %)	41 ± 15 (37 %)	3.2 ± 0.3 (9 %)	< 7	63 ± 12 (19 %)	136 ± 16 (12 %)	0.60 ± 0.06 (10 %)	< 7	13.3 ± 0.6 (5 %)	34 ± 1 (3 %)
U	2.3 ± 0.2 (9 %)	< 1	27 ± 12 (44 %)	4 ± 1 (25 %)	1.7 ± 0.2 (12 %)	< 1	20 ± 4 (20 %)	32 ± 5 (16 %)	0.50 ± 0.05 (10 %)	< 1	5.6 ± 0.4 (7 %)	20 ± 1 (5 %)

Limit of detection is used in the table

*n.d. means “not determined” due to the losses of Si as volatile SiF_4 during digestion of bulk samples with HF

In NP fractions separated by sedimentation, most of the elements could be detected expect Ni, Cu, As, Sn, Te, and Hg in Puyehue sample, Cd and Sn in Tolbachik sample and As, Se, Sn and Bi in Klyuchevskoy sample due to concentrations under limits of detection. RSD ranged from 6% to 52% for Puyehue (the majority of element concentrations being associated to a RSD around 50%) from 3% to 24% for Tolbachik samples and from 0.7% to 18% for Klyuchevskoy sample.

In NP fractions separated by CTFFF, all monitored elements were detected for Tolbachik and Klyuchevskoy samples. Concerning Puyehue sample, 2 major (K and Ca) and 5 trace (As, Se, Cd, Sn, Te) elements were not detected. However, from dimensional analysis, we explained above (3.1.) that there were some losses of NP fraction for Puyehue sample due to adhesion of NPs to the tube wall. Therefore, the amount of recovered NPs was not enough to detect all the elements. RSD ranged from 6% to 47% for Puyehue from 3% to 30% for Tolbachik samples and from 1% to 21% for Klyuchevskoy sample.

In general, all this highlights that the concentrations of all trace elements in NP fractions separated by CTFFF were systematically higher than the concentrations in the fractions separated by sedimentation for Tolbachik and Klyuchevskoy samples. It was not the case for Puyehue sample due to the interaction of NPs with the tube wall during separation by CTFFF. In addition, in Fig 1, it can be seen that the NP fractions separated by sedimentation contained an additional population of particles in the range 400-900 nm. However, on the one hand, in Table 1, trace element concentrations were higher for CTFFF compared to sedimentation. This means that CTFFF enabled more NPs < 400 nm to be recovered than sedimentation. On the other hand, it is interesting to note that despite the interactions of Puyehue particles with the tube wall during CTFFF separation, concentrations (Table 6) were anyway more important than those obtained using filtration method. Therefore, CTFFF caused less NP losses than filtrations and so the separation was more quantitative.

The comparison of RSD considers that repeatability was the worst using filtration as separation method for all samples. In case of Tolbachik and Klyuchevskoy samples, which were not impacted by interaction bias using CTFFF, the RSD values were lower than for Puyehue one. Moreover, RSD were comparable using sedimentation and CTFFF, with a slight tendency to be higher with CTFFF. The maximal value of RSD can be directly linked to the heterogeneity of ashes from which NP fractions were prepared and to the repeatability of the separation method. Thus, Klyuchevskoy appeared to be the most homogeneous sample, closely followed by Tolbachik sample and then Puyehue sample which stand out clearly from the others two ashes. In the same way, sedimentation

seemed to be the most repeatable separation method, closely followed by CTFFF and then filtration, which has not to be recommended to use if the objective is to get a representative information of the whole NP fraction because of the high losses of NPs on the filter.

3.1.3 Weight characterization of bulks and nanoparticle fractions

The weights of NPs in all samples separated by all the different methods were calculated and the results are given in Table 7. The trend observed for NP weights in these samples is in agreement with the trend for elemental concentrations (see *3.2.*) given the calculation of these weights was taken from elemental concentrations. As is seen, the weights of fractions separated by filtration were one order of magnitude lower than the weights of fractions separated by sedimentation and CTFFF. It is to be noted that the weight of NPs separated by filtration of Klyuchevskoy ash was underestimated by using the above-described element-based approach. Indeed, Si, which is the main constitutive element of ashes (SiO_2: 45 – 55%) [118], could not be determined due to small amount of separated NPs. The weight and associated RSD of NPs of Klyuchevskoy and Tolbachik ashes separated by sedimentation and CTFFF were not significantly different. Nevertheless, the weight of Puyehue NPs recovered by CTFFF (0.06 ± 0.02 mg) was about 3 fold lower than this separated by sedimentation (0.22 ± 0.09 mg) and 2 fold higher than this separated by filtration (0.03 ± 0.01 mg). These differences are in agreement with dimensional and elemental information already discussed in the previous parts (NP interactions with tube wall).

Table 7. Calculated weights of NPs separated from volcanic ash samples using filtration, sedimentation, and CTFFF methods

Sample name	Calculated weight of NP fractions, mg(NPs)		
	Filtration	Sedimentation	CTFFF
Puyehue	0.03 ± 0.01	0.22 ± 0.09	0.06 ± 0.02
Tolbachik	0.03 ± 0.01	0.38 ± 0.06	0.45 ± 0.07
Klyuchevskoy	0.017 ± 0.001	0.31 ± 0.03	0.51 ± 0.05

Thus, in the present part of work, the NP fractions of volcanic ashes separated by filtration, sedimentation, and CTFFF were characterized by laser diffraction and electron microscopy methods and analyzed by ICP-MS and ICP-AES. Filtration and CTFFF provided the separation of particles less than 400 nm. The fractions separated by sedimentation were also mainly represented by NPs, which were less than 400 nm; however, this fraction also contained a scarce population of submicron particles (≤ 5%) in the range of 400–900 nm.

The filtration method provided low recoveries of NPs. Indeed, only fine NPs were separated using filtration while larger ones were retained on the filter. As a consequence, the elemental analysis of NP fractions recovered by filtration provided concentrations systematically inferior to those obtained for NP fractions recovered by sedimentation and CTFFF. Most of the trace element concentrations were under limits of detection. Moreover, RSD associated to concentrations were higher for NP fraction separated by filtration than those for NP fraction separated by sedimentation and CTFFF. Thus, filtration enabled separated fraction to be representative to the smaller NP fraction only. Therefore, even though the filtration remains the easiest and the fastest method to use, it is also the least repeatable and the least representative with regard to the NP fraction.

The sedimentation method is commonly used but is time-consuming (48 h). However, this method enabled separated fraction to be representative with regard to the NPs, However, the separated fraction contained a low amount (< 5%) of particles with size between 400 and 900 nm. The repeatability was also high using this method.

Finally, the CTFFF method enabled the fractionation time to be decreased down to 2 h; nevertheless, it required the use of special equipment (planetary centrifuges). This method enabled separated fraction to be representative with regard to the NP fraction with a control of the maximal recovered NP size (400 nm). As NP fractions were more concentrated in CTFFF, this method enabled the separation to be more efficient. The repeatability was slightly lower than with the sedimentation method. The limitation of this method appeared to be the possible interactions between particles as well as between particles and tube wall during the separation process. The main reasons of these interactions can be mineral compositions of separated particles, their surface properties in aqueous suspensions, and an action of centrifugal forces. Nevertheless, these interactions were less critical than the interactions observed between particles and filter using the filtration method.

As a general conclusion to this part of work, CTFFF looks to be the most promising method for the separation of NPs followed by their quantitative elemental analysis. Nevertheless, sedimentation as well as CTFFF can be applied, in particular, to the separation of environmental NPs for their further fractionation and dimensional and elemental characterization using hyphenated methods based on the flow FFF coupled to the laser light scattering detector and ICP-MS.

3.2 Reliability of direct ICP-MS analysis of volcanic ash nanoparticles

For the comprehensive characterization of volcanic ash NPs, a hyphenated technique can be applied. In this case the direct ICP-MS analysis of volcanic ash nanoparticles in the effluent from the separation technique is required. In the present part of work, the ICP-MS determination of major and trace element in suspensions of volcanic ash nanoparticles was carried out after either the acid digestion of the suspensions or using the direct ICP-MS analysis of these suspensions. The results obtained were compared. For confirming the reliability of the direct analysis of NP suspensions by ICP-MS, the digestion procedure under the most severe conditions (the matrix is fully mineralized) was used in the case of "indirect" analysis.

The suspensions of NPs were separated form volcanic ash samples by sedimentation technique. The dimensional characterization of the recovered was described earlier (see *3.1.1*).

NPs of volcanic ash due to high specific surface area and reactivity may sorb trace elements including toxic ones from volcanic gases [6]. This is why exhaustive determination of non-constituent trace element concentrations in NPs is extremely important due to their possible adverse effects to human health and ecosystems [3,11]. The results of the determination of the concentrations of major and trace elements in the suspensions of volcanic ash NP fractions by direct and indirect ICP-MS analyses are given in table 8. In addition, in this table, the uncertainties (U), the relative standard deviation and the relative accuracy bias (B) are presented. The concentrations obtained using both methods were compared except for Sn, Te and Bi, which could be determined only by direct analysis for all samples due to the absence of evaporation and dilution steps as compared to the digestion procedure (concentrations <LOD for indirect analysis). Indeed, the direct analysis enables a sensitivity gain of a factor up to 10 to be obtained compared to the indirect analysis method. For the same reason, the comparison could be made for Ni, Se and Th only for some samples. When the comparison was possible, the presence of a maximum bias of 13%, 10% and 2% can be observed for Puyehue, Tolbachik and Klyuchevskoy NP suspension analysis, respectively. Concerning Klyuchevskoy NP suspension, the majority of concentrations are not significantly different. Only those of Fe and Ce are different, but the accuracy bias was low (inferior to 2%). It is interesting to note that the suspensions from which the biases are both the most numerous and the most important are those from Puyehue and Tolbachik. This suggests that the biases observed come from the nature of the samples and not from the methods used. For Puyehue NP suspension in particular, the concentrations obtained by direct analysis are very often lower than those obtained after acid digestion. One reason for this systematic underestimation

could be the incomplete mass transfer of the elements contained in these NPs when they are not digested. This is not the case for Tolbachik and Klyuchevskoy NP suspensions. In general, for all elements and regardless of the sample considered, the relative accuracy bias is either not significant or less than 10%, except for Pb in the Puyehue sample (13%). The limit value of 10% was considered as a maximum acceptable deviation (MAD) given:

(i) The diversity of mineral phases forming NPs and hence uneven distribution of matrix elements in NP phases (for example, monazite can accumulate light rare earth elements (REE) and cause variations in their concentrations [133]);
(ii) Nanoparticles are not all identical in elemental composition and size; so in direct analysis the sample analyzed (suspension) varies during the introduction time and therefore is less representative of the entire sample than when the sample is analyzed after acid digestion (solution).

Therefore, concentrations presenting a MAD inferior to 10% were considered to be in agreement.

Concerning the relative standard deviation, the acid digestion of suspensions gave RSD over 9% for Pr, Gd, Ho and Pb concentrations in Puyehue ash NP suspension, and only for Pb concentration in Klyuchevskoy ash NP suspension. For all other elements in all samples the RSD were ranging from 1 to 6%. The acid digestion RSD estimates the analytical procedure repeatability (from preparation to ICP-MS analysis) and the heterogeneity of the ash NP suspension samples. The high RSD values obtained for Pb in Puyehue and Klyuchevskoy ash NP suspensions can be explained by the low concentrations of Pb in these samples, which are closed to the limit of detection, knowing that limits of detection are higher for indirect analysis. The high RSD for Pr, Gd and Ho in Puyehue sample cannot be explained by their limits of detection, given the concentrations of these elements are lower in the other samples and however are associated with RSD < 6%. One hypothesis is that the constitution of nanoparticles could have an impact on the repeatability. In the case of the direct analysis of acidified suspensions, the RSD was in the range 2-14%. This RSD estimates both the repeatability and sample heterogeneity, as well as the heterogeneity of the suspension in terms of uneven distribution of elements between particles. These observations are consistent with the observed relative accuracy biases that depend on the nature of the sample.

Therefore, it has shown that the concentrations of major and trace elements determined in the samples of volcanic ash NP fractions by a direct ICP-MS analysis are in agreement with those determined after acid digestion in an autoclave. The results show that suspensions of

Klyuchevskoy volcanic ash NP can be directly analysed by ICP-MS without digestion, the concentrations being not significantly different for direct and indirect analysis. The direct analysis is also possible for most elements of the other two samples whose concentrations in direct and indirect analysis are not significantly different. For other elements, the direct analysis is possible provided that a maximum acceptable deviation has been first defined. As a general conclusion, for an unknown sample, the direct analysis can be performed after assessing the accuracy bias. This opens interesting perspectives for future investigations and comprehensive studies using combined dimensional and elemental characterization based on ICP-MS.

In the present part of this work it has been shown that the concentrations of major and trace elements determined in the samples of volcanic ash NP fractions by a direct ICP-MS analysis are in agreement with those determined after acid digestion in an autoclave. The direct analysis enables the numerous steps of digestion, evaporation and dilution to be avoided. Besides, the advantage of the direct ICP-MS analysis is that generally lower limits of detection can be achieved as compared to the analysis after acid digestion. Some trace elements, which are potentially toxic (for instance Te and Bi), can be determined only by the direct analysis. The results show that suspensions of Klyuchevskoy volcanic ash NP can be directly analysed by ICP-MS without digestion, the concentrations of elements are not significantly different for the direct and indirect analyses. The direct analysis is also possible for most elements of the other two samples (Al, Y, Ce, Ho, Cu, Se, Tl, Pb, Th of Tolbachik sample, Y, La, Ce, Pr, Gd, Tl, Th of Puyehue sample); concentrations determined by the direct and indirect analysis being not significantly different. For other elements (Fe, La, Pr, Gd, Ni of Tolbachik sample, Al, Fe, Ho, Cu of Puyehue sample), the direct analysis is possible, however, maximum acceptable deviation has to be assessed. It can be concluded that for an unknown sample, the direct analysis can be performed after assessing the accuracy bias. This opens interesting perspectives for comprehensive studies using combined dimensional and elemental characterisation based on laser light scattering and ICP-MS.

Table 8. Concentration of elements in NP fraction from Puyehue, Tolbachik, and Klyuchevskoy volcanic ashes as obtained by ICP-MS (mean ± U* and RSD** into brackets)

Element	LOD		Puyehue			Tolbachik			Klyuchevskoy		
	Direct analysis	After digestion	Direct analysis	After digestion	Relative accuracy bias	Direct analysis	After digestion	Relative accuracy bias	Direct analysis	After digestion	Relative accuracy bias
1	**2**	**3**	**4**	**5**	**6**	**7**	**8**	**9**	**10**	**11**	**12**
	mg L^{-1}				***%***	***mg L^{-1}***		***%***	***mg L^{-1}***		***%***
Al	0.002	0.01	0.23 ± 0.02 (4 %)	0.29 ± 0.01 (2 %)	10	1.1 ± 0.1 (5 %)	1.18 ± 0.02 (1 %)	no bias	1.1 ± 0.1 (5 %)	1.14 ± 0.04 (2 %)	no bias
Fe	0.01	0.02	0.10 ± 0.01 (5 %)	0.123 ± 0.002 (1 %)	9	1.3 ± 0.1 (4 %)	1.59 ± 0.02 (1 %)	10	0.62 ± 0.08 (6 %)	0.73 ± 0.02 (1 %)	1
	µg L^{-1}				***%***	***µg L^{-1}***		***%***	***µg L^{-1}***		***%***
Y	0.001	0.001	0.13 ± 0.02 (8 %)	0.17 ± 0.02 (6 %)	no bias	0.4 ± 0.1 (13 %)	0.40 ± 0.01 (1 %)	no bias	0.19 ± 0.02 (5 %)	0.21 ± 0.02 (5 %)	no bias
La	0.002	0.002	0.10 ± 0.02 (10 %)	0.12 ± 0.01 (4 %)	no bias	0.4 ± 0.1 (13 %)	0.28 ± 0.01 (2 %)	4	0.11 ± 0.03 (13 %)	0.07 ± 0.01 (6 %)	no bias
Ce	0.002	0.002	0.22 ± 0.06 (13 %)	0.27 ± 0.02 (4 %)	no bias	0.8 ± 0.2 (13 %)	0.58 ± 0.02 (2 %)	no bias	0.18 ± 0.01 (3 %)	0.164 ± 0.002 (1 %)	2
Pr	0.001	0.003	0.028 ± 0.004 (7 %)	0.035 ± 0.006 (9 %)	no bias	0.073 ± 0.004 (3 %)	0.081 ± 0.001 (1 %)	4	0.028 ± 0.004 (8 %)	0.023 ± 0.003 (6 %)	no bias
Gd	0.001	0.001	0.04 ± 0.01 (14 %)	0.04 ± 0.01 (11 %)	no bias	0.11 ± 0.02 (10 %)	0.084 ± 0.002 (1 %)	5	0.036 ± 0.002 (3 %)	0.033 ± 0.003 (5 %)	no bias
Ho	0.0004	0.001	0.0051 ± 0.0004 (4 %)	0.007 ± 0.001 (11 %)	7	0.015 ± 0.002 (7 %)	0.015 ± 0.002 (6 %)	no bias	0.008 ± 0.001 (6 %)	0.010 ± 0.001 (5 %)	no bias
Ni	0.1	1	< LOD	< LOD	n.d.***	13.6 ± 0.5 (2%)	16 ± 1 (3%)	6	< LOD	< LOD	n.d.***
Cu	0.3	1	2.4 ± 0.1 (2%)	2.0 ± 0.1 (3%)	10	14 ± 2 (7%)	15 ± 1 (3%)	no bias	7 ± 2 (14%)	6.5 ± 0.8 (6%)	no bias
Se	0.3	0.9	< LOD	< LOD	n.d.***	11 ± 1 (5 %)	10 ± 1 (5 %)	no bias	1.5 ± 0.2 (6 %)	< LOD	n.d.***
Sn	0.03	0.1	0.19 ± 0.04 (11%)	< LOD	n.d.***	0.33 ± 0.08 (12%)	< LOD	n.d.***	0.23 ± 0.01 (2%)	< LOD	n.d.***

Table 7 (continued)

1	2	3	4	5	6	7	8	9	10	11	12
Te	0.01	0.02	< LOD	< LOD	n.d.***	0.12 ± 0.02 (8 %)	< LOD	n.d.***	0.09 ± 0.02 (10 %)	< LOD	n.d.***
Tl	0.001	0.002	0.06 ± 0.01 (8%)	0.063 ± 0.001 (1%)	no bias	0.24 ± 0.01 (2%)	0.21 ± 0.02 (5%)	no bias	0.065 ± 0.006 (5%)	0.064 ± 0.004 (3%)	no bias
Pb	0.1	0.2	0.61 ± 0.06 (5%)	0.4 ± 0.1 (13%)	13	1.34 ± 0.08 (3%)	1.2 ± 0.1 (4%)	no bias	0.37 ± 0.05 (7%)	0.32 ± 0.08 (13%)	no bias
Bi	0.01	0.02	0.06 ± 0.02 (13 %)	< LOD	n.d.***	0.157 ± 0.008 (2 %)	< LOD	n.d.***	0.04 ± 0.01 (12 %)	< LOD	n.d.***
Th	0.004	0.004	0.027 ± 0.006 (12 %)	0.030 ± 0.002 (3 %)	no bias	0.04 ± 0.01 (11 %)	0.049 ± 0.002 (2 %)	no bias	< LOD	< LOD	n.d.***

* *U* is expanded uncertainty calculated as $k \times SD$ $(k = 2)$ according to Eurachem/CITAC guide: Quantifying Uncertainty in Analytical Measurement [134]

** *RSD* is the relative standard deviation calculated from the three replicates

*** n.d. means not determined because at least one of concentrations measured by indirect and direct analyses were under the LOD

3.3 Characterization of volcanic ash nanoparticles and study of their fate in aqueous medium by asymmetric flow field-flow fractionation – multidetection

The objective of the present part of work is to implement an analytical strategy based on the multidetection offering the possibility of dimensional and elemental characterization of nanoparticles of volcanic ash in their size continuum. Thus, (i) the nanoparticulate fraction of a volcanic ash sample was characterized by identifying the different populations, and (ii) the temporal fate of these different populations was investigated in terms of dissolution, aggregation and settling out.

Klyuchevskoy ash sample was considered for this study. It was chosen because (i) it is among the volcanoes producing the most ash on Earth; (ii) the methods for the chemical characterization were previously developed and are validated; and (iii) the elemental composition of its ash, and in particular of the separated nanoparticle fraction is known. In addition, the repeatability of results of the separation and elemental analysis of Klyuchevskoy nanoparticle fraction was the highest among the studied ash samples. The ash of the Klyuchevskoy volcano can therefore serve as a test sample for a more detailed physico-chemical evaluation of its nanoparticle fraction, which is of environmental, morphological, and biogeochemical interest.

The elemental content was exhaustively described in sections *3.1.2* and *3.2*. Briefly, the major element content of ash was: aluminum (Al, (86 ± 9) mg g^{-1}) and iron (Fe, (62 ± 6) mg g^{-1}); silicon (Si), was also present (determined in the nanoparticle fraction by direct elemental analysis) but could not be determined accurately in the ash due to the formation of volatile components during the mineralization step. These major elements were under oxide forms, expected to represent at least 15% (Al_2O_3), about 10% (Fe_2O_3), and 50% (SiO_2) respectively, according to the usual distribution observed in basaltic volcanic ash. REE, which are also constitutive of ash, were found in this material, especially lanthanum (La, (7 ± 1) µg g^{-1}). In addition, the main trace element (in terms of concentration) detected in this ash was copper (Cu, (68 ± 7) µg g^{-1}).

3.3.1 Comparison of volcanic ash particle sedimentation process in deionized water and a synthetic river water

The nanoparticle fraction was recovered from Klyuchevskoy ash sample by sedimentation using two aqueous solutions (synthetic river water and deionized water) as was mentioned. Results of PSD measured depending on time of sedimentation are given in figure.

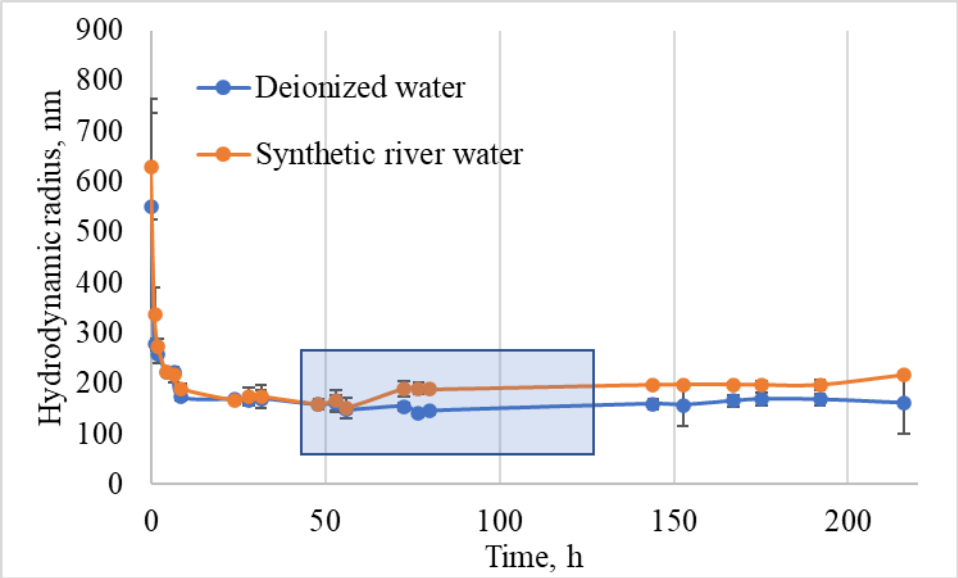

Figure 9. Monitoring of the suspension generated with deionized water and synthetic river water. The blue rectangle represents the selected 72-hour study area, indicated from 0 to 72 hours in the text, for simplicity

The choice of these “simple solutions” was motivated by the objective of intrinsically characterizing nanoparticles and their properties, which is a prerequisite for particle knowledge. Thus, the suspension monitoring revealed similar behaviour with both solutions: first a rapid decrease in size for 9 hours, then stabilization from 48 hours with a very slow increase at least for 130 hours, and then a faster increase. In this last part of the curve, the standard deviation associated with the radius also appeared larger, which generally corresponds to the presence of aggregates. As a result, deionized water and a settling time of 48 hours were used to generate the suspension (hereafter named “initial suspension”). The settling time of 48 hours is in agreement with calculation with the Stokes law, giving similar time for a micrometric cut-off. Operationally, this means that after 24h mixing and 48h of sedimentation, the supernatant taken as the initial suspension was collected (15 mL) for the rest of the study. Then, the study was conducted over 72 hours.

The repeatability of the preparation of the initial suspension was evaluated from 10 independent sub-aliquots: it was 7% in amount of NP generated. The curves representing the particle size as a function of time were similar, with r = 0.9584 and a variation of 5% in maximum size from one

distribution to another. The main characteristics of the initial suspension of the ash nanoparticle fraction were: conductivity of (9.1 ± 0.1) µS cm^{-1}, pH of (6.8 ± 0.1) and Zeta potential of (–40 ± 1) mV.

3.3.2 Dimensional and elemental characterization

The characterization carried out by A4F-UV-MALS-ICP-MS enabled the sets of fractograms presented in Fig. 1 to be obtained. The profile of all the fractograms is similar, with 3 maxima, suggesting the presence of 3 main peaks related to 3 populations of nanoparticles. To refine this observation, increase the resolution and thus better define these 3 populations, the signals were deconvoluted. The corresponding peaks, identified as P1, P2 and P3, are presented on the UV-Vis fractogram only (Figure 10) for clarity reason. Complementarily, Table 9 (Part A) presents the dimensional characteristics of these 3 populations. They appear polydisperse with ranges of sizes (second column in Table 9) larger than 100 nm in gyration radii (rG), whatever the population considered. The comparison of this size range with the value of rG at the top of the peak confirms the slight asymmetry of P1 (tailing) and P2 (leading), observed in Figure 10, while P3 is symmetrical. This suggests size distributions and/or hydrodynamic behaviour specific to each population of nanoparticles corresponding to these peaks. From an analytical point of view, these three populations were significantly separated, with resolution factors of (1.01 ± 0.11) and (0.58 ± 0.08) between P1 and P2, and P2 and P3 respectively. In addition, focusing on the first part of the rG curve (part corresponding to a uniform variation of the grey curve plotted at the top of Figure 10) and adjusting the variations of rG exponentially, the selectivity varied from 0.76 to 0.47. The variation of the gyration radius over the entire fractionated range does not appear uniform: there is a discontinuity with a change of slope around 15.5 min, which corresponds to the top of the peak P2. Compared with the variation of the rG of the standard nanospheres, the radius of gyration thus tended to increase more rapidly than expected up to the peak of P2 (i.e. between about 10 and 15.5 min), then less quickly afterwards (i.e. from 16 to 20 min). This particular profile suggests that the elution behaviour in the A4F channel is dependent on the populations. The elution behaviour may be related to the NP internal mass distribution (because of the NP shape and/or constitution heterogeneity), and/or to NP interactions with the separation channel A4F membrane. Usually, the observed interactions between inorganic nanoparticles and membrane are mainly attributed to the surface electrical charge of nanoparticles rather than purely to their chemical composition. However, the electrical charge depends on the composition and structure of the surface material, as well as the size and shape of the nanoparticles [51]. So, and by anticipating the chemical characterization below, the singular hydrodynamic behaviour of P2 is necessarily related to the

morphological difference (i.e. the difference in shape and/or structure) of this population compared to P1 and P3. The elution slightly faster than would be expected would then originate from (i) an internal mass distribution so heterogeneous that it gave the nanoparticles P2 a tumbling motion and/or (ii) a negative surface electric charge greater than those of the other populations, inducing more repulsion with the membrane and therefore a higher position in the A4F channel.

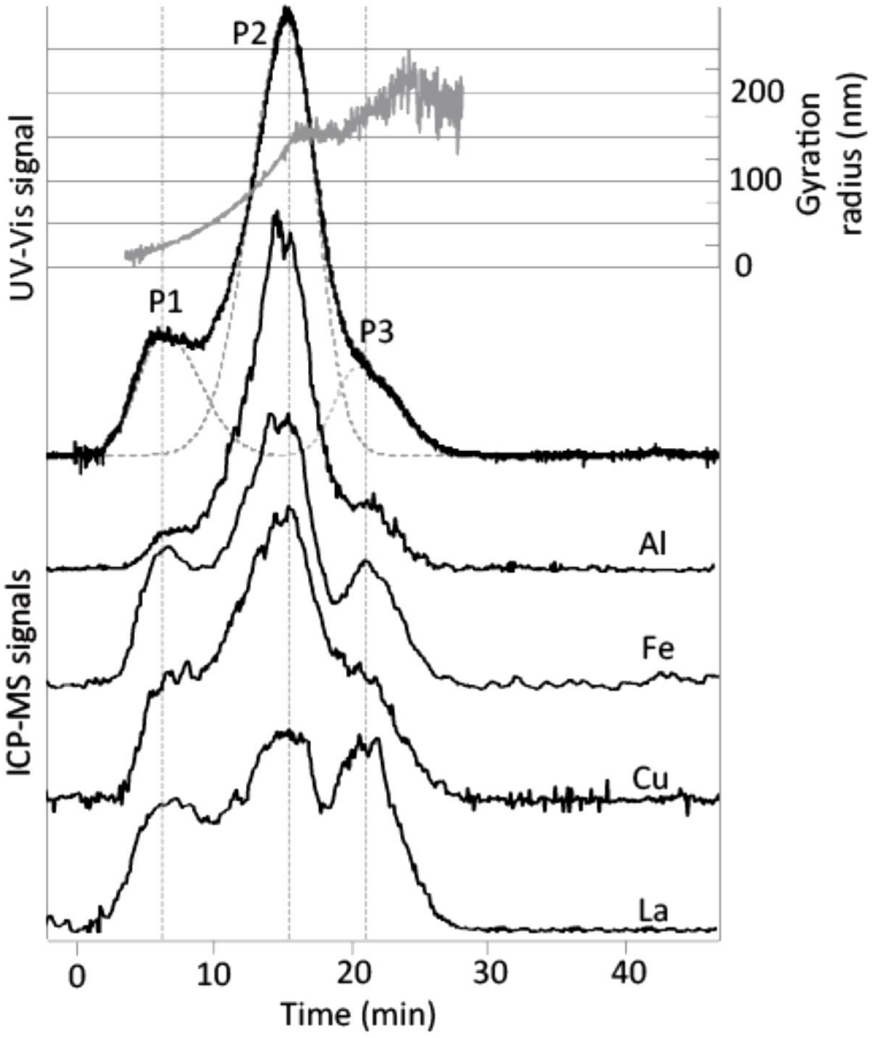

Figure 10. Typical fractograms of the initial suspension of the Klyuchevskoy volcano ash nanoparticle fraction, with the three deconvolved populations (P1, P2 and P3).

Table 9. Main dimensional characteristics and elemental composition of NPs and NP deconvoluted populations from Klyuchevskoy volcanic ashes

	A) Dimensional			B) Concentrations (average ± SD (RSD), in μg L^{-1} of suspension [(2)]) and *recoveries (R ± SD %)*				
	Gyration radii (nm)		Shape index		Major elements		Trace elements	
	At the peak top	Min-Max [Range] at the basis		Total NPs	Al	Fe	Cu	La
Total sample after "direct analysis" [(1)]				15500 ± 1500 (10%)	1100 ± 50 (5%)	620 ± 40 (6%)	7 ± 1 (14%)	0.110 ± 0.015 (13%)
Total sample	–		–	15148 ± 1621 (11%)	1075 ± 75 (7%)	618 ± 55 (9%)	5.76 ± 0.75 (13%)	0.076 ± 0.091 (12%)
Total fractionated sample *Recovery, R%*	–	5 – 250 [245]	–	14390 ± 1789 (12%) *95 ± 5%*	1109 ± 38 (4%) *103 ± 3%*	612 ± 15 (3%) *99 ± 2%*	5.66 ± 0.62 (11%) *98 ± 2%*	0.079 ± 0.010 (13%) *99 ± 2%*
P1	42 ± 4	10– 135 [125]	1.56 ± 0.07	2857 ± 353 (12%)	88.0 ± 3.1 (3%)	145.8 ± 4.4 (3%)	0.97 ± 0.11 (3%)	0.0199± 0.0026 (3%)
P2	137 ± 8	25– 205 [200]	1.95 ± 0.05	9623 ± 1190 (12%)	874 ± 31 (4%)	340 ± 10 (4%)	3.42 ± 0.38 (4%)	0.0328± 0.0043 (4%)
P3	185 ± 6	120–250 [130]	1.12 ± 0.07	1910 ± 236 (12%)	146.9 ± 5.1 (3%)	125.9 ± 3.8 (3%)	1.26 ± 0.14 (3%)	0.0262± 0.0034 (3%)

[(1)] NP and elemental concentrations from section *3.2*

[(2)] The elemental concentrations are expressed in mass of element per volume of suspension

The calculation of the index shape enables these differences to be quantified and therefore compared. Whatever the population considered, this indicator had a value greater than 1 (Table 9, third column) because of a faster elution than that of standard nanospheres. This result can be compared to the electron microscopy images (see micrographs of Klyuchevskoy NP fraction in Figure 8) and the resulting shape distribution. The distribution of nanoparticles observed as a function of their aspect ratio (ar) showed that one third of the NPs had an ar equal or greater than 1.5. The aspect ratio of an object is defined as the ratio between the longest dimension and the shortest dimension of the considered object. The obtained values of ar are given in Figure 11. These results confirm that the shape index values reflect a gap in sphericity of the nanoparticles of volcanic ash.

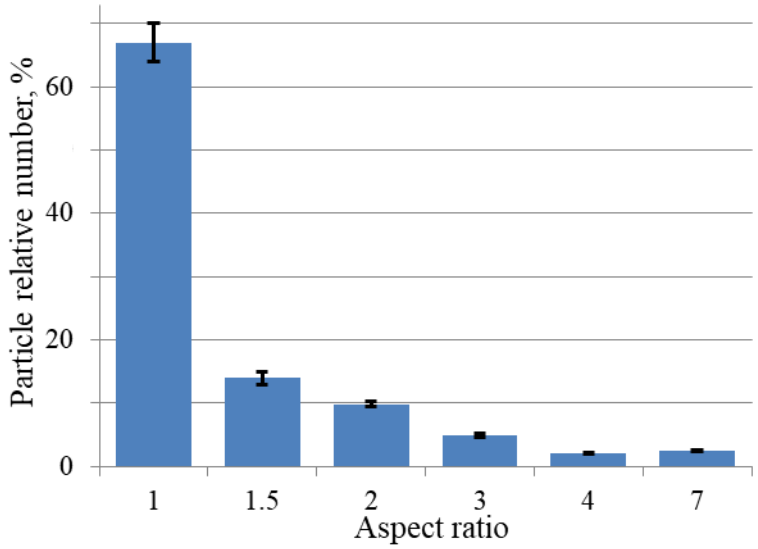

Figure 11. Morphological study; values of aspect ratio distribution of the observed particles from micrographs of Klyuchevskoy NP fraction

The dimensional characterization was completed by the consideration of the UV-Vis spectra. Indeed, the wavelength at the absorption maximum depends, among other things, on the size, geometry and structural state of the surface of the particles. The concavity of the spectrum can also give a size indication. The spectra selected at the top of the 3 peaks of the fractograms are shown in Figure 12. Their general shape with absorption maximum is typical for metal oxides such as silica, aluminum oxides and iron [121,135,136]. For P1, the absorption maximum is at a wavelength of 294 nm; the spectrum is also the most concave shaped (see Figure 12B). This confirms that the P1 population consists of particles of smaller mean size compared to the other two populations. Same absorption maxima at 300 nm and similar shape of the P2 and P3 spectra

suggest closer dimensional characteristics for these two populations. All this is in agreement with the gyration radius values presented in Table 9.

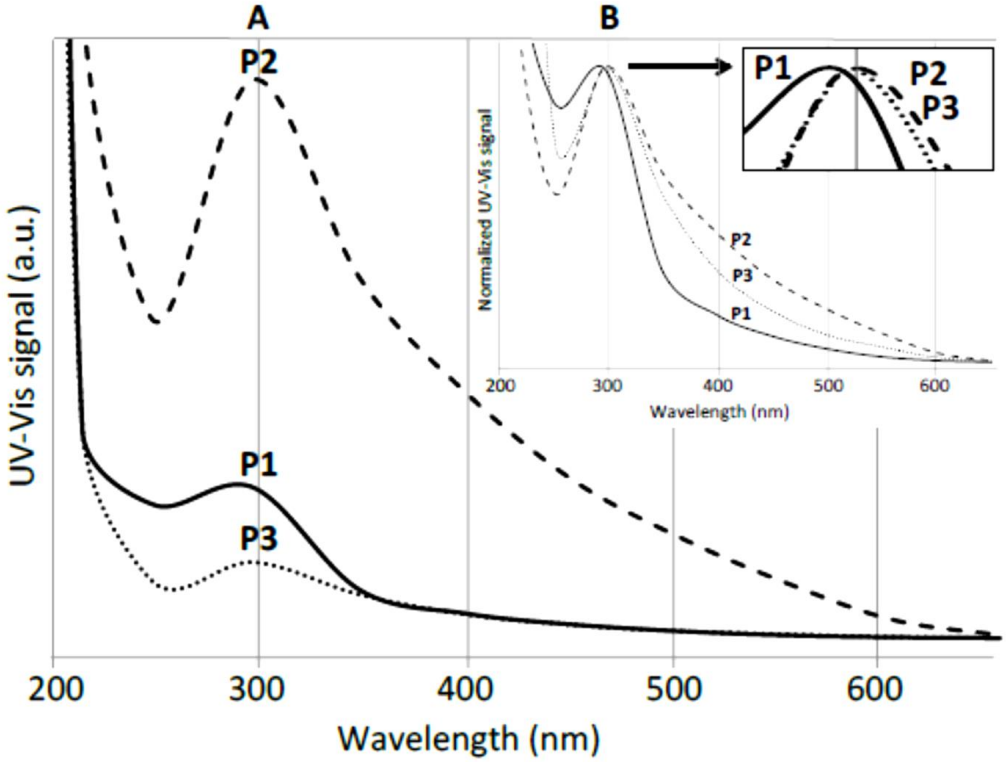

Figure 12. Typical UV-Vis spectra taken at the top of the 3 peaks (corresponding to the 3 populations P1, P2 and P3) of the fractogram of the initial suspension of the Klyuchevskoy volcano ash nanoparticle fraction, given as A) absolute and B) normalized.

All concentrations of nanoparticles and elements obtained in the initial unfractionated (bulk sample) and fractionated suspension, as well as in the 3 deconvoluted populations are reported in Table 9 Part B). The following information can be inferred from the examination of these concentrations:

(i) P1, P2 and P3 represent respectively 20, 67 and 13% of the nanoparticle fraction.

(ii) The recovery (R%) of 100% found for all the elements monitored (i.e. the elements were only present in the nanoparticle phase of the suspension) means there was no dissolution of the NPs during the preparation of the initial suspension.

(iii) Considering more particularly the 2 major elements monitored, it was possible to calculate the composition in the corresponding oxides in the 3 populations of NPs. The results obtained are

presented in Figure 13. The chemical distribution and therefore the concentrations within each population are specific to each of the 3 populations. In particular, the percentage of Al_2O_3 in P1 was 2.5 to 3 times lower than in P2 and P3, whereas the percentages of Cu and La in P3 was 2 times higher than in P1. The percentages of Fe_2O_3 and of La in P2 were the lowest of the 3 populations. To summarize, the distribution of elements that were constitutive or not, major or trace, was specific to each NP population identified. No correlation between the percentages of these different elements was found within each population. This is relevant regarding the fractograms of these 4 elements since they all have singular shapes. In addition, compared to the percentages in volcanic ash (in particular 16% Al_2O_3 and 9% Fe_2O_3), it can be seen that the distribution in P2 and especially in P1 was very different from that of the bulk.

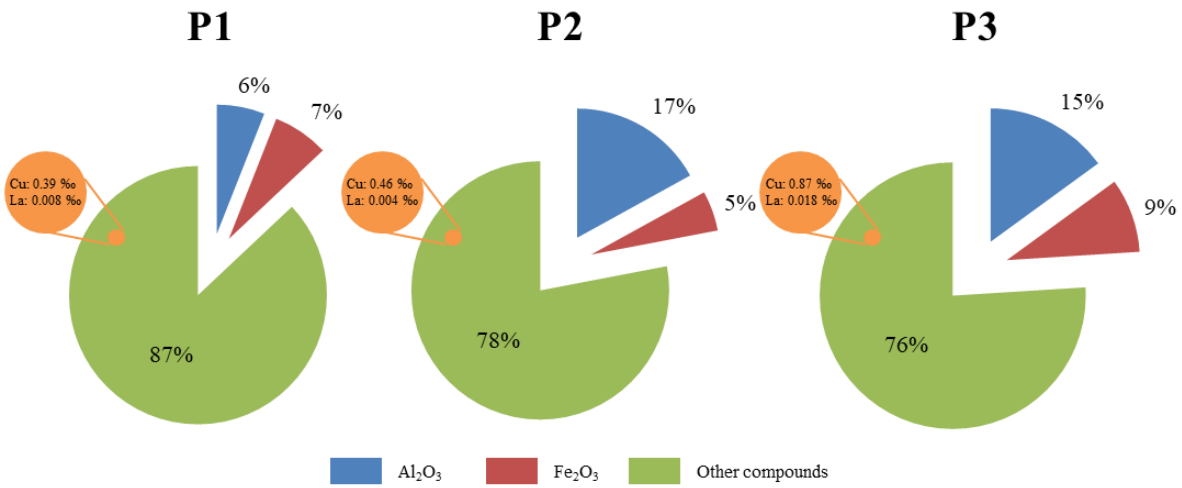

Figure 13. Distribution of elements and oxides in the populations P1, P2 and P3 in the initial suspension of the Klyuchevskoy volcano ash nanoparticle fraction. Precision is ±1 on the last digit of each percentage value

3.3.3 Temporal monitoring

To complete the acquisition of knowledge about nanoparticles of volcanic ash, their fate was monitored temporally. In particular, this involved evaluating the possible phenomena of dissolution, aggregation and/or sedimentation occurring in the suspension. Figure 14 presents the UV-Vis fractograms for visualizing these phenomena. In addition, Figure 15 aims to quantify these phenomena. It can be noted that:

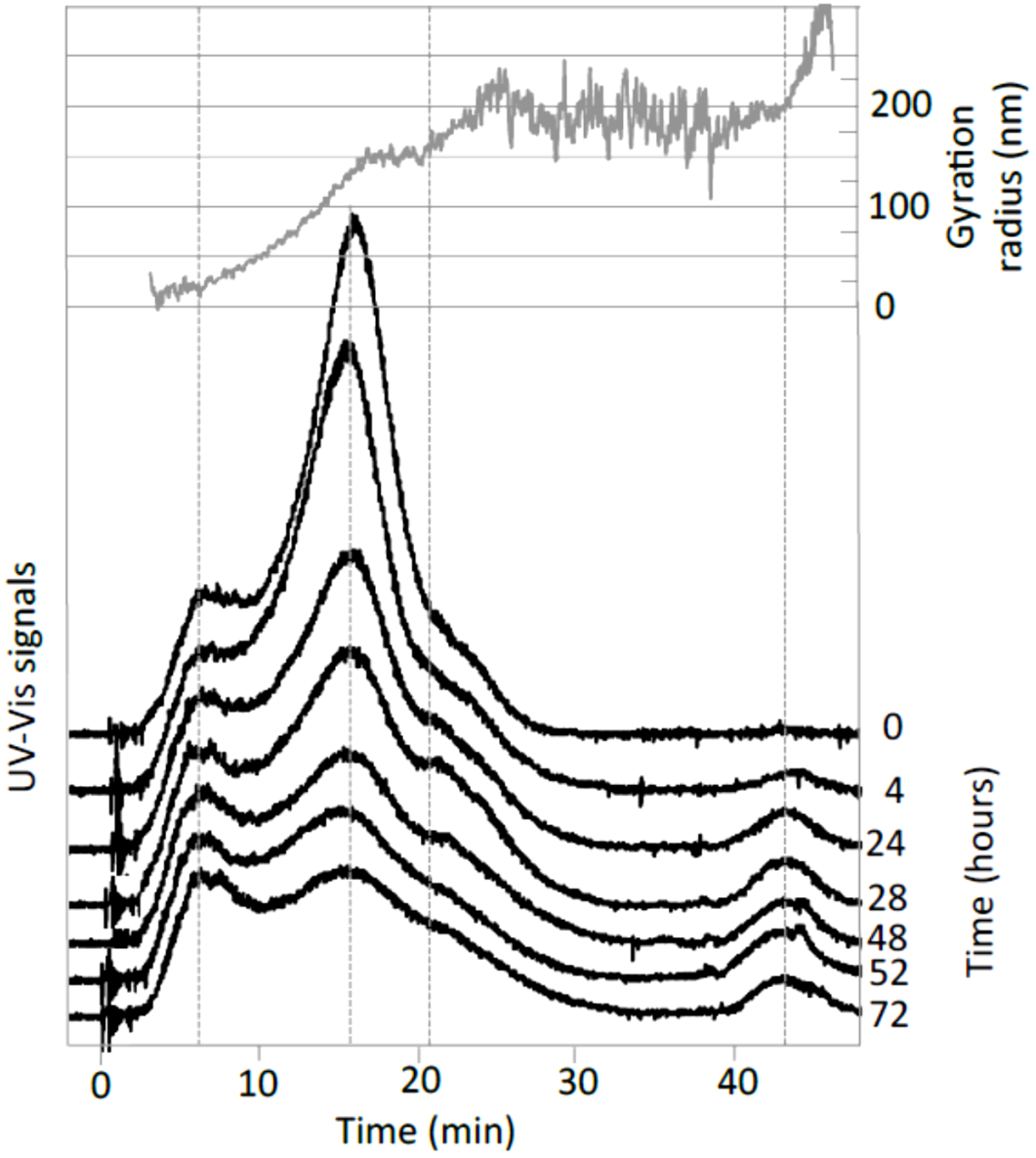

Figure 14. Fractograms showing the 72-hour evolution of the suspension of the Klyuchevskoy nanoparticle fraction. The variation in size as a function of the elution time reported (in gray, at the top) corresponds to 72 hours.

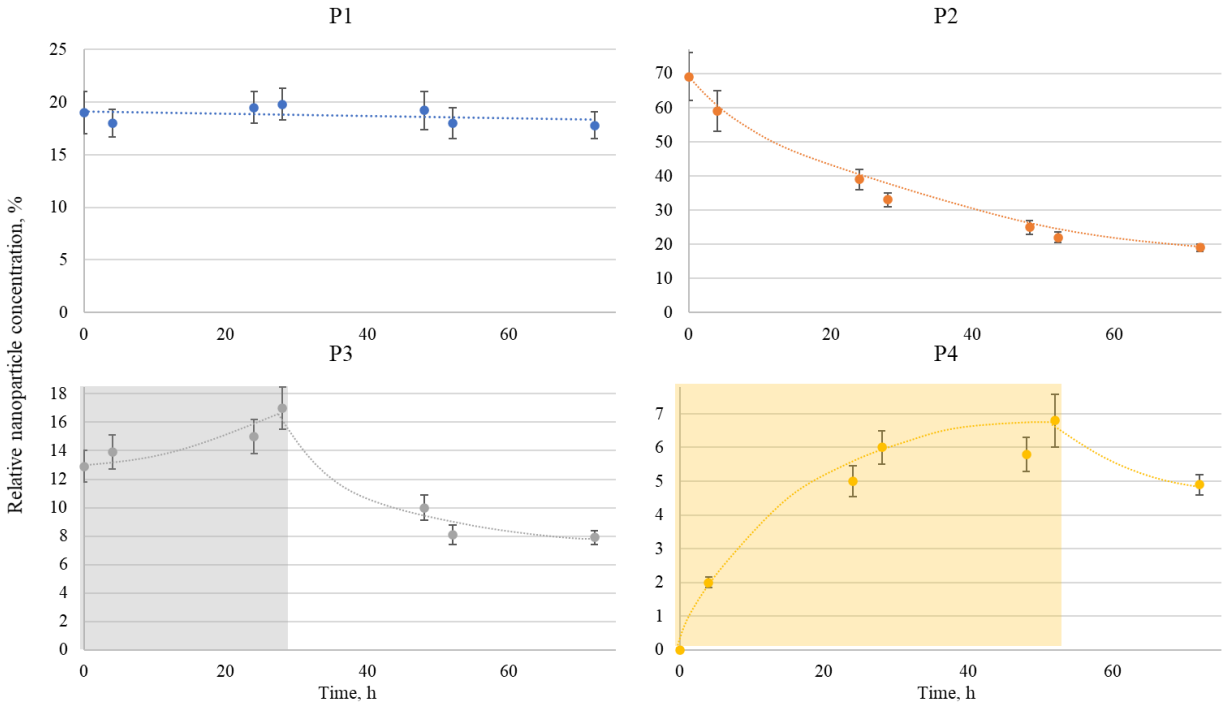

Figure 15. Evolution of the different populations identified in the suspension of the Klyuchevskoy nanoparticle fraction. The concentrations are given in percentage relative to the total concentration of nanoparticles in the initial suspension

(i) The rG variation as a function of the elution time (grey curve in Figure 10) changed little after 72 hours. In particular the discontinuity observed and previously discussed (attributed to the elution of P2) remained. This suggests that the observed populations do not change in terms of chemical composition/surface state/surface charge.

(ii) The concentration of the P1 population did not vary significantly ((96 ± 4)% remained in suspension at 72 hours). The P2 concentration decreased throughout the monitoring duration, with about 60% less NPs at 72 hours. Compared to the initial concentration, the P3 concentration first increased by about 25% at 28 hours (Figure 15), and then decreased by 25% at 72 hours. The decrease in P2 and P3 concentrations suggests either dissolution, or aggregation phenomena such that the nanoparticles no longer appeared in the population considered, nor even in the overall NP fraction in suspension due to settling out. However, it can also be noted that the recovery did not change during the monitoring, always remaining between 95 and 100%. This demonstrates that if there was loss of NPs in the suspension, it was not due to the dissolution of the nanoparticles. Concerning the apparent increase of P3 at the beginning of the monitoring, it could be due to the aggregation of P2, which would have produce objects eluting at the same time as P3. This is relevant given the shape of the P3 peak (Figure 14), which appears both higher and with a tailing towards larger sizes.

(iii) Simultaneously, the fourth population (P4) appeared on the fractograms after 40 minutes of elution. It corresponded to objects whose gyration radii were larger than the other populations, up to more than 300 nm. The slope of the rG variation also changed and became higher. This suggests that these objects had sizes that increased faster than expected, which is typical of aggregates [137]. The P4 concentration (UV-Vis) increased up to 52 hours, then decreased, as it can be seen both in Fig.4 (UV-Vis peak) and Figure 15 (curve shape). The existence of the 3 populations P1, P2 and P3 in the initial suspension and their temporal evolution, suggest that P4 resulted from an aggregation mainly of P2 NPs. The chemical distribution confirms this origin. Indeed, in the initial suspension, the Al/Fe ratio of P2 was 3.4; that of P3 was 1.6. In P4, this ratio was close to 3 in the first part of the temporal monitoring. P4 resulted from aggregation also involving P3 after 30 hours, the Al/Fe ratio then being between that of P2 and P3.

(iv) Beyond 50 hours, the P4 population also decreased. This suggests that the aggregation process progressively led to the formation of aggregates large enough to settle out of the suspension. Overall, the nanoparticle fraction in suspension decreased by approximately 40% after 72 hours of monitoring.

(v) The fact that the rG variation was similar between the initial state and after 72 hours suggests that the aggregation phenomena involved all the particles within the populations concerned, without sufficient size discrimination to be detected by MALS.

To complete these observations and attempt to distinguish "simple aggregation" (i.e. aggregates remained in the suspension) and aggregation with setting out, Figure 16 shows the UV-Vis spectra at the peak tops corresponding to the populations whose surface area varied significantly during monitoring (i.e. P2, P3 and P4). The spectra of the P1 population were not presented because they remained similar over time. Overall, the absorption maximum at 300 nm is observed for all populations and all times, which was expected with respect to the composition of NPs, consisting essentially of metal oxides.

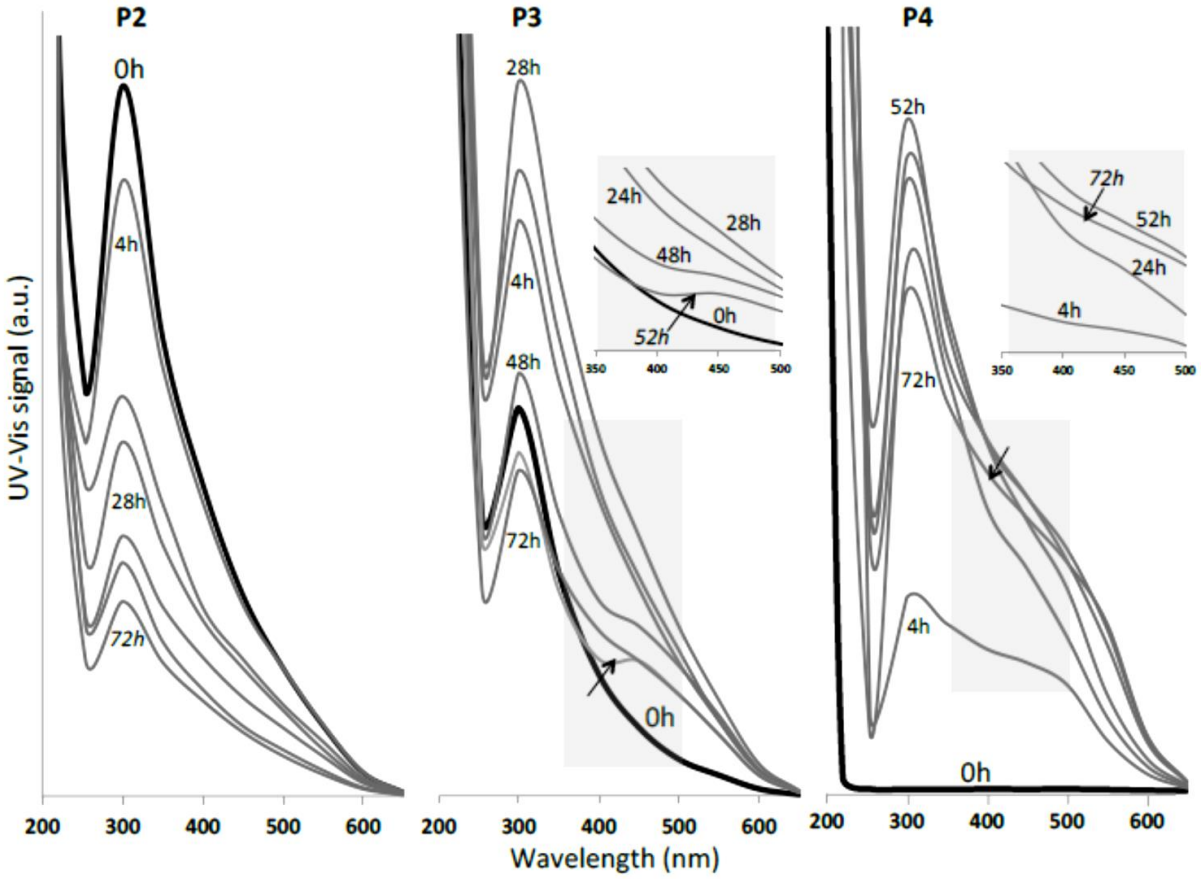

Figure 16. UV-Vis spectra at the top of the 3 peaks of the fractograms seen in Figure 14 (i.e. the 3 populations P2, P3 and P4).

For the population P2, the spectra intensity decreased without changing spectra shapes over time. This reflected a decrease in concentration without observable change in size. For P3, the spectra between 0 and 28 hours increased in intensity without changing shape. From 48 hours, the intensity decreased and a secondary peak appeared in the visible region at 450 nm. This was particularly observable at 52 hours (marked with an arrow in Figure 16) and less at 72 hours. This peak could be attributed to light scattering of aggregates. The concentration of aggregates was the highest at 52 hours. The UV-Vis spectra of population P4 were similar at all times when it was observed, with two maxima around 300 and 450-500 nm. This confirms that P4 resulted from the aggregation of P2 and/or P3: the particles both absorbed due to their surface chemical composition (close for P2 and P3) and scattered the light because of their size large enough to enable this phenomenon to be observed. This phenomenon remained significant at 72 hours (marked with an arrow in Figure 16), although the peak at 450-500 nm decreased slightly. It could further be observed on this spectrum that the peak at 300 nm decreased more significantly, the lower intensity of these 2 maxima reflecting a loss of suspended material, as also observed in Figures 14 and 15.

The implementation of AF4-UV–Vis-MALS-ICP-MS coupling thus enabled the following information to be acquired:

– The nanoparticle fraction of the Klyuchevskoy volcano ash initially contained 3 polydisperse populations, differing in size, composition with respect to monitored elements and behaviour in suspension in Milli-Q water at pH 6.8.

– This fraction did not dissolve over the study.

– The population of nanoparticles P1 represented approximately 20% by weight in the initial suspension and had gyration radii less than 140 nm. These nanoparticles remained in suspension without settling, and no phenomenon of aggregation could be observed for the 72 h of monitoring.

– The populations P2 and P3 represented approximately 80% by weight in the initial suspension (67 and 13%, respectively) and had gyration radii between 25 and 250 nm. These nanoparticles aggregated so that, at the end of the study, their concentration in suspension had decreased by 30 and 60%, respectively.

– The difference in both quantitativity and kinetics of aggregation/sedimentation of these 3 populations appeared to be mainly related to their chemical composition and their sphericity deviation, these characteristics being specific to each population

– A new population P4 appeared in the suspension due to the aggregation of nanoparticles P2 mainly. The radii of aggregates were up to 300 nm. This P4 population represented only around 6 to 7% of the initial fraction of nanoparticles. The concentration of this population decreased beyond 50 h.

– The behaviour of these 4 populations suggests that P2 and P3 mainly and rapidly settled out of the suspension, possibly after aggregation.

– Consequently, sedimentation induced decreasing of the elements present in the suspension, in particular the major and trace elements monitored.

Thus, the present study illustrates the advantage of being able to discriminate between different populations of nanoparticles according to their size, elemental composition and hydrodynamic behaviour, because these characteristics induce a different temporal behaviour. This information enables the fate of NPs of volcanic ash and the elements they may contain to be understood and the associated physicochemical phenomena to be quantified. This is particularly important since the NPs generated can (i) contain toxic and/or potentially impacting elements and/or (ii) carry elements by sorption occurring in aqueous medium. The type of information that can be acquired via AF4-UV–Vis-MALS-ICP-MS coupling therefore opens new perspectives for future environmental monitoring. However, several analytical challenges remain inherent in the nature of the matrix, in particular the large number of elements and their very low levels of concentration. Obviously, the methodological development effort must concern the entire process, from sample preparation to analysis, and from total determination to determination in the size continuum within a necessarily multi-technique approach. But this effort must aim above all to be able to reach all the metals and metalloids contained in the ashes, which is still today a limit analytical point.

3.4 Fractionation and characterization of volcanic ash nanoparticles by coiled tube field-flow fractionation, laser diffraction, scanning electron microscopy and inductively coupled plasma mass-spectrometry

In the final part of work the fractionation and characterization of volcanic ash nanoparticles were additionally performed using the combination of CTFFF, LD, SEM, and ICP-MS. For this, a new CTFFF fractionation procedure has been investigated. The procedure consists of two steps: recovering of submicron particle fraction and subsequent fractionation of recovered fraction. It should be noted that the proposed procedure has been used for the first time. Klyuchevskoy volcanic ash sample was considered as test sample due to reasons described earlier in *3.3.*

3.4.1 Recovering of submicron particle fraction from ash sample

The first step of CTFFF was developed based on the fractionation procedure of CTFFF described in *2.3.3.*

The initial Klyuchevskoy volcanic ash with mass of 1 g was prepared as slurry with 10 mL of water (1 g of ash and 10 mL deionized water). This was made in a 15 mL polypropylene tube. After contact, the tube was closed with cap and intensively shaken for two minutes.

Then, this slurry was introduced at flow rate 25 mL/min into the rotating coil column (RCC) by the use of a peristaltic pump. The RCC was preliminary filled with 20 mL deionized water. During the introduction of the slurry, the RCC did not rotate (ω = 0 rpm). The inner capacity of the column is 20 mL and particulate matter has an even distribution along the column. Thus, the resulting mixture in the column is equivalent to a suspension composed of 1 g of ashes in 20 mL water. Then, the column was rotated at 600 rpm and water was continuously fed into the column. During the rotation, large particles (>1 μm) of ash are held on the tube wall by the complex action of centrifugal forces and small particles (<1 μm) are eluted by the continuously fed water. The total time of the column rotation is 15 min. The separation of submicrometric particle fraction was achieved at a flow rate of 4 mL min^{-1}. The CTFFF procedure parameters of recovering of submicrometric particle fraction were experimentally chosen after series of preliminary tests.

The elution process of the total submicron particle fraction was monitored by spectrophotometer (λ = 254 nm). The part of the fraction considered for the second step of the separation process was collected into 50 mL polypropylene tube. The fractogram of elution of this submicron particle fraction is shown in Figure 17. The volume of collected submicrometric fraction was 20 mL, while time of collection was 300 s. The volume of total submicrometric fraction was 41.5 mL; time – 620 s.

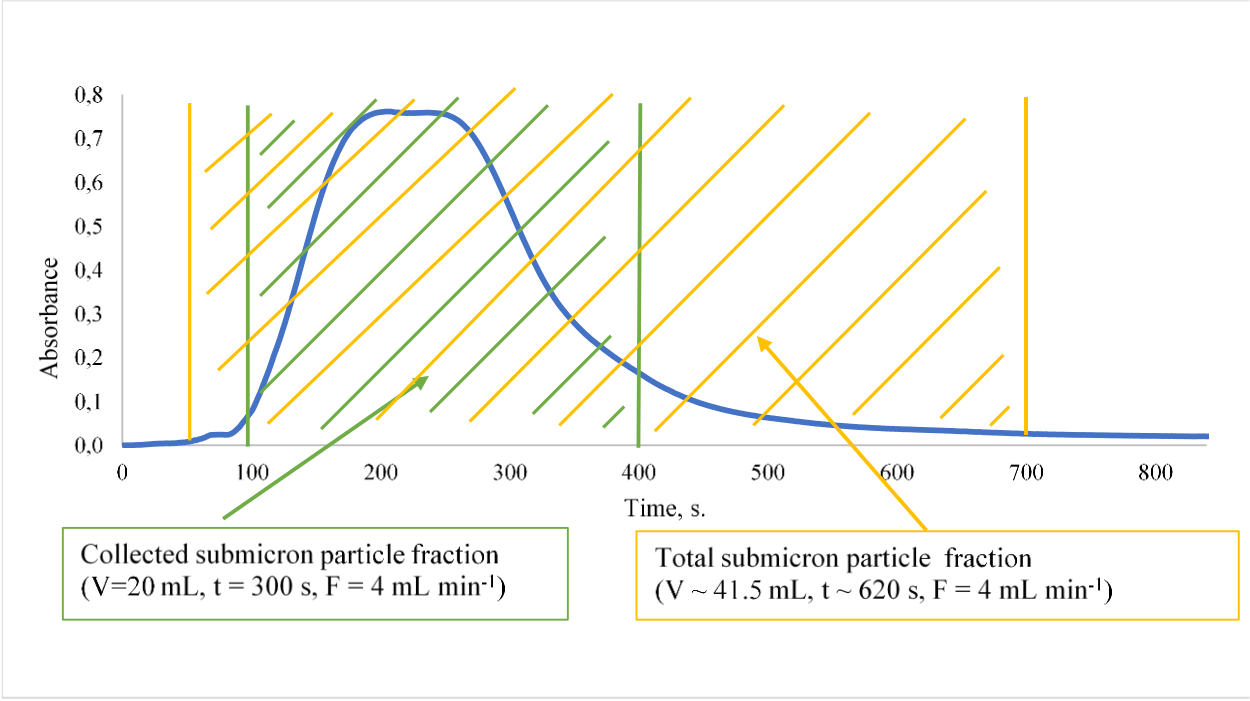

Figure 17. Fractogram of elution of submicron particle fraction.

The green color highlights the part of curve (Figure 17) that corresponds to the collected fraction of submicron particles. The volume of collected submicron particle fraction was 20 mL. The gold color (Figure 17) highlights the part of curve that corresponds to entire fraction of submicron particles. The volume of entire submicron particle fraction was about 41.5 mL. For further investigation of submicron particle fraction, 20 mL of the fraction was collected to avoid its excessive dilution.

After recovering, collected submicron particle fraction was characterized by laser diffraction and scanning electron microscopy techniques. The results of characterization are given in Figure 18. It has been shown (Figure 18*a*) that the recovered submicron particle fraction has bimodal PSD with maxima at 102 and 521 nm. The PSD have range from 40 to 1000 nm. The microphotographs (Figure 18*b*) confirmed the results obtained by LD.

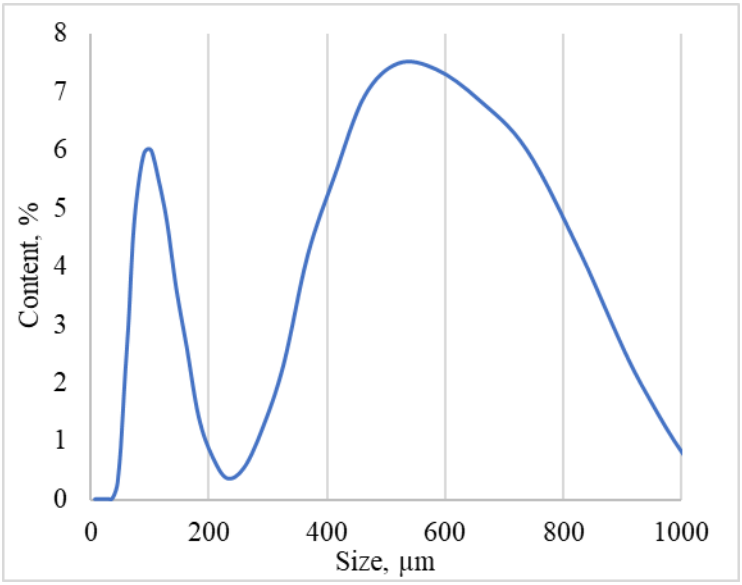

(a)

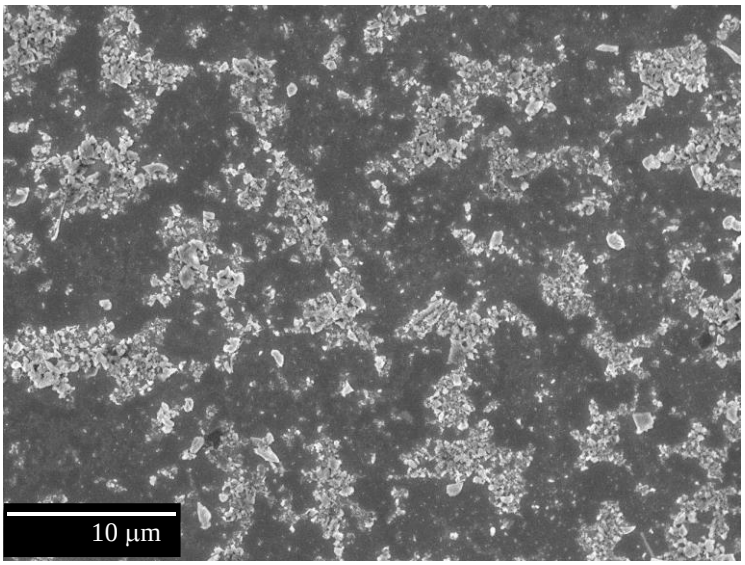

(b)

Figure 18. Particle size distribution obtained by laser diffraction and typical microphotograph obtained by scanning electron microscopy of the submicron particle fraction recovered from Klyuchevskoy volcanic ash.

The main parameters of first step of new CTFFF fractionation procedure can be given as follows:

- Initial mass of ashes = 1 g;
- Flow rate of mobile phase during CTFFF separation is 4 mL min^{-1};
- Speed of rotation of planetary centrifuge is 600 rpm;
- Volume of collected submicron particle fraction is 20 mL;
- Total volume of recovered submicron particle fraction is 41.5 mL.

3.4.2 Separation of submicron particle fraction into three different populations

Initially, aliquot of 2 mL was taken from submicron particle fraction (20 mL) recovered at the first step of new CTFFF separation procedure for further separation. This aliquot was introduced at flow rate 0.9 mL min^{-1} into the column by the use of the peristaltic pump. The RCC was preliminarily filled with deionized water and did not rotate ($\omega = 0$ rpm).

After the injection of sample, the column was run and rotated at 800 rpm. It should be noted that the direction of flow and direction of CTFFF rotation are opposite. The inner capacity of the column was same as at the first step (20 mL).

The separation of submicrometric fraction was achieved at a stepwise decreasing of flow rates. The flow rates and corresponding applying time of these flow rates were chosen in order to provide the uniform distribution of different size fractions inside the tube of CTFFF. The flow rates and corresponding time are indicated in Table 10. The flow rates were chosen after the series of preliminary tests. The number of flow rates (n=4) was chosen to recover three populations with different size.

Table 10. The flow rates and corresponding time used at the second step of new CTFFF fractionation procedure to provide the separation of submicron fraction of Klyuchevskoy volcano ash into three different populations. The submicron particle fraction was separated at the first step of new CTFFF fractionation procedure.

Flow rate, mL min^{-1}	Time, s*	Equivalent to volume of carrier flow, mL
0.9	366 s	5 mL
0.6	800 s	5 mL
0.3	1000 s	5 mL
0.1	3000 s	5 mL
	Total volume	20 mL (=inner capacity of the column)

* time was chosen to provide the pumping of 5 mL of carrier fluid at each flow rate

When the distribution of population along the channel in RCC was finished, the column was stopped (0 rpm). Then, the populations distributed inside the column were recovered by elution at a flow rate of 4.5 mL min^{-1}. The separated populations were collected in polypropylene tubes according to the fractogram curve (Figure 19). The volume of each fraction was 4 mL. The total volume of the 5 populations (seen in Figure 19) was 20 mL (5 x 4 mL), and the total volume of eluted carrier was about 33.5 mL.

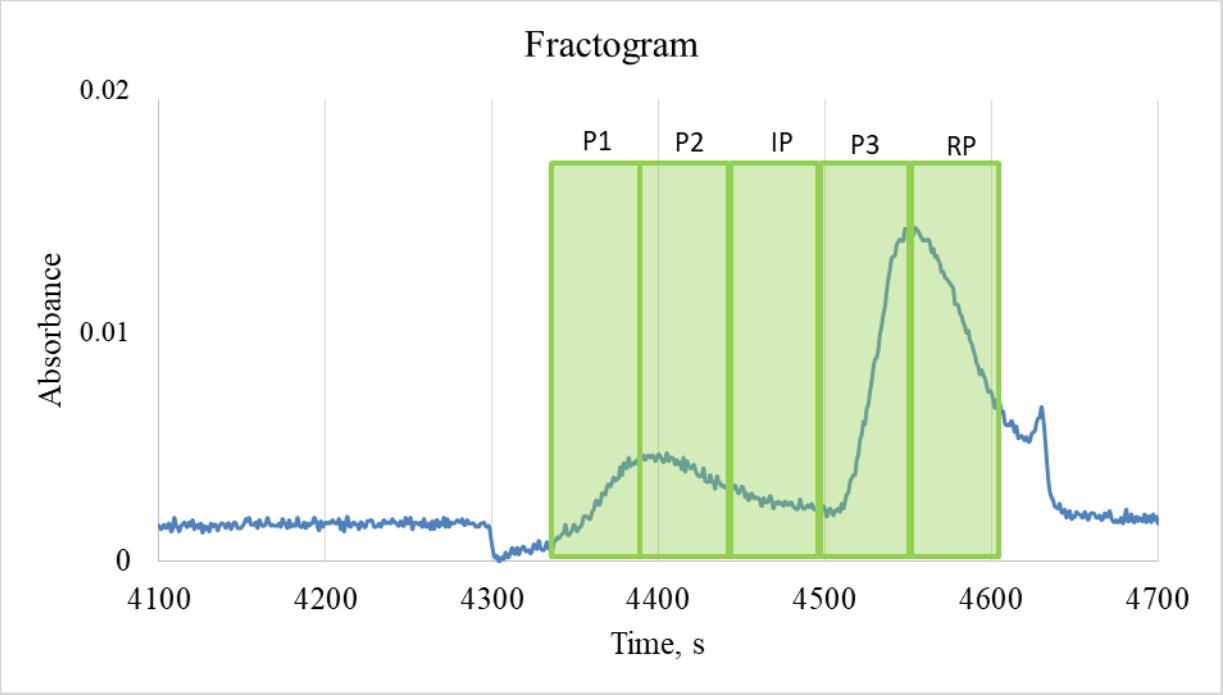

Figure 19. Fractogram of populations separated from submicron particle fraction; P1 – population 1, P2 – population 2, PF – interim population, P3 – population 3, PF – residual population. Elution was performed at a flow rate of 4.5 mL min^{-1}.

The areas highlighted on the fractogram (Figure 19) correspond to the collected populations. The 3 submicron particle populations (simply named Populations 1, 2 and 3 = P1, P2 and P3) were characterized by LD and SEM techniques. The obtained PSD of collected populations is illustrated in Figure 20. The microphotographs are given in Figure 21. Population 1 consists of particles with size less than 50 nm. Population 2 consists of particles with size from 50 to 200 nm. Population 3 consists of particles with size less than 1000 nm. The microphotographs of separated populations confirm the results obtained by LD. Interim population was collected to avoid cross-contamination of populations 2 and 3. The last collected population is residual.

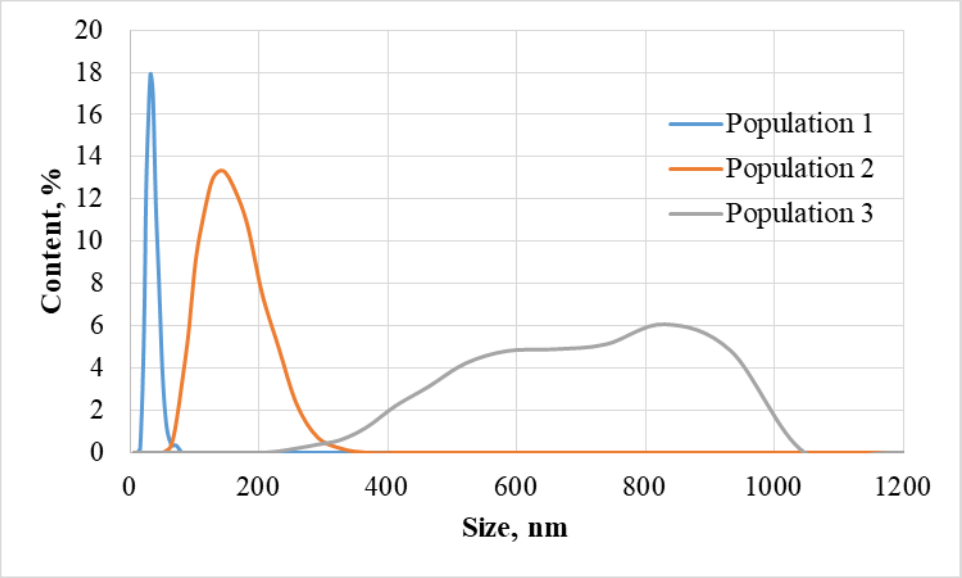

Figure 20. Particle size distribution of population 1, 2, and 3 separated from submicron fraction as obtained by laser diffraction

The main parameters of the second step of new CTFFF fractionation procedure can be given as follows:

- Volume of the recovered at 1st step submicron particle fraction injected into CTFFF for the second step is 2 mL;
- Speed of rotation of planetary centrifuge is 800 rpm;
- The directions of flow and RCC rotations are in opposite;
- Flow rates of mobile phase for distribution of populations to be recovered from submicron particle fraction were 0.9, 0.6, 0.3, and 0.1 mL min^{-1}, respectively;
- Elution flow rate was 4.5 mL min^{-1};
- Final volume of each population collected (i.e. of P1, of P2, of P3) is 4 mL;
- Total volume for recovering the 5 fractions = 33.5 mL;

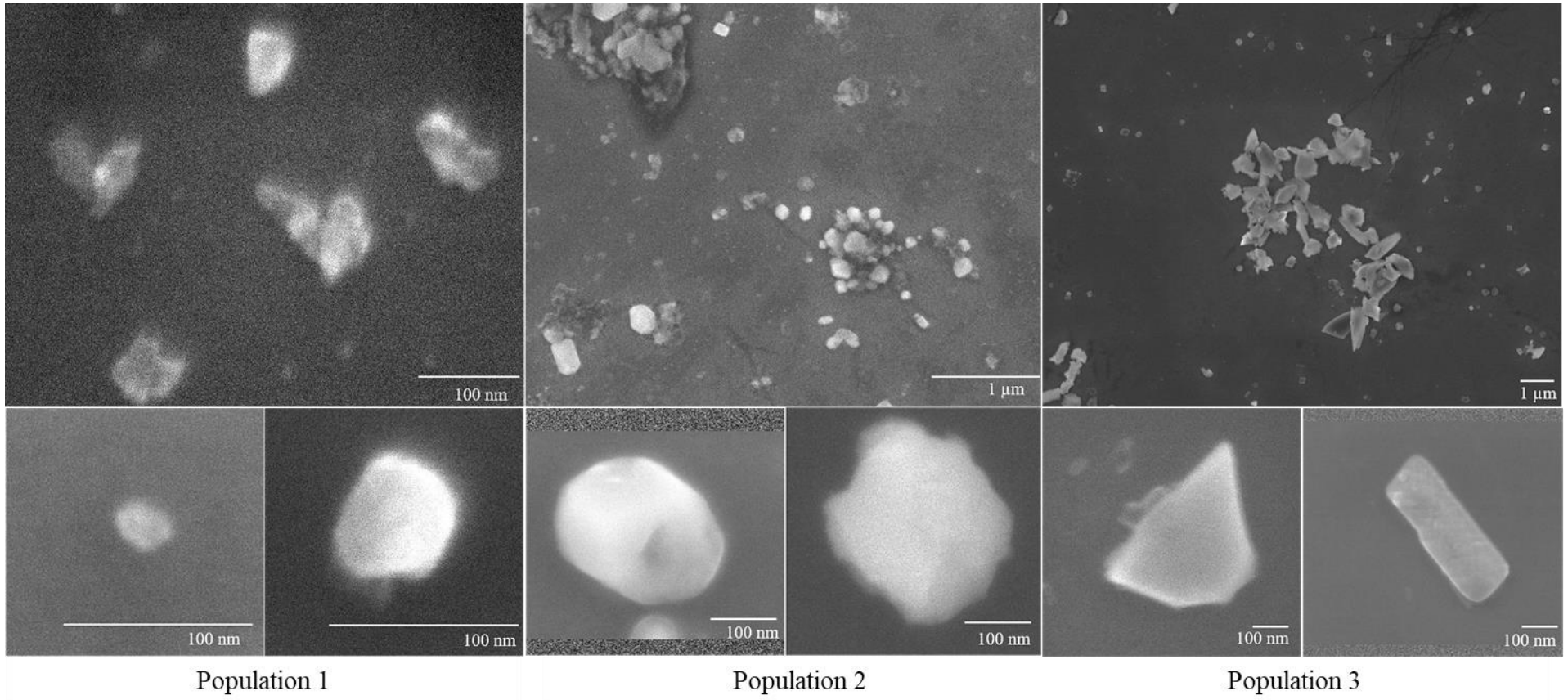

Figure 21.Microphotographs of population 1, 2, and 3 separated from submicron particle fraction as obtained by scanning electron microscopy

3.4.3 Elemental analysis of separated populations

After characterization, the populations separated from submicron particle fraction were directly analyzed by ICP-MS. The reliability of direct analysis of volcanic ash was shown previously in *3.2.* The recovered populations were not diluted before analysis. The results of analysis are provided in table 11. The concentration unit μg L^{-1} refer to the 4 mL volume of each fraction.

Table 11. Elemental concentration in population 1, 2, and 3 separated from submicron particle fraction as obtained by ICP-MS

Element	LOD	LOQ	Population 1 (<50 nm)	Population 2 (50-200 nm)	Population 3 (200-1000 nm)
	Concentration, μg L^{-1}				
Al	1.0	1.1	2.8±0.2	2.3±0.2	60±4
Fe	0.3	0.5	2.4±0.4	1.7±0.1	42±8
Ni	0.01	0.02	0.18±0.03	0.017±0.004	0.03±0.01
Cu	0.09	0.17	< LOD	< LOD	0.23±0.03
As	0.05	0.09	0.09±0.02	0.12±0.02	< LOD
Se	0.38	0.57	< LOD	< LOD	< LOD
Y	0.001	0.001	< LOD	< LOD	0.012±0.002
Sn	0.02	0.04	< LOD	< LOD	< LOD
Te	0.01	0.03	< LOD	< LOD	< LOD
La	0.001	0.002	< LOD	< LOD	0.0037±0.0003
Ce	0.001	0.002	< LOD	< LOD	0.0093±0.003
Pr	0.001	0.002	< LOD	< LOD	0.0012±0.0002 (< LOQ)
Nd	0.002	0.004	< LOD	< LOD	0.007±0.001
Gd	0.001	0.003	< LOD	< LOD	0.0025±0.0005
Dy	0.0006	0.0007	< LOD	< LOD	0.0013±0.0003
Ho	0.0004	0.0006	< LOD	< LOD	0.00041±0.00007 (< LOQ)
Tl	0.002	0.004	< LOD	< LOD	< LOD
Pb	0.09	0.19	< LOD	< LOD	0.127±0.003 (< LOQ)
Bi	0.002	0.003	< LOD	< LOD	< LOD
Th	0.001	0.001	< LOD	< LOD	< LOD

The concentrations of most elements in the populations under study were under LOD. This can be explained by dilution process at the first and second steps of the new CTFFF fractionation procedure. For further and more sophistication investigation of new proposed CTFFF fractionation procedure, CTFFF can be coupled online with detectors for size characterization. In addition, the pre-concentration of separated populations can enhance the results of elemental analysis.

General conclusion and Perspectives

The present doctoral thesis has been focused on the development of a new approach to the investigation of environmental nanoparticles. The proposed approach is based on the complementary use of asymmetric flow field-flow fractionation and coiled tube field-flow fractionation techniques. The main findings of the present doctoral thesis can be summarized as follows:

1. CTFFF, filtration, and sedimentation techniques applied to the recovery of nanoparticles from bulk polydisperse samples have been comparatively studied. The advantages and limitations of listed separation techniques are evaluated.

It has been shown that the filtration method provides low recoveries of NPs. Indeed, only fine NPs were separated using filtration while larger ones were retained on the filter. As a consequence, the elemental analysis of NP fractions recovered by filtration provided concentrations systematically inferior to those obtained for NP fractions recovered by sedimentation and CTFFF. The concentrations of most trace elements were under limits of detection. Moreover, RSD for the concentrations of elements in NP fractions separated by filtration were higher than for those separated by sedimentation and CTFFF. Therefore, even though the filtration remains the easiest and the fastest method to use, it is at the same time the least repeatable and the least representative for the separation of NP fraction.

The sedimentation method is commonly used but is time-consuming (48 h). However, this method enabled separated fraction to be representative to the NP fraction containing a low amount (<5%) of particles with size between 400 – 900 nm. The repeatability was also the best using this method.

CTFFF method enabled the fractionation time to be decreased down to 2 h, nevertheless it required the use of a special equipment (planetary centrifuges). This method enabled separated fraction to be representative to the NP fraction with a control of the maximal recovered NP size (400 nm for this paper). As NP fractions were more concentrated using CTFFF, this method enabled the separation to be more quantitative. The repeatability was slightly lower than with the sedimentation method. The limit of this method appeared to be the possible interactions between particles as well as between particles and tube wall during the separation process. The main reasons of these interactions can be mineral compositions of separated particles, their surface properties in

aqueous suspensions, and an action of centrifugal forces. Nevertheless, these interactions were less critical than the interactions observed between particles and filter using the filtration method.

2. The reliability of direct ICP-MS analysis of volcanic ash nanoparticles has been demonstrated. The direct analysis enables the numerous steps of digestion, evaporation, and dilution to be avoided. Besides, the interest of the direct ICP-MS analysis is that generally lower limits of detection can be achieved as compared to analysis after acid digestion. Some trace elements, which are potentially toxic (for instance Te and Bi), can be determined only by direct analysis.

3. The implementation of A4F-UV-MALS-ICP-MS coupling provided the information of different population of volcanic ash nanoparticles. The results obtained illustrate the advantage of being able to discriminate between different populations of nanoparticles according to their size, elemental composition and hydrodynamic behaviour, because these characteristics induce a different temporal behaviour. This information enables the fate of NPs of volcanic ash and the elements they may contain to be understood and the associated physicochemical phenomena to be quantified.

4. A new CTFFF fractionation procedure has been proposed. This procedure includes two steps. The first step is the recovery of submicron particle fraction from initial sample. The second step is the separation of submicron particle fraction obtained at the first step into three subpopulations. It should be noted that both first and second steps are performed by using CTFFF technique. For the first time, this procedure has been successfully applied to the fractionation of volcanic ash sample. Three populations with size < 50, 50-200, and 200-1000 nm were recovered. The results of fractionation were confirmed by laser diffraction and scanning electron microscopy techniques.

5. The advantages of complementary application of CTFFF and A4F have been demonstrated. It should be stressed that CTFFF technique has an increased separation capacity as compared to A4F, while A4F has an increased resolution. CTFFF can be applied to the separation of natural NPs from volcanic ash samples for their further fractionation, dimensional and elemental characterization using hyphenated methods based on the A4F coupled to laser light scattering and ICP-MS. Thus, CTFFF can be considered as a relevant tool for the pre-treatment of bulk polydisperse samples in the studies of environmental nanoparticles. It can be concluded that the

developed approach of complementary use of CTFFF and A4F can be served as the basis of the unified methodology applicable to the study of environmental NPs.

Based on the results obtained, possible perspectives can be formulated as follows:

1. The new CTFFF fractionation procedure requires further investigation in order to increase the number of populations separated from submicron particle fractions and, hence, decrease bounds of the particle size distribution of these recovered populations. This investigation can be performed by online coupling of CTFFF techniques with detectors for size characterization. Moreover, for the same reason, the performing of additional experiments is needed, in particular, the other numbers and values of flow rates used at the second step of the new CTFFF separation procedure can be tested.

2. The application field of the complementary use of A4F and CTFFF should be expanded. The developed approach may serve as successful tool for environmental monitoring; apart from volcanic ash NPs it can be used for the study of environmental NPs of other origins, for instance, soils and street dust.

3. This approach may be used not only for environmental but also for material studies. Due to CTFFF capability to separate a large quantity of analytes with a very wide range of sizes, it can be successfully used for purification and separation of various powder materials in micrometer size range for their further investigation by A4F-UV-MALS-ICP-MS hyphenated technique. Therefore, their complementary use looks rather promising.

References

[1] ISO/TS 80004-2: Nanotechnologies, Vocabulary, Part 2: Nano-objects, International Organization for Standardization, 2015.

[2] S. Faucher, P. Le Coustumer, G. Lespes, Nanoanalytics: history, concepts, and specificities, Environ. Sci. Pollut. Res., (2018) 1–15.

[3] C. Buzea, I.I. Pacheco, K. Robbie, Nanomaterials and nanoparticles: Sources and toxicity, Biointerphases, 2 (2007) MR17–MR71.

[4] M.S.M.S. Ermolin, P.S.P.S. Fedotov, Separation and characterization of environmental nano- and submicron particles, Rev. Anal. Chem., 35 (2016) 185–199.

[5] G. Lespes, S. Faucher, V.I. Slaveykova, Natural Nanoparticles, Anthropogenic Nanoparticles, Where Is the Frontier?, Front. Environ. Sci., 8 (2020) 71.

[6] M.S.M.S. Ermolin, P.S.P.S.P.S. Fedotov, N.A.N.A.N.A. Malik, V.K.V.K. Karandashev, Nanoparticles of volcanic ash as a carrier for toxic elements on the global scale, Chemosphere, 200 (2018) 16–22.

[7] D.A. Taylor, Dust in the wind, Environ. Health Perspect., 110 (2002).

[8] J. Houghton, Global warming, Reports Prog. Phys., 68 (2005) 1343–1403.

[9] E.C. Maters, P. Delmelle, S. Bonneville, Atmospheric Processing of Volcanic Glass: Effects on Iron Solubility and Redox Speciation, Environ. Sci. Technol., 50 (2016) 5033–5040.

[10] S. Bains, R.D. Norris, R.M. Corfield, K.L. Faul, Termination of global warmth at the Palaeocene/Eocene boundary through productivity feedback, Nature, 407 (2000) 171–174.

[11] E. Navarro, A. Baun, R. Behra, N.B. Hartmann, J. Filser, A.-J. Miao, A. Quigg, P.H. Santschi, L. Sigg, Environmental behavior and ecotoxicity of engineered nanoparticles to algae, plants, and fungi, Ecotoxicology, 17 (2008) 372–386.

[12] F.A. Messaud, R.D. Sanderson, J.R. Runyon, T. Otte, H. Pasch, S.K.R. Williams, An overview on field-flow fractionation techniques and their applications in the separation and characterization of polymers, Prog. Polym. Sci., 34 (2009) 351–368.

[13] C. Mélin, A. Perraud, N. Christou, R. Bibes, P. Cardot, M.-O. Jauberteau, S. Battu, M. Mathonnet, New ex-ovo colorectal-cancer models from different SdFFF-sorted tumor-initiating cells, Anal. Bioanal. Chem., 407 (2015) 8433–8443.

[14] E. Esposito, L. Ravani, M. Drechsler, P. Mariani, C. Contado, J. Ruokolainen, P. Ratano, P. Campolongo, V. Trezza, C. Nastruzzi, R. Cortesi, Cannabinoid antagonist in nanostructured lipid carriers (NLCs): Design, characterization and in vivo study, Mater. Sci. Eng. C, 48 (2015) 328–336.

[15] C. Contado, A. Pagnoni, A new strategy for pressed powder eye shadow analysis: Allergenic metal ion content and particle size distribution, Sci. Total Environ., 432 (2012) 173–179.

[16] A. Samontha, C. Nipattamanon, J. Shiowatana, A. Siripinyanond, Toward better understanding of salt-induced hen egg white protein aggregation using field-flow fractionation, J. Agric. Food Chem., 56 (2008) 8809–8814.

[17] M.S. Ermolin, P.S. Fedotov, E.A. Levashov, E.Y. Savonina, A.I. Ivaneev, Field-flow fractionation of metallic microparticles in a rotating coiled column, Mendeleev Commun., 26 (2016).

[18] P.S. Fedotov, N.G. Vanifatova, V.M. Shkinev, B.Y. Spivakov, Fractionation and characterization of nano- and microparticles in liquid media, Anal. Bioanal. Chem., 400 (2011) 1787–1804.

[19] J.B. Miller, J.M. Harris, E.K. Hobbie, Purifying colloidal nanoparticles through ultracentrifugation with implications for interfaces and materials, Langmuir, 30 (2014) 7936–7946.

[20] F. Bonaccorso, M. Zerbetto, A.C. Ferrari, V. Amendola, Sorting nanoparticles by centrifugal fields in clean media, J. Phys. Chem. C, 117 (2013) 13217–13229.

[21] L.E. Spelter, H. Nirschl, Classification of Fine Particles in High-Speed Centrifuges, Chem. Eng. Technol., 33 (2010) 1276–1282.

[22] J.C. Giddings, A New Separation Concept Based on a Coupling of Concentration and Flow Nonuniformities, Sep. Sci., 1 (1966) 123–125.

[23] G. Lespes, J. Gigault, S. Battu, Field Flow Fractionation, in: Anal. Sep. Sci., Wiley-VCH Verlag GmbH & Co. KGaA, Weinheim, Germany, 2015: pp. 1143–1176.

[24] A.C. Makan, M.J. Spallek, M. du Toit, T. Klein, H. Pasch, Advanced analysis of polymer emulsions: Particle size and particle size distribution by field-flow fractionation and dynamic light scattering, J. Chromatogr. A, 1442 (2016) 94–106.

[25] P.-A.A. Faye, N. Vedrenne, M.A. De la Cruz-Morcillo, C.-C.C. Barrot, L. Richard, S. Bourthoumieu, F. Sturtz, B. Funalot, A.-S.S. Lia, S. Battu, New Method for Sorting Endothelial and Neural Progenitors from Human Induced Pluripotent Stem Cells by Sedimentation Field Flow Fractionation, Anal. Chem., 88 (2016) 6696–6702.

[26] D.Y. Kang, C.H. Eum, S. Lee, Characterization of Fly Ash by Field-Flow Fractionation Combined with SPLITT Fractionation and Compositional Analysis by ICP-OES, Bull. Korean Chem. Soc., 35 (2014) 69–75.

[27] T.A. Maryutina, E.Y. Savonina, P.S. Fedotov, R.M. Smith, H. Siren, D.B. Hibbert, Terminology of separation methods (IUPAC Recommendations 2017), Pure Appl. Chem.,

90 (2018) 181–213.

[28] M.S. Ermolin, P.S. Fedotov, A.I. Ivaneev, V.K. Karandashev, A.A. Burmistrov, Y.G. Tatsy, Assessment of elemental composition and properties of copper smelter-affected dust and its nano- and micron size fractions, Environ. Sci. Pollut. Res., 23 (2016).

[29] M.S. Ermolin, P.S. Fedotov, A.I. Ivaneev, V.K. Karandashev, N.N. Fedyunina, A.A. Burmistrov, A contribution of nanoscale particles of road-deposited sediments to the pollution of urban runoff by heavy metals, Chemosphere, 210 (2018) 65–75.

[30] P.S. Fedotov, M.S. Ermolin, V.K. Karandashev, D. V. Ladonin, Characterization of size, morphology and elemental composition of nano-, submicron, and micron particles of street dust separated using field-flow fractionation in a rotating coiled column, Talanta, 130 (2014) 1–7.

[31] J.C. Giddings, A System Based on Split-Flow Lateral-Transport Thin (SPLITT) Separation Cells for Rapid and Continuous Particle Fractionation, Sep. Sci. Technol., 20 (1985) 749–768.

[32] S. Gupta, P.M. Ligrani, M.N. Myers, J.C. Giddings, Resolution deterioration and optimal operating conditions in centrifugal SPLITT fractionation Part II: Unstable density gradients, J. Microcolumn Sep., 9 (1997).

[33] B.N. Barman, P.S. Williams, M.N. Myers, J.C. Giddings, Split-Flow Thin (SPLITT) Cell Separations Operating under Sink-Float Mode Using Centrifugal and Gravitational Fields, Ind. Eng. Chem. Res., 57 (2018) 2267–2276.

[34] J. Storey, P. Douglas, P. Ligrani, K. Morten, Buoyancy-driven continuous SPLITT fractionation: A new technique for separation of microspheres, Sep. Sci. Technol., 44 (2009) 1895–1922.

[35] A. De Momi, J.R. Lead, Size Fractionation and Characterisation of Fresh Water Colloids and Particles: Split-Flow Thin-Cell and Electron Microscopy Analyses, Environ. Sci. Technol., 40 (2006) 6738–6743.

[36] T.F. Kinde, D. Dutta, A microfluidic SPLITT device for fractionating low-molecular weight samples, Anal. Chem., 85 (2013) 7167–7172.

[37] A. Capuano, V. Mulloni, A. Adami, L. Lorenzelli, Continuous extraction of proteins with a miniaturized electrical split-flow cell equipped with suspended splitters fabricated by dry film lamination, Sensors Actuators B Chem., 273 (2018) 627–634.

[38] J.C. Giddings, Field-flow fractionation: analysis of macromolecular, colloidal, and particulate materials, Science, 260 (1993) 1456–65.

[39] L.J. Gimbert, K.N. Andrew, P.M. Haygarth, P.J. Worsfold, Environmental applications of flow field-flow fractionation (FIFFF), TrAC Trends Anal. Chem., 22 (2003) 615–633.

[40] J.C. Giddings, F.J. Yang, M.N. Myers, Flow-field-flow fractionation: a versatile new separation method, Science, 193 (1976) 1244–5.

[41] R.D. Vaillancourt, W.M. Balch, Size distribution of marine submicron particles determined by flow field-flow fractionation, Limnol. Oceanogr., 45 (2000) 485–492.

[42] M. Baalousha, B. Stolpe, J.R. Lead, Flow field-flow fractionation for the analysis and characterization of natural colloids and manufactured nanoparticles in environmental systems: A critical review, J. Chromatogr. A, 1218 (2011) 4078–4103.

[43] J. Hee Song, W. Kim, D. Woon Lee, Comparison of Retention Behavior of Various Polystyrene Latex Particles and Gold Colloids on Different Channel Walls in Flow Field-Flow Fractionation, J. Liq. Chromatogr. Relat. Technol., 26 (2003) 3003–3035.

[44] S. Auer, I. Bindeman, P. Wallace, V. Ponomareva, M. Portnyagin, The origin of hydrous, high-δ18O voluminous volcanism: diverse oxygen isotope values and high magmatic water contents within the volcanic record of Klyuchevskoy volcano, Kamchatka, Russia, Contrib. to Mineral. Petrol., 157 (2009) 209–230.

[45] J.Y. Ahn, K.H. Kim, J.Y. Lee, P.S. Williams, M.H. Moon, Effect of asymmetrical flow field-flow fractionation channel geometry on separation efficiency, J. Chromatogr. A, 1217 (2010) 3876–3880.

[46] C.R.M. Bria, F. Afshinnia, P.W. Skelly, T.M. Rajendiran, P. Kayampilly, T.P. Thomas, V.P. Andreev, S. Pennathur, S. Kim Ratanathanawongs Williams, Asymmetrical flow field-flow fractionation for improved characterization of human plasma lipoproteins, Anal. Bioanal. Chem., 411 (2019) 777–786.

[47] K. Eskelin, M. Poranen, Controlled Disassembly and Purification of Functional Viral Subassemblies Using Asymmetrical Flow Field-Flow Fractionation (AF4), Viruses, 10 (2018) 579.

[48] M. Lampi, H.M. Oksanen, F. Meier, E. Moldenhauer, M.M. Poranen, D.H. Bamford, K. Eskelin, Asymmetrical flow field-flow fractionation in purification of an enveloped bacteriophage ϕ6, J. Chromatogr. B, 1095 (2018) 251–257.

[49] G. Krebs, T. Becker, M. Gastl, Characterization of polymeric substance classes in cereal-based beverages using asymmetrical flow field-flow fractionation with a multi-detection system, Anal. Bioanal. Chem., 409 (2017) 5723–5734.

[50] V. Kestens, G. Roebben, J. Herrmann, Å. Jämting, V. Coleman, C. Minelli, C. Clifford, P.-J. De Temmerman, J. Mast, L. Junjie, F. Babick, H. Cölfen, H. Emons, Challenges in the size analysis of a silica nanoparticle mixture as candidate certified reference material, J. Nanoparticle Res., 18 (2016) 171.

[51] S. Faucher, G. Charron, E. Lützen, P. Le Coustumer, D. Schaumlöffel, Y. Sivry, G.

Lespes, Characterization of polymer-coated CdSe/ZnS quantum dots and investigation of their behaviour in soil solution at relevant concentration by asymmetric flow field-flow fractionation – multi angle light scattering – inductively coupled plasma - mass spectro, Anal. Chim. Acta, 1028 (2018) 104–112.

[52] S. Serrano, M.A. Gomez-Gonzalez, P.A. O'Day, F. Laborda, E. Bolea, F. Garrido, P.A. O'Day, F. Laborda, E. Bolea, F. Garrido, Arsenic speciation in the dispersible colloidal fraction of soils from a mine-impacted creek, J. Hazard. Mater., 286 (2015) 30–40.

[53] K.M. Kuhn, E. Neubauer, T. Hofmann, F. von der Kammer, G.R. Aiken, P.A. Maurice, Concentrations and Distributions of Metals Associated with Dissolved Organic Matter from the Suwannee River (GA, USA), Environ. Eng. Sci., 32 (2015) 54–65.

[54] C.W. Cuss, M.W. Donner, I. Grant-Weaver, T. Noernberg, R. Pelletier, R.N. Sinnatamby, W. Shotyk, Measuring the distribution of trace elements amongst dissolved colloidal species as a fingerprint for the contribution of tributaries to large boreal rivers, Sci. Total Environ., 642 (2018) 1242–1251.

[55] J.R. Lead, K.J. Wilkinson, Environmental Colloids and Particles: Current Knowledge and Future Developments, in: Environ. Colloids Part., John Wiley & Sons, Ltd, Chichester, UK, 2007: pp. 1–15.

[56] C. Cascio, D. Gilliland, F. Rossi, L. Calzolai, C. Contado, Critical Experimental Evaluation of Key Methods to Detect, Size and Quantify Nanoparticulate Silver, Anal. Chem., 86 (2014) 12143–12151.

[57] Y. Ito, Trends in countercurrent chromatography, TrAC Trends Anal. Chem., 5 (1986) 142–147.

[58] P.S. Fedotov, M.S. Ermolin, O.N. Katasonova, Field-flow fractionation of nano- and microparticles in rotating coiled columns, J. Chromatogr. A, 1381 (2015) 202–209.

[59] Y. Ito, M. Weinstein, I. Aoki, R. Harada, E. Kimura, K. Nunogaki, The Coil Planet Centrifuge, Nature, 212 (1966) 985–987.

[60] P.S. Fedotov, B.Y. SpivakovP, V.M. Shkinev, B.Y. Spivakov, V.M. Shkinev, Possibility of Field-Flow Fractionation of Macromolecules and Particles in a Rotating Coiled Tube, Anal. Sci., 16 (2000) 535–536.

[61] P.S. Fedotov, V.A. Kronrod, O.N. Kasatonova, Simulation of the motion of solid particles in the carrier liquid flow in a rotating coiled column, J. Anal. Chem., 60 (2005) 310–316.

[62] A. Szparaga, T. Kowalkowski, B. Buszewski, Mathematical modeling of full feed depletion split-flow lateral-transport thin self-adjustable channels (FFD-SPLITT-SA), J. Chromatogr. A, 1552 (2018) 67–72.

[63] S.R. Springston, M.N. Myers, J.C. Giddings, Continuous Particle Fractionation Based on

Gravitational Sedimentation in Split-Flow Thin Cells, Anal. Chem., 59 (1987) 344–350.

[64] S. Gupta, P.M. Ligrani, J.C. Giddings, Investigations of Performance Characteristics Including Limitations Due to Flow Instabilities in Continuous SPLITT Fractionation, Sep. Sci. Technol., 32 (1997) 1629–1655.

[65] C. Contado, F. Dondi, R. Beckett, J.C. Giddings, Separation of particulate environmental samples by SPLITT fractionation using different operating modes, Anal. Chim. Acta, 345 (1997) 99–110.

[66] A. De Momi, J.R. Lead, Behaviour of environmental aquatic nanocolloids when separated by split-flow thin-cell fractionation (SPLITT), Sci. Total Environ., 405 (2008) 317–323.

[67] G. Blo, C. Conato, C. Contado, F. Fagioli, F. Dondi, Quantitative Splitt Fractionation of Lagoon Sediments, Ann. Chim., 94 (2004) 617–628.

[68] M.H. Kwon, Y.J. Moon, E.C. Jung, K.H. Lee, S. Lee, Size-sorting of micron-sized particles using two gravitational SPLITT fractionation (GSF) connected in a series (Tandem GSF), Bull. Korean Chem. Soc., 32 (2011) 681–686.

[69] S. Lee, S.K. Cho, J.W. Yoon, S.H. Choi, J.H. Chun, C.H. Eum, H. Kwen, Removal of aggregates from micron-sized polymethyl methacrylate (pmma) latex beads using full feed depletion mode of gravitational splitt fractionation (ffd-gsf), J. Liq. Chromatogr. Relat. Technol., 33 (2010) 27–36.

[70] M.H. Moon, H.J. Kim, S.Y. Kwon, S.J. Lee, Y.S. Chang, H. Lim, Pinched inlet split flow thin fractionation for continuous particle fractionation: Application to marine sediments for size-dependent analysis of PCDD/Fs and metals, Anal. Chem., 76 (2004) 3236–3243.

[71] M.H. Moon, D. Kang, H. Lim, J.E. Oh, Y.S. Chang, Continuous fractionation of fly ash particles by SPLITT for the investigation of PCDD/Fs levels in different sizes of insoluble particles, Environ. Sci. Technol., 36 (2002) 4416–4423.

[72] C. Contado, F. Riello, G. Blo, F. Dondi, Continuous split flow-thin cell fractionation of starch particles, J. Chromatogr. A, 845 (1999) 303–316.

[73] C.H. Eum, B.K. Kim, D.Y. Kang, S. Lee, Characterization of Asian dust using steric mode of sedimentation field-flow fractionation (Sd/StFFF), Anal. Sci. Technol., 25 (2012) 476–482.

[74] A. Santoro, R. Terzano, L. Medici, M. Beciani, A. Pagnoni, G. Blo, Colloidal mercury (Hg) distribution in soil samples by sedimentation field-flow fractionation coupled to mercury cold vapour generation atomic absorption spectroscopy, J. Environ. Monit., 14 (2012) 138–145.

[75] S. Assemi, S. Sharma, S. Tadjiki, K. Prisbrey, J. Ranville, J.D. Miller, Effect of Surface Charge and Elemental Composition on the Swelling and Delamination of Montmorillonite

Nanoclays Using Sedimentation Field-flow Fractionation and Mass Spectroscopy, Clays Clay Miner., 63 (2015) 457–468.

[76] J. Soto-Alvaredo, F. Dutschke, J. Bettmer, M. Montes-Bayón, D. Pröfrock, A. Prange, Initial results on the coupling of sedimentation field-flow fractionation (SdFFF) to inductively coupled plasma-tandem mass spectrometry (ICP-MS/MS) for the detection and characterization of TiO_2 nanoparticles, J. Anal. At. Spectrom., 31 (2016) 1549–1555.

[77] M.A. Gomez-Gonzalez, A. Voegelin, J. Garcia-Guinea, E. Bolea, F. Laborda, F. Garrido, Colloidal mobilization of arsenic from mining-affected soils by surface runoff, Chemosphere, 144 (2016) 1123–1131.

[78] K.J. Tindale, P.J. Patel, D. Wallschläger, Characterization of colloidal arsenic at two abandoned gold mine sites in Nova Scotia, Canada, using asymmetric flow-field flow fractionation-inductively coupled plasma mass spectrometry, J. Environ. Sci. (China), 49 (2016) 189–196.

[79] S. Harguindeguy, P. Crançon, M. Potin Gautier, F. Pointurier, G. Lespes, Colloidal mobilization from soil and transport of uranium in (sub)-surface waters, Environ. Sci. Pollut. Res., 26 (2019) 5294–5304.

[80] S. Holzmann, A. Missong, H. Puhlmann, J. Siemens, R. Bol, E. Klumpp, K. von Wilpert, Impact of anthropogenic induced nitrogen input and liming on phosphorus leaching in forest soils, J. Plant Nutr. Soil Sci., 179 (2016) 443–453.

[81] S. Baken, I.C. Regelink, R.N.J. Comans, E. Smolders, G.F. Koopmans, Iron-rich colloids as carriers of phosphorus in streams: A field-flow fractionation study, Water Res., 99 (2016) 83–90.

[82] J.J.M. De Klein, J.T.K. Quik, P.S. Bäuerlein, A.A. Koelmans, Towards validation of the NanoDUFLOW nanoparticle fate model for the river Dommel, the Netherlands, Environ. Sci. Nano, 3 (2016) 434–441.

[83] W.X. Wang, M. Chen, L. Guo, W.X. Wang, Size partitioning and mixing behavior of trace metals and dissolved organic matter in a South China estuary, Sci. Total Environ., 603–604 (2017) 434–444.

[84] M. Xie, M. Chen, W.X. Wang, Spatial and temporal variations of bulk and colloidal dissolved organic matter in a large anthropogenically perturbed estuary, Environ. Pollut., 243 (2018) 1528–1538.

[85] N. Gottselig, J. Sohrt, D. Uhlig, V. Nischwitz, M. Weiler, W. Amelung, Groundwater controls on colloidal transport in forest stream waters, Sci. Total Environ., 717 (2020) 134638.

[86] B.F. Trueman, T. Anaviapik-Soucie, V. L'Hérault, G.A. Gagnon, Characterizing colloidal

metals in drinking water by field flow fractionation, Environ. Sci. Water Res. Technol., 5 (2019) 2202–2209.

[87] H.S. Ferreira, B. Moreira-Alvarez, A.R. Montoro Bustos, J.R. Encinar, J.M. Costa-Fernández, A. Sanz-Medel, Capabilities of asymmetrical flow field – Flow fractionation on-line coupled to different detectors for characterization of water-stabilized quantum dots bioconjugated to biomolecules, Talanta, 206 (2020) 120228.

[88] P. Llano-Suárez, D. Bouzas-Ramos, J.M. Costa-Fernández, A. Soldado, M.T. Fernández-Argüelles, Near-infrared fluorescent nanoprobes for highly sensitive cyanide quantification in natural waters, Talanta, 192 (2019) 463–470.

[89] R. Aznar, F. Barahona, O. Geiss, J. Ponti, T. José Luis, J. Barrero-Moreno, Quantification and size characterisation of silver nanoparticles in environmental aqueous samples and consumer products by single particle-ICPMS, Talanta, 175 (2017) 200–208.

[90] Y. jie Chang, Y. hsin Shih, C.H. Su, H.C. Ho, Comparison of three analytical methods to measure the size of silver nanoparticles in real environmental water and wastewater samples, J. Hazard. Mater., 322 (2017) 95–104.

[91] S. Motellier, N. Pelissier, J.G. Mattei, Contribution of single particle inductively coupled plasma mass spectrometry and asymmetrical flow field-flow fractionation for the characterization of silver nanosuspensions Comparison with other sizing techniques, J. Anal. At. Spectrom., 32 (2017) 1348–1358.

[92] S. Motellier, N. Pélissier, J.G. Mattei, Aging of silver nanocolloids in sunlight: Particle size has a major influence, Environ. Chem., 15 (2018) 450–462.

[93] K.A. Huynh, E. Siska, E. Heithmar, S. Tadjiki, S.A. Pergantis, Detection and Quantification of Silver Nanoparticles at Environmentally Relevant Concentrations Using Asymmetric Flow Field-Flow Fractionation Online with Single Particle Inductively Coupled Plasma Mass Spectrometry, Anal. Chem., 88 (2016) 4909–4916.

[94] J. Jiménez-Lamana, V.I. Slaveykova, Silver nanoparticle behaviour in lake water depends on their surface coating, Sci. Total Environ., 573 (2016) 946–953.

[95] J.M. Pettibone, J. Liu, In Situ Methods for Monitoring Silver Nanoparticle Sulfidation in Simulated Waters, Environ. Sci. Technol., 50 (2016) 11145–11153.

[96] H. El Hadri, V.A. Hackley, Investigation of cloud point extraction for the analysis of metallic nanoparticles in a soil matrix, Environ. Sci. Nano, 4 (2017) 105–116.

[97] H. El Hadri, S.M. Louie, V.A. Hackley, Assessing the interactions of metal nanoparticles in soil and sediment matrices-a quantitative analytical multi-technique approach, Environ. Sci. Nano, 5 (2018) 203–214.

[98] D. Ruhland, K. Nwoko, M. Perez, J. Feldmann, E.M. Krupp, AF4-UV-MALS-ICP-

MS/MS, spICP-MS, and STEM-EDX for the Characterization of Metal-Containing Nanoparticles in Gas Condensates from Petroleum Hydrocarbon Samples, Anal. Chem., 91 (2019) 1164–1170.

[99] L. Krause, E. Klumpp, I. Nofz, A. Missong, W. Amelung, N. Siebers, Colloidal iron and organic carbon control soil aggregate formation and stability in arable Luvisols, Geoderma, 374 (2020) 114421.

[100] O.N. Katasonova, P.S. Fedotov, B.Y. Spivakov, M.N. Filippov, Behavior of Solid Microparticles in Their Fractionation on a Rotating Coiled Column, J. Anal. Chem., 58 (2003) 473–477.

[101] M.S. Ermolin, P.S. Fedotov, A.I. Ivaneev, V.K. Karandashev, N.N. Fedyunina, V.V. Eskina, Isolation and quantitative analysis of road dust nanoparticles, J. Anal. Chem., 72 (2017).

[102] M.S. Ermolin, P.S. Fedotov, V.K. Karandashev, V.M. Shkinev, Methodology for separation and elemental analysis of volcanic ash nanoparticles, J. Anal. Chem., 72 (2017) 533–541.

[103] V.M. Shkinev, M.S. Ermolin, P.S. Fedotov, A.P. Borisov, V.K. Karandashev, B.Y. Spivakov, A set of analytical methods for the estimation of elemental and grain-size composition of volcanic ash, Geochemistry Int., 54 (2016) 1252–1260.

[104] O.N. Katasonova, P.S. Fedotov, V.K. Karandashev, B.Y. Spivakov, Application of rotating coiled columns to the fractionation of soil particles and to the sequential extraction of heavy-metal species from silty, dusty, and sandy fractions, J. Anal. Chem., 60 (2005) 684–690.

[105] M.S. Ermolin, P.S. Fedotov, K.N. Smirnov, O.N. Katasonova, B.Y. Spivakov, O.A. Shpigun, Field-flow fractionation of microparticles in a rotating coiled column for the preparative separation of sorption materials, J. Anal. Chem., 70 (2015) 1207–1212.

[106] T. Kowalkowski, A. Szparaga, M. Pastuszak, Role of micrometer sediment particles (SPLITT fractionation) in phosphorus speciation and its recycling in lakes, Environ. Earth Sci., 73 (2015) 1779–1788.

[107] S. Lee, T.W. Lee, S.K. Cho, S.T. Kim, D.Y. Kang, H.D. Kwen, S.K. Lee, C.H. Eum, Implementation of splitter-less SPLITT fractionation and its application to large scale-fractionation of sea sediment, Microchem. J., 95 (2010) 11–19.

[108] C. Huguet, G.J. de Lange, Ö. Gustafsson, J.J. Middelburg, J.S. Sinninghe Damsté, S. Schouten, Selective preservation of soil organic matter in oxidized marine sediments (Madeira Abyssal Plain), Geochim. Cosmochim. Acta, 72 (2008) 6061–6068.

[109] M. Portnyagin, K. Hoernle, G. Avdeiko, F. Hauff, R. Werner, I. Bindeman, V. Uspensky,

D. Garbe-Schönberg, Transition from arc to oceanic magmatism at the Kamchatka-Aleutian junction, Geology, 33 (2005) 25.

[110] Standard NF ISO 18772 Soil quality — Guidance on leaching procedures for subsequent chemical and ecotoxicological testing of soils and soil materials, International Organization for Standardization, 2014.

[111] R. Sahai, MEMBRANE SEPARATIONS | Filtration, Encycl. Sep. Sci., (2000) 1717–1724.

[112] T. Kinoshita, The method to determine the optimum refractive index parameter in the laser diffraction and scattering method, Adv. Powder Technol., 12 (2001) 589–602.

[113] Y.A. Karpov, V.A. Orlova, Modern methods of autoclave sampling in chemical analysis of substances and materials, Zavod. Lab., 73 (2007) 4–11.

[114] V.A. Khvostikov, V.K. Karandashev, V.A. Orlova, Autoclave system for specimens opening for element analyses, 3599526 C1 RU. №2015120258/05, 2016.

[115] V.K. Karandashev, V.A. Khvostikov, S. V. Nosenko, Z.P. Burmii, Stable Highly Enriched Isotopes in Routine Analysis of Rocks, Soils, Grounds, and Sediments by ICP-MS, Inorg. Mater., 53 (2017) 1432–1441.

[116] V.K. Karandashev, A.N. Turanov, T.A. Orlova, A.E. Lezhnev, S. V. Nosenko, N.I. Zolotareva, I.R. Moskvitina, Use of the inductively coupled plasma mass spectrometry for element analysis of environmental objects, Inorg. Mater., 44 (2008) 1491–1500.

[117] B. Magnusson, U. Ornemark, eds., Eurachem Guide: The Fitness for Purpose of Analytical Methods - A Laboratory Guide to Method Validation and Related Topics, Second, 2014.

[118] M.J. Le Bas, A.L. Streckeisen, The IUGS systematics of igneous rocks, J. Geol. Soc. London., 148 (1991) 825–833.

[119] M. Lægdsmand, K.G. Villholth, M. Ullum, K.H. Jensen, Processes of colloid mobilization and transport in macroporous soil monoliths, Geoderma, 93 (1999) 33–59.

[120] M. Aliofkhazraei, Handbook of nanoparticles, Springer International Publishing, 2015.

[121] M. Meier, J. Ungerer, M. Klinge, H. Nirschl, Formation of porous silica nanoparticles at higher reaction kinetics, Powder Technol., 339 (2018) 801–808.

[122] S. Dubascoux, I. Le Hécho, M. Potin Gautier, G. Lespes, On-line and off-line quantification of trace elements associated to colloids by As-Fl-FFF and ICP-MS, Talanta, 77 (2008) 60–65.

[123] G. Liu, J. Wang, W. Xue, J. Zhao, J. Wang, X. Liu, Effect of the size of variable charge soil particles on cadmium accumulation and adsorption, J. Soils Sediments, 17 (2017) 2810–2821.

[124] G. Liu, J. Wang, X. Liu, X. Liu, X. Li, Y. Ren, J. Wang, L. Dong, Partitioning and geochemical fractions of heavy metals from geogenic and anthropogenic sources in various soil particle size fractions, Geoderma, 312 (2018) 104–113.

[125] E. Padoan, C. Romè, F. Ajmone-Marsan, Bioaccessibility and size distribution of metals in road dust and roadside soils along a peri-urban transect, Sci. Total Environ., 601–602 (2017) 89–98.

[126] J. Hofman, H. Bartholomeus, S. Janssen, K. Calders, K. Wuyts, S. Van Wittenberghe, R. Samson, Influence of tree crown characteristics on the local PM 10 distribution inside an urban street canyon in Antwerp (Belgium): A model and experimental approach, Urban For. Urban Green., 20 (2016) 265–276.

[127] H. Guénet, E. Demangeat, M. Davranche, D. Vantelon, A.-C. Pierson-Wickmann, E. Jardé, M. Bouhnik-Le Coz, E. Lotfi, A. Dia, J. Jestin, Experimental evidence of REE size fraction redistribution during redox variation in wetland soil, Sci. Total Environ., 631–632 (2018) 580–588.

[128] C. Niyungeko, X. Liang, C. Liu, Z. Liu, M. Sheteiwy, H. Zhang, J. Zhou, G. Tian, Effect of biogas slurry application rate on colloidal phosphorus leaching in paddy soil: A column study, Geoderma, 325 (2018) 117–124.

[129] Y. Imoto, T. Yasutaka, M. Someya, K. Higashino, Influence of solid-liquid separation method parameters employed in soil leaching tests on apparent metal concentration, Sci. Total Environ., 624 (2018) 96–105.

[130] E. Paineau, I. Bihannic, C. Baravian, A.M. Philippe, P. Davidson, P. Levitz, S.S. Funari, C. Rochas, L.J. Michot, Aqueous suspensions of natural swelling clay minerals 1 structure and electrostatic interactions, Langmuir, 27 (2011) 5562–5573.

[131] T.J. Jones, K. McNamara, J. Eychenne, A.C. Rust, K. V. Cashman, B. Scheu, R. Edwards, Primary and secondary fragmentation of crystal-bearing intermediate magma, J. Volcanol. Geotherm. Res., 327 (2016) 70–83.

[132] S.B. Mueller, P.M. Ayris, F.B. Wadsworth, U. Kueppers, A.S. Casas, P. Delmelle, J. Taddeucci, M. Jacob, D.B. Dingwell, Ash aggregation enhanced by deposition and redistribution of salt on the surface of volcanic ash in eruption plumes, Sci. Rep., 7 (2017) 45762.

[133] R.C. Vickery, Chemistry of the Lanthanons, Academic Press, New York, 1953.

[134] S.L.R. Ellison, A. Williams, Eurachem/CITAC Guide: Quantifying Uncertainty in Analytical Measurement, Third, 2012.

[135] I.M. El-Nahhal, J.K. Salem, S. Kuhn, T. Hammad, R. Hempelmann, S. Al Bhaisi, Synthesis and characterization of silica coated and functionalized silica coated zinc oxide

nanomaterials, Powder Technol., 287 (2016) 439–446.

[136] M.H. Mahdieh, H. Mozaffari, Characteristics of colloidal aluminum nanoparticles prepared by nanosecond pulsed laser ablation in deionized water in presence of parallel external electric field, Phys. Lett. Sect. A Gen. At. Solid State Phys., 381 (2017) 3314–3323.

[137] J. Gigault, B. Grassl, G. Lespes, Size characterization of the associations between carbon nanotubes and humic acids in aqueous media by asymmetrical flow field-flow fractionation combined with multi-angle light scattering, Chemosphere, 86 (2012) 177–182.

Appendix

Appendix 1. List of publications

Within frameworks of the doctoral thesis, three articles have been published in international scientific journals, one article has been submitted. The results of doctoral thesis were presented and discussed on two international scientific conferences.

Articles:

1. **Ivaneev A.,** Ermolin M., Fedotov P., Faucher S., Lespes G. Sedimentation field-flow fractionation in thin channels and rotating coiled columns: from analytical to preparative scale separations // Separation & Purification Reviews. 2020. Published online. https://doi.org/10.1080/15422119.2020.1784940
2. **Ivaneev A.,** Faucher S., Ermolin M., Karandashev V., Fedotov P., Lespes G. Separation of nanoparticles from polydisperse environmental samples: comparative study of filtration, sedimentation, and coiled tube field-flow fractionation // Analytical and bioanalytical chemistry. 2019. № 411. P. 8011-8021.
3. **Ivaneev A.,** Faucher S., Fedyunina N., Karandashev V., Ermolin M., Fedotov P., Lespes G. Reliability of the direct ICP-MS analysis of volcanic ash nanoparticles // International Journal Environmental Analytical Chemistry. 2019. Vol. 99, № 4. P. 369–379.
4. Faucher S., **Ivaneev A.**, Fedotov P., Lespes G. Characterization of volcanic ash nanoparticles and study of their fate in aqueous medium by asymmetric flow field-flow fractionation – multidetection // Environmental science and Pollution research. 2020. submitted.

Conference abstracts:

5. Ivaneev A., Faucher S., Fedyunina N., Karandashev V., Ermolin M., Fedotov P., Lespes G., Reliability of the direct ICP-MS analysis of volcanic ash nanoparticles // European Winter Conference on Plasma Spectrochemistry. Pau, France, 2019. (poster presentation).
6. Ivaneev A., Faucher S., Ermolin M., Fedotov P., Karandashev V., Lespes G. Comparative study of the techniques applied to the separation of nanoscale particles from volcanic ash samples // 3rd International Caparica Christmas Conference on Sample Treatment, Caparica, Portugal, 2018. (oral presentation).

Appendix 2. Contribution of co-authors in published works

I have participated in all the stages of doctoral work: planning and performing experiments, discussions of results obtained, and writing articles. I performed preliminary tests, pre-treatment of volcanic ash samples under study, their fractionation by CTFFF, membrane filtration, and sedimentation, filtration of recovered fractions, their characterization by LD, direct ICP-MS analysis of separated nanoparticle, investigation of the new CTFFF fractionation procedure.

Petr Fedotov and Gaëtane Lespes – proposition the goals of the doctoral work, planning of experiments, discussion of results, and edition of articles.

Stéphane Faucher – planning of experiments, performing A4F experiments, discussion of results obtained, and edition of articles.

Mikhail Ermolin – planning of experiments, participation in CTFFF experiments, discussion of results obtained and edition of articles.

Vasily Karandashev – digestion of samples, performing ICP-AES and ICP-MS analysis of digested samples, discussion of results

Natalia Fedyunina – participation in experiment of volcanic NPs direct analysis by ICP-MS, discussion of results.

Appendix 3. Abstract

Environmental particles, especially nanoparticles (NPs), have a potential risk for human health and ecosystems due to their ubiquity, specific characteristics and properties (extremely high mobility in the environment, abilities of accumulation of toxic elements and penetration in living organisms) and, hence, should be scrutinized. The study of environmental NPs remains a challenge for analytical chemistry. In fact, NPs in a polydisperse environmental sample may represent only one thousandth or less of the bulk sample. Consequently, a considerable sample weight must be handled to separate amount of NP fraction sufficient for their dimensional and quantitative characterization. The group of field-flow fractionation (FFF) techniques can serve as a relevant basis for the development of methodology applicable to the study of environmental NPs.

This doctoral thesis focuses on the use of asymmetrical flow and coiled tube field-flow fractionation techniques (A4F and CTFFF, respectively) in the investigation of environmental particulate samples. The results obtained demonstrate the advantages of these techniques applied to the study of volcanic ash nanoparticles. It should be highlighted that CTFFF technique has an increased separation capacity as compared to A4F, while A4F has an increased resolution. CTFFF was applied to the separation of NPs from environmental samples and a new CTFFF procedure was proposed. Dimensional and elemental characterization was carried out using A4F coupled to laser light scattering and ICP-MS. Furthermore, the results related to the investigation of stability of environmental nanoparticles are also given.

Keywords: Coiled tube field-flow fractionation techniques, Asymmetrical flow field-flow fractionation, Environmental particles, Environmental nanoparticles, Volcanic ashes

Appendix 4. Résumé

Les particules environnementales, particulièrement les nanoparticules (NP), présentent un risque potentiel pour la santé humaine et les écosystèmes en raison de leur ubiquité, de leurs caractéristiques et de leurs propriétés spécifiques. Plus particulièrement les NP ont une mobilité extrêmement élevée dans l'environnement, une capacité à associer, voire à concentrer des éléments toxiques et à pénétrer dans les organismes vivants. Les nanoparticules doivent donc être considérées avec une attention particulière dans les études environnementales. Néanmoins, l'étude des NP dans l'environnement demeure un défi pour la chimie analytique. En effet, les nanoparticules dans un échantillon environnemental polydispersé peuvent représenter seulement un millième ou moins de la masse de l'échantillon global. Par conséquent, une masse d'échantillon considérable doit être manipulé pour séparer une quantité de nanoparticules suffisante pour leur caractérisation dimensionnelle et leur quantification. L'ensemble des techniques de fractionnement par flux−force (FFF) peut servir de base pertinente pour le développement d'une méthodologie applicable à l'étude des NP environnementales.

Cette thèse de doctorat se concentre sur l'utilisation des techniques de fractionnement flux-force asymétrique et en colonne tournante (A4F et CTFFF, respectivement) dans l'étude d'échantillons environnementaux de particules. Les résultats obtenus mettent en évidence les avantages de l'utilisation de ces techniques appliquées à des nanoparticules de cendres volcaniques. Il convient de souligner que la technique de CTFFF a une capacité de séparation accrue par rapport à l'A4F, tandis que l'A4F a une grande résolution. La CTFFF a été utilisée pour la séparation de NP d'échantillons de cendres volacniques. Une nouvelle procédure de fractionnement en colonne tournante a également été proposée. La caractérisation dimensionnelle et élémentaire de ces NP a été réalisée en utilisant le couplage entre l'A4F, la diffusion de la lumière multi-angle et l'ICP-MS. Complémentairement, la stabilité de ces nanoparticules y est abordée.

Mots-cles: Fractionnement flux-force en colonne tournante, Fractionnement flux-force asymétrique, Particules environnementales, Nanoparticules environnementales, Cendres volcaniques.